Compartmentalisation of cAMP in Brown Adipocytes

Dissertation

zur

Erlangung des Doktorgrades (Dr. rer. nat.)

der

Mathematisch-Naturwissenschaftlichen Fakultät

der

Rheinischen Friederich-Wilhelms-Universität Bonn

vorgelegt von

Sukanya Arcot Kannabiran

aus

Bhopal, Indien

Bonn 2022

Angefertigt mit der Genehmigung der Mathematisch-Naturwissenschaftlichen Fakultät der Rheinischen Friedrich-Wilhelms-Universität Bonn

1. Gutachter: Prof. Dr. Alexander Pfeifer

2. Gutachterin: Prof. Dr. Christa Müller

Tag der Promotion: 19.01.2022

Erscheinungsjahr: 2022

Acknowledgements

I would like to express my heartfelt gratitude to Prof. Dr. Alexander Pfeifer for giving me the opportunity to be a part of his working group and entrusting me with two novel and exciting projects. I would like to thank him for his time, supervision and support during the time of my PhD thesis.

I am grateful to Prof. Dr. Christa Müller for her support with the GPR18 project, advice as my second supervisor, and her warmth during each and every retreat organised by the graduate school in Bonn.

I am deeply indebted to Prof. Dr. Viacheslav Nikolaev for his encouragement, his willingness to be available at any time point and having supervised, coordinated my work and providing me with materials from Hamburg. I am very grateful for his unending support, without whom I wouldn't be where I stand today. He has been a blessing in disguise, and a mentor who I would always live up to as long as I continue my scientific journey.

I am thankful to Dr. Dominic Gosejacob for his constructive criticism, teaching me the importance to have an eye for detail and instilling in me the thought to always ask the right questions while performing experiments. I am indebted to him for his time, nerves and most importantly, his patience. I am glad that the two of us survived this journey with plenty of memories.

I have also been lucky to have the constant support of my mentors Dr. Josefine Reber and Dr. Noah Morruzi who have always had my back and encouraged me to go on, when times were rough. I would also like to extend my gratitude to Dr. Martin Jastroch who encouraged me to take up this opportunity in Bonn. I also feel privileged to have been a part of the lab of Prof. Dr. Martin Klingenspor at the Technical University of Munich where my liking for adipose tissue biology stems from. For this, I am deeply grateful to Dr. Tobias Fromme for his excellent lectures on Mitochondrial biology and his brilliance in the method of teaching.

I am grateful to the whole working group of Prof. Pfeifer for their advice, help, support and kindness. The unending support of the professors and colleagues of the Graduate school in Bonn (GRK1873, Batch of 2016) who have been wonderful and fun to be with made my doctoral studies worthwhile.

I would like to thank my friends, Sandhya, Malavika, and Nandita, who despite of living in three different time zones across the globe have constantly supported and encouraged me. I could feel at home in Bonn. The full credit for this goes to Joschka, Eva, Elena, Victoria, Jaspal,

Rafael, Laura and others for their immense support and company at all times and making my stay memorable.

A major portion of this thesis was written when I had relocated to Hamburg to be a part of the working group of Prof. Dr. Dr. Andreas Guse at the University Medical Center, Hamburg-Eppendorf. I am very grateful and happy to have a high-spirited mentor as Prof. Guse, who is extremely supportive and fun to work with. I am thrilled to be here and also thankful to have the constant support and motivation of the entire group.

Finally, I am grateful to my parents, Sheela and Kannabiran, who have been my strongest pillars. Ma and Appa, thank you for your support and always motivating me to never give up. They say better late, than never. This one goes to you!

Abstract

The second messenger, 3',5'-cyclic adenosine monophosphate (cAMP) plays an important role in governing the function and differentiation of brown adipocytes. Upon the stimulation of the G_s-coupled G protein-coupled receptors (GPCRs) adenylate cyclases are activated, which in turn produce cAMP. In cells, the levels of cyclic nucleotide regulated and controlled by phosphodiesterases (PDEs). This tight regulation of PDEs over cAMP enables them to generate subcellular microdomains. Given the importance of cAMP in brown adipocyte signalling, not much is known about how the spatio-temporal architecture of cAMP in adipocytes is organised. This study focussed on monitoring the cAMP dynamics real-time in pre- and mature murine brown adipocytes upon the activation of G_s-coupled GPCRs, namely the most widely studied different β-adrenergic receptors (β-ARs) and with some preliminary insights on adenosine (A_{2A} and A_{2B}) receptors. The expression of different PDEs and their various subtypes were confirmed via immunoblotting and qPCR analysis. Of interest for this study were PDE2, PDE3 and PDE4. Subcellular fractionation of these PDEs in brown adipocytes revealed their localisation mainly in the cytosol. Therefore, live cell imaging was established in murine pre- and mature brown adipocytes isolated from transgenic mice expressing a cytosolic Förster Resonance Energy Transfer (FRET) based biosensor (Epac1-camps).

Firstly, cAMP compartmentation was studied in individual β-AR subtypes. Under the activation of every β-AR subtype, PDE4 was the main regulator of cytosolic cAMP in brown preadipocytes. While in mature adipocytes, upon β_1-AR activation, PDE3 and PDE4 tightly controlled cAMP pools. This could be due to the upregulation of PDE3 on protein levels upon differentiation. Surprisingly, increase in PDE3 protein expression had no influence on controlling β_3-induced cAMP, and the control of PDE4 was diminished in mature brown adipocytes. This led to a possible hypothesis that different loco-regio pools of cAMP could exist in brown adipocytes, one involving association of β_1-AR with PDE3/4 in the cytosol, while another could be one with β_3-AR more controlled by PDEs from other membrane compartments. These results could be recapitulated functionally, wherein lipolysis assay revealed that PDE3/4 tightly control β_1-AR activated, whereas this control was lost in β_3-AR initiated cAMP facilitating brown adipocyte lipolysis.

Upon the stimulation of G_s-coupled adenosine receptors (A_{2A} and A_{2B}), PDE2 and PDE4 tightly control cAMP compartmentation in preadipocytes and the reason for this could also be that these PDEs are lowly expressed on protein levels. The regulation of PDE3 and PDE4 on A_{2A} and A_{2B} receptor-initiated cAMP was similar to the pattern observed with β_3-AR activation

indicating that these PDEs regulate receptors involved in process of activating brown adipocyte thermogenesis similarly.

Kurzfassung

Der sekundäre Botenstoff 3‘,5‘-zyklisches Adenosinmonophosphat (cAMP) spielt eine wichtige Rolle bei der Steuerung der Funktion und Differenzierung von braunen Adipozyten. Bei Stimulation von G_s-gekoppelten G Protein-gekoppelten Rezeptoren (GPCRs) werden meistens Adenylatzyklasen aktiviert, die wiederum cAMP produzieren. In Zellen wird der Gehalt an zyklischen Nukleotiden durch Phosphodiesterasen (PDEs) reguliert und kontrolliert. Diese strenge Regulierung durch PDEs ermöglicht es, subzelluläre Mikrodomänen von cAMP zu erzeugen. Obwohl cAMP eine wichtige Rolle in der Signaltransduktion von braunen Adipozyten spielt, ist nicht viel darüber bekannt, wie die räumlich-zeitliche Verteilung von cAMP in Adipozyten organisiert ist. Diese Studie konzentrierte sich auf die Echtzeit-Überwachung der cAMP-Dynamik in prä- und reifen braunen Adipozyten der Maus nach der Aktivierung von G_s-gekoppelten GPCRs. Untersucht wurden dabei die gut bekannten β-Adrenorezeptoren (β-ARs) und in Ansätzen die Adenosin (A_{2A} und A_{2B}) Rezeptoren. Die Expression verschiedener PDEs und ihrer verschiedenen Subtypen wurden mittels Immunoblotting und qPCR-Analyse bestätigt. Von Interesse für diese Studie waren PDE2, PDE3, und PDE4. Die subzelluläre Fraktionierung dieser PDEs in Bildgebung lebender Zellen in prä- und reifen braunen Adipozyten zeigte, dass sie hauptsächlich im Zytosol lokalisiert sind. Daher wurde die Bildgebung lebender Zellen in prä- und reifen braunen Adipozyten etabliert: die Adipozyten wurden aus transgenen Mäusen, die einen zytosolischen Förster Resonance Energy Transfer (FRET)-basierten Biosensor (Epac1-camps) exprimieren, isoliert.

Zunächst wurde die Kompartimentierung von cAMP in einzelnen β-AR-Subtypen untersucht. Bei der Aktivierung jedes β-AR-Subtyps war PDE4 der Hauptregulator von zytosolischem cAMP in braunen Präadipozyten, während in reifen Adipozyten nach β_1-AR-Aktivierung PDE3 und PDE4 streng kontrollierte cAMP-Pools bildeten. Dies könnte auf die Hochregulierung von PDE3 auf Proteinniveaus bei der Differenzierung zurückzuführen sein. Überraschenderweise hatte eine Erhöhung der PDE3-Proteinexpression keinen Einfluss auf die Kontrolle von β_3-induziertem cAMP und der Einfluss von PDE4 war in reifen braunen Adipozyten vermindert. Dies führte zu der möglichen Hypothese, dass in braunen Adipozyten verschiedene Loco-Regio-Pools von cAMP existieren könnten, von denen einer die Assoziation von β_1-AR mit PDE3/4 im Zytosol beinhaltet, während ein anderer eher durch die Verknüpfung von β_3-AR mit PDEs aus anderen Membrankompartimenten kontrolliert wird. Diese Ergebnisse konnten funktionell rekapituliert werden: der Lipolyse-Assay zeigte, dass PDE3/4 β_1-AR-aktiviertes cAMP streng kontrollierte, während diese Kontrolle bei β_3-AR-initiiertem cAMP verloren ging, was die Lipolyse von braunen Adipozyten erleichtert.

Bei Stimulation von G_s-gekoppelten Adenosinrezeptoren (A_{2A} und A_{2B}) kontrollieren PDE2 und PDE4 die cAMP-Kompartimentation in Präadipozyten eng und es könnte sein, dass diese PDEs auf Proteinebene schwach exprimiert werden. Die Regulation von A_{2A}- und A_{2B}-Rezeptor-initiiertem cAMP durch PDE3 und PDE4 ähnelte dem Muster, dass bei der β_3-AR-Aktivierung beobachtet wurde, was darauf hindeutet, dass diese PDEs Rezeptoren regulieren, die am Prozess der Aktivierung der Thermogenese der braunen Adipozyten beteiligt sind.

Table of Contents

List of Figures

List of Tables

List of Units

C	Celcius
H	Hour
µm	Micrometer
µL	Microliter
mA	Miliampere
Min	Minute
mL	Milliliter
Mm	Millimolar
Nm	Nanometer
Ms	Milliseconds
M	Molar
L	Liter
Sec	Second
V	Volt

List of Symbols

Alpha	α
Beta	β
Degree	°
Gamma	γ
Ground state	S_0
Energy of photons	h_v
Excited state	S_0
FRET ratio corrected	$FRET_{corr}$
FRET ratio	FRET
Number of experiments	N
Spectral bleedthrough factor	b

List of Abbreviations

4-AAP	4-aminoantipyrine
5‘-AMP	5’- adenosine monophosphate
5‘-GMP	5’- guanosine monophosphate
β-AR	β-Adrenergic receptors
β_1-AR	β_1-Adrenergic receptor
β_2-AR	β_2-Adrenergic receptor
β_3-AR	β_3-Adrenergic receptor
A_{2A}	Adenosine A_{2A} receptor
A_{2B}	Adenosine A_{2B} receptor
AC	Adenylyl cyclase
ADP	Adenosine-5’-diphosphate
Ago	Agonist
APS	Ammonium peroxydisulfate
ATGL	Adipose tissue triglyceride lipase
ATP	Adenosine-5’-triphosphate
BA	Brown adipocytes
BAT	Brown adipose tissue
BMI	Body mass index
BSA	Bovine serum albumin
cAMP	3‘,5‘-cyclic adenosine monophosphate
$CaCl_2$	Calcium chloride
cGMP	3‘,5‘-cyclic guaonsine monophosphate
CFP	Cyan fluorescent protein
CNGC	Cyclic nucleotide gated channels
CNS	Central nervous system
CO_2	Carbon-dioxide
DAG	Diacyl glycerol
DAP	Dihydroxyacetone phosphate
DM	Differentiation medium
DMEM	Dulbecco’s modified eagle’s medium
DMSO	Dimethyl sulfoxide
DNA	Deoxyribonucleic acid
EGTA	Ethylene glycol-bis(β-aminoethyl ether)-*N*,*N*,*N*′,*N*′-tetraacetic acid
ELISA	Enzyme-linked immunosorbent assay

Epac	Exchange protein directly activated by cAMP
Epac1	Exchange protein directly activated by cAMP-1
ER	Endoplasmic reticulum
ESPA	N-ethyl-*N*-(3-sulfopropyl) *m*-anisidine
EtOH	Ethanol
FBS	Fetal bovine serum
FDA	Food and drug adminstration
FFA	Free fatty acid
Fsk	Forskolin
FRET	Förster resonance energy transfer
GAF	cyclic *G*MP, *A*denylyl cyclase, *F*hlA
GEF	Guanine nucleotide exchange factor
gWAT	Gonadal white adipose tissue
GK	Glycerol kinase
G-1-P	Glycerol-1-phosphate
GPCR	G protein-coupled receptor
GM	Growth medium
GPO	Glycerol Phosphate Oxidase
GTP	Guanosine triphosphate
G_s	Stimulatory G-proteins
HCl	Hydrochloric acid
HEPES	N-(2-hydroxyethyl)-piperazine-N'-2-ethansulfonic acid
HPRT	Hypoxanthine-guanine-phosphoribosyltransferase
IB_{cells}	Isolation Buffer for Cells
H_2O_2	Hydrogen peroxide
HSL	Hormone sensitive lipase
IM	Induction medium
iWAT	Inguinal white adipose tissue
iBAT	Intrascapular brown adipose tissue
KCl	Potassium chloride
kDa	Kilo Dalton
LED	Light emitting diode
LR	Linker region
LSM	Laser scanning confocal microscopy
MAM	Mitochondrial associated membranes
MSC	Mesenchymal stem cells

MeOH	Methanol
MRB	Mitochondrial resuspension buffer
mRNA	Messenger RNA
NaCl	Sodium chloride
NaF	sodium fluoride
NaOH	Sodium hydroxide
Na_3VO_4	Sodium orthovanadate
NE	Norepinephrine
ORO	Oil Red O
P	Passage
PAGE	Polyacrylamid gel electrophoresis
PBS	Phosphate buffered saline
PCR	Polymerase chain reaction
PDE	Phosphodiesterase
PFA	Paraformaldehyde
pGC	Particulate guanylyl cyclases
PIP_2	Phosphatidylinositol 4,5- bisphosphate
PKA	Protein kinase A
PKC	Protein kinase C
PKG	Protein kinase G
P/S	Penicillin/streptomycin
qPCR	Real time quantitative PCR
RIPA	Radioimmunoprecipitation assay
ROI	Region of interest
RPM	Rotations per minute
RT	Room temperature
SBT	Spectral bleed through
SERCA	Sarcoplasmic/endoplasmic reticulum calcium ATPase
sCMOS	scientific Complementary metal–oxide–semiconductor
s.e.m	Standard error of the mean
SDS	Sodium dodecyl sulphate
sGC	Soluble guanylyl cyclases
SNS	Sympathetic nervous system
SR	Sarcoplasmic reticulum
SV-40	Simian virus 40
T3	Triiodothyronine

TC	Tissue culture
TBS	Tris buffered saline
TEMED	N, N, N', N'-tetramethylethylenediamine
TG	Transgenic
UCP1	Uncoupling protein 1 (*ucp1*)
UCR	Upstream conserved regions
WA	White adipocytes
WAT	White adipose tissue
WHO	World Health Organisation
WT	Wild type
YFP	Yellow fluorescent protein

I. Compartmentalisation of cAMP in brown adipocytes

1. Introduction

1.1. Obesity and the role of the brown adipose tissue

Obesity occurs as a state of energy imbalance wherein the energy intake exceeds energy expenditure leading to the storage of excess fat [2]. The prevalence of obesity and its related comorbidities namely hypertension, heart diseases, diabetes, ischemic strokes and certain types of cancer have made it the major cause of global mortality and morbidity [3,4]. The World Health Organisation (WHO) reported 13% of the world's population in 2016 (Figure 1) and as of 2019, about 39 million children under the age of five to be obese respectively [1]. Therefore, there is a growing need to understand underlying causes and identify mechanisms to prevent the manifestation of obesity and its related diseases.

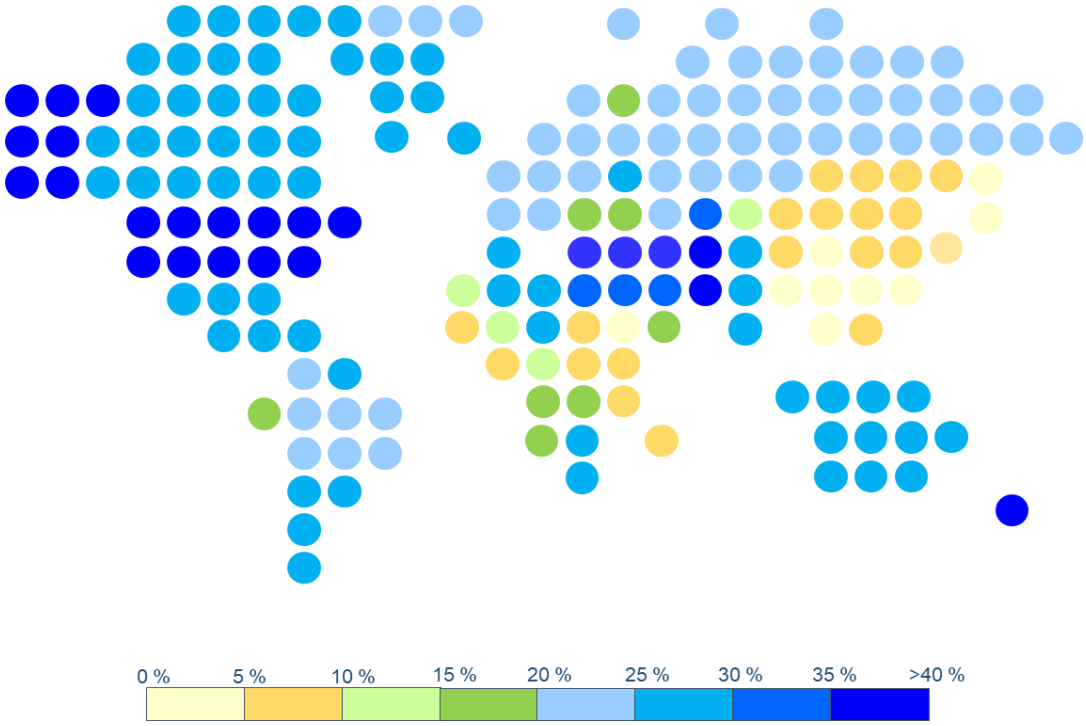

Figure 1.: Representation of the prevalence of obesity worldwide. A map representing the percentage of adult men and women that are obese throughout the world as reported by the WHO in 2016. The statistics and the figure were adapted from WHO [1]. WHO – World Health Organisation.

A logical attempt to curb obesity would be to target a reduction in energy intake and/or increase energy expenditure [2]. In light to this, activation of one of the fundamental adipose organs, the brown adipose tissue (BAT) in humans is an interesting therapeutic target to combat obesity. This therapeutic potential of the BAT stems from its ability to perform thermogenesis which correlates inversely to the body mass index (BMI) and adiposity increasing whole-body energy expenditure and metabolism [5–11].

1.1.1. Insights on the different adipose tissue depots in mammals

In mammals, two main adipose tissue depots namely, the white adipose tissue (WAT) and BAT form the fundamental unit of the adipose organ [12]. The WAT is comprised of white adipocytes (WA), which are large spherical cells 60-80 µM in diameter [13]. They are characterised by a large unilocular lipid droplet making up 90% of the cell volume, the nucleus and small mitochondria are present within the rim of the cytoplasm with its main function being that of energy storage [13] (Figure 2).

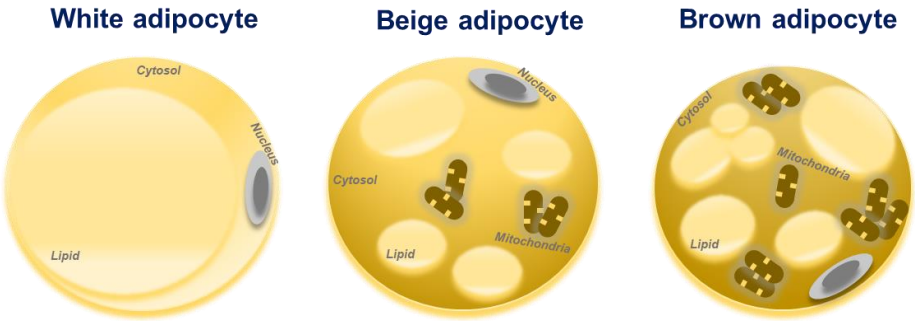

Figure 2.: Different types of adipocytes in mammals. The different types of adipocytes namely white adipocytes, beige adipocytes and brown adipocytes characterised by their differences in morphology and function. The figure has been adapted from studies by Cinti 2009 [13] and Pfeifer and Hoffmann, 2015 [16].

The BAT is composed of its functional unit, brown adipocytes (BA) which are about 30-50 µM in diameter [13]. The cytoplasm of BA is characterised by multilocular lipid droplets and many mitochondria (Figure 2) [12,13]. The main function of the BA is to dissipate energy and produce heat. This remarkable capacity of the BAT is due to the presence of uncoupling protein 1 (UCP1) in the inner mitochondrial membrane [8]. UCP1 confers to the thermogenic potential of the BAT without perturbing the synthesis or breakdown of adenosine monophosphate (ATP). UCP1 diminishes the proton gradient by uncoupling cellular respiration and mitochondrial ATP synthesis by converting the energy of substrate oxidation to heat [8,14] . Apart from the classical WA and BA, another type of BA within the WAT depots termed beige or brite adipocytes has been identified.

Beige/brite adipocytes share similar characteristics to that of classical BA, namely the existence of multilocular lipid droplets, several mitochondria and the expression of UCP1

(Figure 2). Beige/brite adipocytes are also denoted as inducible brown adipocytes in WAT [15–17]. In mice, the most predominant BAT depot is the intrascapular BAT (iBAT) present in the anterior subcutaneous region and comprise of brown adipocytes. The WAT located subcutaneously close to the hind limbs forms the inguinal WAT (iWAT) made up of white and beige adipocytes and is located in proximity of the gonads, forming the gonadal white adipose tissue (gWAT) composed of mainly WA [12,13] (Figure 3). In humans, BAT is mainly found in the neck, perirenal and supruaclavicular region made up of white, brown and beige adipocytes.

Beige cells are also found in the subcutaneous fat of humans and exhibit characteristics of the classical white adipose tissue (Figure 3) [5,10,11].

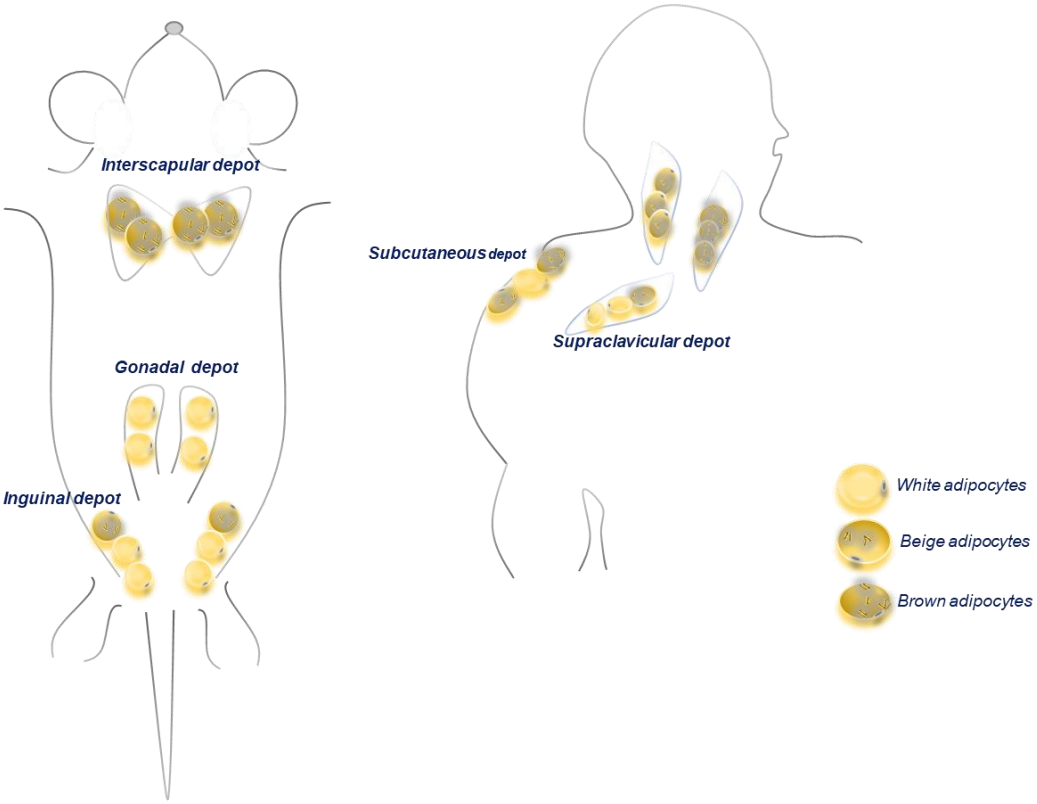

Figure 3.: Location of different adipose tissue depots in mice and humans. In mice, the three main adipose tissue depots are the iBAT, iWAT and gWAT. In humans, the subcutaneous adipose tissue forms main adipose tissue depot, and BAT is localised in the neck, and supraclavicular region. The figure was adapted from study by Bartelt and Heeren, 2015 [5]. iBAT- interscapular brown adipose tissue, iWAT - inguinal white adipose tissue, gWAT – gonadal white adipose tissue.

1.1.2. Activation and function of the brown adipose tissue

The physiological activation of BAT occurs upon cold exposure when the sympathetic nervous system releases norepinephrine (NE) [18] which binds to the β-adrenergic receptors (β-ARs). β-ARs are the most extensively studied G protein-coupled receptors (GPCRs) involved in the activation and function of BAT [19]. They comprise three subtypes: β_1, β_2 and β_3-ARs all of which are coupled to stimulatory G-proteins (G_s) and are expressed in the BAT [8,20,21].

The functional significance of the brown adipocyte thermogenic activity in the context of metabolic efficiency, altered metabolism upon subjection to different physiological conditions are often studied in certain species of mammals namely: mice, rats, Djungarian and Syrian hamsters [8]. In rodents, of the three β-ARs expressed in brown adipocytes, functionally relevant are β_1- and β_3-ARs that exhibit different functions [8]. Upon treatment with NE, at earlier stages of differentiation, proliferating adipocytes in culture showed an increase in the β_1-AR induced cAMP [20]. The following finding by Bronnikov.et al [20] was also the first study to have reported the function of adipocyte proliferation to be completely controlled by the activation of classical β_1-ARs [20].

In rodents and humans, β_3-ARs are the most widely studied receptors [8]. In humans, studies have proved the activation of BAT by β_3-ARs to play a role in metabolism [7,22] and to stimulate a process called lipolysis which facilitates the breakdown of stored lipids into free fatty acids [23]. A recent study, however questioned the role of β_3-ARs in stimulating BAT thermogenesis in humans. Interestingly, their novel finding indicated that in humans, BAT thermogenesis and lipolysis is mediated by the pharmacological stimulation of β_2-ARs and not by β_3-ARs, and that β_2-ARs are co-expressed with UCP1 [24].

It is essential to understand the mechanism of the classical activation of BAT in mammals. Treatment with NE leads to the activation of β_3-ARs wherein they couple to adenylyl cyclases (AC), triggering the classical canonical pathway of adipocyte activation as described below [8,20,21]. After the binding of NE to the β-ARs, adenylyl cyclases are activated which causes an increase in the concentration of the intracellular second messenger, 3', 5'- cyclic adenosine monophosphate (cAMP) [25]. The major effector of cAMP, protein kinase A (PKA) [26,27] then mediates activation of both adipose tissue triglyceride lipase [28] and hormone sensitive lipase [29] causing the breakdown of storage lipids to free fatty acids. Free fatty acids then bind to and activate the BAT-specific mitochondrial protein, UCP1. UCP1 increases the mitochondrial proton leak stopping the synthesis of ATP, facilitating thermogenesis where the energy of substrate oxidation is converted into heat (Figure 4) [14]

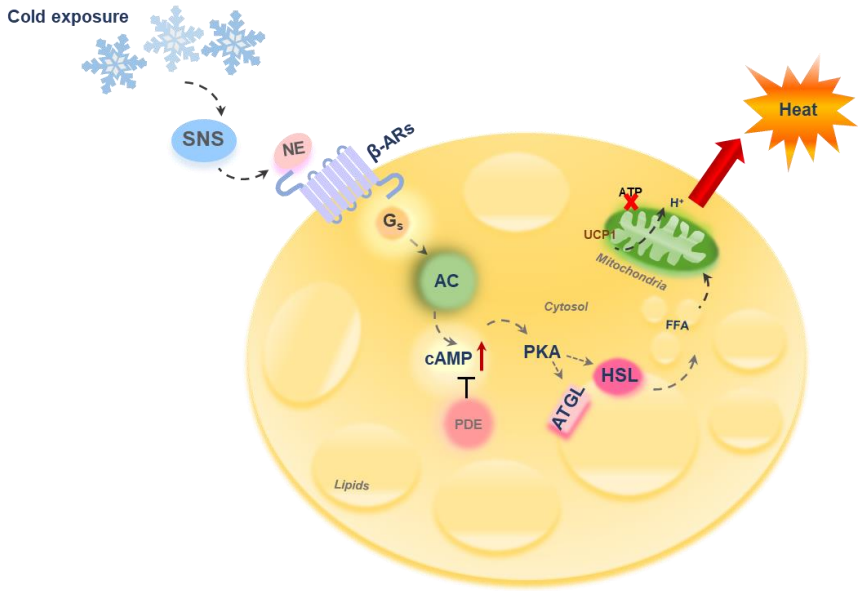

Figure 4.: Schematic representation of the activation of the UCP1 regulating thermogenesis in brown adipocytes. A representation of canonical brown adipocyte thermogenesis wherein the mitochondrial ATP synthesis is uncoupled by UCP1 as a result of the activation of β-ARs upon cold exposure. SNS – Sympathetic nervous system, NE- norepinephrine, β-ARs – β-adrenergic receptors, G_s - Stimulatory G-proteins, AC - Adenylyl cylases, cAMP - Cyclic adenosine monophosphate, PKA – Protein kinase A, ATGL- adipose tissue triglyceride lipase, HSL – Hormone sensitive lipase, PDE – phosphodiesterase, FFA – Free fatty acids, ATP – Adenosine triphosphate, UCP1 – Uncoupling protein 1. This figure has been modified and adapted from studies by Cannon and Nedergaard, 2008; Fredriksson et al., 2001 [8,27].

Over the years, attempts have been made in comprehending the biology of BAT. In this context, other signalling effectors and GPCRs have been studied. Apart from cAMP, noteworthy to mention is another main second messenger 3',5'-cyclic guanosine monophosphate (cGMP). It is generated by soluble guanylyl cyclases (sGC) and particulate guanylyl cyclases (pGC) [30]. cGMP has also been shown to be an important regulator of BAT function and interscapular BA differentiation via the effector protein kinase G (PKG) [31].

Interestingly, another class of GPCRs, the purinergic receptors – adenosine receptors, A_{2A} and A_{2B} receptors have newly been studied. They have also gained importance in the context of treating obesity. In mammals, these receptors have been reported to activate PKA and stimulate thermogenesis [32,33].

1.2. An overview on the role of phosphodiesterases

The functioning of the BAT via activation of different β-ARs or other GPCRs should demand mechanisms that are tightly regulated within the cell. The regulation of β-AR signalling has been well studied in cardiac myocytes [34] but how this occurs in the BAT is unknown. In cells, the levels of both second messengers cAMP and cGMP exist as a balance of their production and degradation. While the former occurs as a result of GPCR activation, the latter is governed

by phosphodiesterases (PDEs) and is their only route for degradation. PDEs play an important role in shaping intracellular pools of cyclic nucleotides thereby regulating major signalling events [35,36]. These intracellular enzymes generate distinct subcellular cyclic nucleotide microdomains by hydrolysing cAMP to 5'- adenosine monophosphate (5'-AMP) inactivating PKA or cGMP to 5'-guanosine monophosphate (5'-GMP) inactivating PKG and their respective downstream effectors [34]. All PDEs encompass carboxy-terminal catalytic cores that are conserved. Their amino-terminal regions exhibit differences amongst families, subfamilies, isoforms and have various functional roles [37]. PDEs are classified into 11 families, encoded by 21 genes encompassing roughly 100 isoforms. Of the 11 families based on their affinity to the substrate, they hydrolyse different cyclic nucleotides. PDE4, 7, 8 are cAMP-specific; PDE5, 6, 9 are cGMP specific and PDE1, 2, 3, 10, 11 are cAMP and cGMP-specific, or are called dual-specific PDEs due to their ability to hydrolyse both cAMP and cGMP (**Fehler! Verweisquelle konnte nicht gefunden werden.**) [38,39]. Over the years, the function and role of PDE2, PDE3 and PDE4 families of PDEs have been extensively studied in different cell types [38].

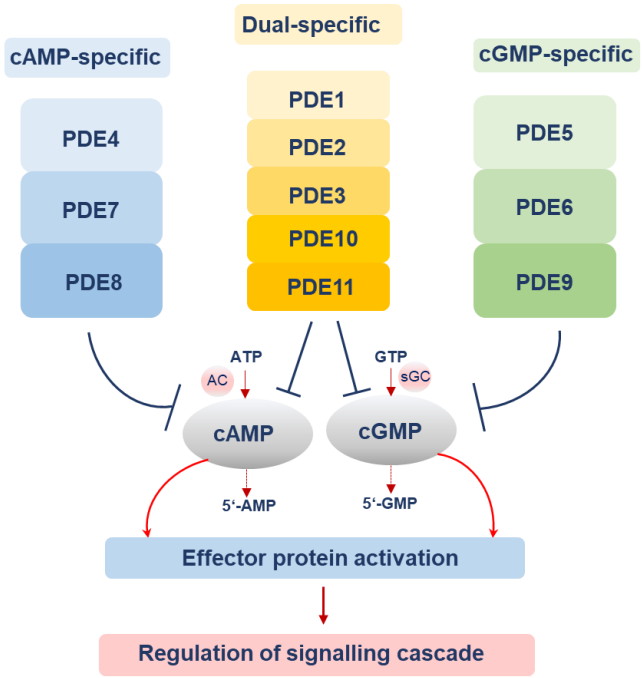

Figure 5.: Second messenger specificity of various phosphodiesterases. Different classes of PDEs classified as cAMP-specific (in blue), dual-specific (in yellow) and cGMP-specific (in green) PDEs based on the second messenger they degrade and their regulation of signalling cascades. This figure has been adapted from the study published by Pavlaki and Nikolaev, 2018 [37]. PDE- Phosphodiesterase, AC - Adenylyl cylases, cAMP – 3',5'-Cyclic adenosine monophosphate, sGC – Soluable guanylyl cyclases, cGMP – 3', 5'- Cyclic guanosine monophosphate, ATP – Adenosine triphosphate, 5'-AMP – 5'-adenosine monophosphate, GTP - Guanosine triphosphate, 5'-GMP - 5'-adenosine monophosphate.

1.2.1. Phosphodiesterase 2

PDE2 family is comprised of three isoforms namely PDE2A1, PDE2A2 and PDE2A3 which arise from a single gene PDE2A [37]. They are localised in different parts of the cell due to their varying N-terminal domains. Of the 11 families of PDEs, 5 families (PDE 2, 5, 6, 10 and 11) contain two small-molecule binding domains called cyclic *G*MP, *A*denylyl cyclase, *F*hlA (GAF) domains and are equipped with dual substrate specificity for cAMP and cGMP. The binding of cGMP allosterically to the GAF domain of PDE2 causes the hydrolysis of cAMP [40,41] making this specific class of PDE to hydrolyse cAMP at a ~10 fold higher rate. It is the only PDE known to hydrolyse cAMP in this manner. Therefore, PDE2 has been stated to play an important role in cAMP/cGMP degradation and crosstalk [42]. PDE2A1 was found to be located in the cytosol of murine heart and peripheral tissues [43]. PDE2A2 is present in the mitochondrial matrix of murine liver, brain [44], neonatal rat ventricular myocytes [45] and also, has recently been identified in brite/beige adipocytes [46]. PDE2A3 is membrane-associated and is mostly found in the brain [43].

A few noteworthy discoveries with respect to PDE2A biology is that it has been implicated in regulating mitochondrial morphology in neonatal rat ventricular myocytes and mouse embryonic fibroblasts [45], it regulates heart rate and arrythmias in mice [47]. A novel evidence also shows that the stimulation of β-ARs with NE in white adipocytes followed by PDE2A inhibition enhanced white adipocyte browning and reduced mitophagy [46]. This was a preliminary study highlighting the importance of PDE2A inhibition as a tool to treat metabolic disorders, especially in the context of treating obesity [46].

1.2.2. Phosphodiesterase 3

PDE3 family is comprised of 2 subfamilies: PDE3A and PDE3B which are transcribed from two different genes PDE3A contains 3 isoforms: PDE3A1, PDE3A2 and PDE3A3 which are formed via alternative initiation sites of transcription and translation. PDE3A1 was found to be localised in the sarcoplasmic reticulum (SR) [48] and caveolin-rich membrane microdomains [49], PDE3A2 has been reported to be present on the microsomal and cytosolic fractions [50] and PDE3A3 in the cytosolic fraction [50] of the myocardium respectively. PDE3B is localised in germinal neuroepithelium, neurons, human T-lymphocytes, monocyte-derived macrophages, and in particulate fractions – endoplasmic reticulum (ER) of differentiating 3T3-L1 adipocytes [51]. PDE3 hydrolyses cAMP and cGMP in a mutually competitive manner, and hence it is termed as a cGMP - inhibited PDE. PDE3 and its isoforms have been reported to perform and control many functions in different cell types [38,51]. To name a few: PDE3A isoforms together with the various anchoring, scaffold, and adaptor proteins organize themselves into multiprotein signalling complexes in the heart, which help in protection from

contractile dysfunction, as well as increased mortality arising due to lethal arrhythmic events like sustained ventricular tachycardia [52–54]. The activation of PDE3B has been reported to control the anti-lipolytic activity of insulin in adipocytes [51,55]. PDE3B levels are elevated in vascular smooth muscle cells in rats, and therefore has helped in understanding the progression of cardiovascular diseases [56] and its inhibition has also been reported to improve renin secretion in rats [57]. Knock-out of PDE3B in mice has shown to improve browning of WAT, minimal increase in weight gain post consumption of high-fat diet, reduction in fat deposition, increased β-oxidation due to higher mitochondrial biogenesis and increased oxygen consumption upon the intraperitoneal injection of β_3-AR agonist, CL316243 (CL) [58]. This also highlights the importance of PDE3B inhibition as a potential therapeutic target in the treatment of obesity.

1.2.3. Phosphodiesterase 4

The four major PDE4 subfamilies are - PDE4A, PDE4B, PDE4C and PDE4D which encode over 20 isoforms having a high affinity for cAMP. Each unique isoform of PDE4 contains an N-terminal region containing a targeting domain, and/or upstream conserved regions (UCR) 1 and 2. The UCRs are linked to each other and the catalytic domain via a linker region (LR) 1 and 2 [59]. PDE4 isoforms are categorised into long, short, super-short and dead-short isoforms based on the size and the presence of UCRs [60]. PDE4 and their isoforms are localised in different cell types and tissues namely: airway and vascular smooth muscle, vascular endothelium, leukocytes, brain and the heart [38,61]. PDE4 isoforms exhibit a variety of roles that have been reported in the cardiovascular system. To name a few examples of the role played by the isoforms of PDE4: PDE4D5 when recruited to the site of β_2-AR site by β-arrestins has been described to mediate a switch in G-protein receptor signalling from G_s to G_i signalling in cardiac myocytes [62]. Inhibition of PDE4A in specific models of transgenic mice contributes to amplified β-AR induced cAMP responses [63]. A study showed that the genetic ablation of PDE4B in mice contributed to a regulation of energy balance as it supressed obesity induced inflammation wherein the WAT of these mice had low levels of TNF-α and macrophage infiltration, and exhibited increased locomotor activity [64]. The knockout of PDE4A also improved conditions of obesity-driven depression due to the restoration of cAMP/PKA signalling in the hypothalamus [65]. Therefore, PDE4 also functions as an interesting therapeutic target to combat obesity and its associated clinical complications.

1.3. Insights into the concept of compartmentalisation

The activation of GPCRs present at the surface of a cell leads to the activation of subsequent signal transduction pathways and triggering of various effector molecules [66]. This has led to the question of where and how long the activated-GPCR signalling is active in the cell and if

different specific subcellular microdomains for different types of GPCR-driven signals exist. Furthermore, the question is how a cell could generate a diverse set of responses working with the same set of second messengers. The potential answer to this lies in the precise segregation of signalling pathways due to spatial and temporal resolution of how the second messengers (cAMP and cGMP) are generated and catabolised [67,68]. This concept has been termed compartmentalisation. Compartmentalisation was first observed in cardiac myocytes in the early 1980's while an elevation in cAMP concentration was observed when different ligands were administered [69].

The extensively studied ubiquitous second messenger cAMP is known to diffuse rapidly within a cell (200-700 µm/s) eliciting a myriad of global intracellular responses. The measurement of second messenger dynamics of the two important cyclic nucleotides namely, cAMP and cGMP dynamics is regulated by PDEs [38]. Understanding the nature of complexity of the PDEs systems in regulating levels of the second messengers, cAMP and cGMP have made it clear that cells can express several PDE types and their respective isoforms, and that the localisation of these PDEs could be the main regulator of local concentrations of cAMP or cGMP in a cell [38]. Studies on understanding how PDEs act as ''sinks'' to reduce the concentration of cAMP concentration in space and shorter time periods at localised areas within a cell has gained importance in the recent years [67,70]. However, traditional biochemical approaches like radioimmunoassays, enzyme-linked immunosorbent assays (ELISA) are unsuitable to determine cAMP concentrations at a subcellular level as they require disruption of a large number of cells and tissues. This leads to the measurement of overall levels of second messengers. This also makes the visualisation of cyclic nucleotide dynamics real-time in subcellular microdomains very difficult to interpret [71]. However, a solution to this would be to use a more sensitive approach that would aid the measurement of real-time dynamics of cyclic nucleotides with high spatial and temporal resolution in live cells.

Another approach to measure second messengers is to use biosensors. One example is the use of cyclic nucleotide gated channels (CNGC). CNGCs are nonselective cation channels in the plasma membrane, consisting of four subunits which have intracellular binding sites for cAMP and cGMP. Upon binding of cyclic nucleotides, there is an activation of these ion channels [72] causing an increase in cation current and intracellular calcium [73] which is either measured by patch-clamping or calcium sensitive dyes [74]. However, the main limitation of the CNGC based biosensor was its poor selectivity to cAMP or cGMP, and its restriction to only one membrane (sarcolemmal) compartment [71].

1.3.1. Förster resonance energy transfer – a tool to study intracellular cAMP compartmentalisation

A widely used technique that enables the measurement of cAMP in living cells and tissues with high spatial and temporal resolution is Förster resonsance energy transfer (FRET) [75]. This approach of non-radiative energy transfer was described in the 1940's by Theodor Förster [76]. A FRET biosensor consists of a binding domain of the molecule of interest flanked between two fluorescent proteins that act as energy acceptors or donors. The donor and acceptor proteins have to be in a close proximity of less than 10 nm for the energy transfer to take place and many biological processes happen within this spatial range at which FRET occurs [77]. Binding of the molecule of interest to its binding domain causes a conformational change which leads to an altered distance and change in the state of energy levels from ground state (S_0) to excited state (S_1) between the donor and acceptor proteins as explained by the Jablonski diagram [78] (Figure 6). As the distance between the donor and the excited acceptor decreases, the transferred energy increases. The FRET measurements are then expressed ratiometrically as FRET traces [71,75].

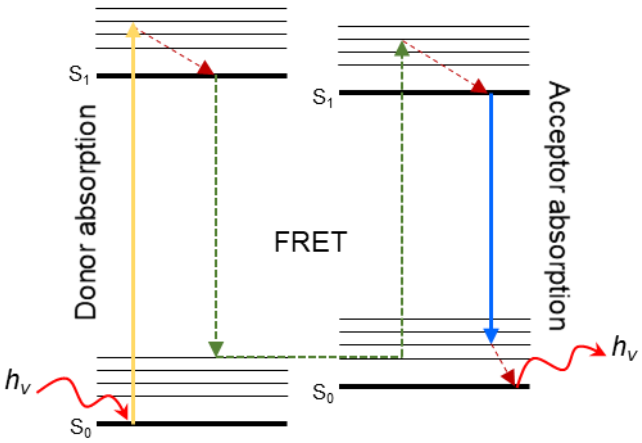

Figure 6.: The effect of FRET explained by Jablonski diagram. FRET occurs when the energy released from the relaxation of the donor is taken up by a suitable acceptor at proximity. This leads to the excitation of the electrons and the emission of the photons of the acceptor fluorescent protein. This figure was adapted from the study by Frackowiak, 1988 [78]. FRET – Förster resonance energy transfer, S_0 – Ground state, S_1 – Excited state, h_v – Energy of photon.

1.3.2. FRET-based biosensors

Several FRET sensors have been developed over the years to study the real-time dynamics of cAMP [79–81]. FRET based biosensors can be introduced into any cell type by transfection, viral transduction or can be expressed in transgenic animal models [68,75,82,83].

The first FRET biosensor to study the real-time dynamics of cAMP was based on PKA [84]. These sensors were based on fluorescent proteins coupled to the subunits of PKA and these sensors were the first of their kind to elucidate the role of PDE3 and PDE4 in neonatal ventricular cardiac myocytes [36,82,85]. However, PKA-based cAMP biosensors have a serious limitation that their 4 subunits should form a heterotetramer for them to be functional and their possible interaction with endogenous PKA subunits in the cell could result in slow sensor kinetics [79].

To overcome these difficulties, a new generation of biosensors was developed based on the exchange protein directly activated by cAMP (Epac) which is an important cAMP effector protein. Epac is comprised of the cAMP-binding site and a catalytic domain [86]. For this study, a FRET biosensor based on exchange protein directly activated by cAMP 1 (Epac1), Epac1-camps was used. This sensor consists of single cAMP-binding domain of Epac1 sandwiched between cyan fluorescent protein (CFP, donor) and yellow fluorescent protein (YFP, acceptor), which can be expressed in cells or the cells of interest can by isolated from transgenic mice (TG) that express this sensor under the control of CMV enhancer and chicken β-actin promotor [68]. Binding of cAMP to the cAMP binding domain of Epac1 causes a conformational change leading to a decrease in YFP fluorescence and an increase in CFP fluorescence due to an increase in the distance between the two fluorophores (Figure 6) [75]. This FRET biosensor has an EC_{50} for cAMP in the range of 2.4 µM enabling visualization of higher cAMP concentrations [79,80]. This sensor has been well characterised and has been successfully used in cardiac myocytes to report rapid changes in cAMP at a high temporal resolution and various PDE-regulated microdomains have been discovered [49,87].

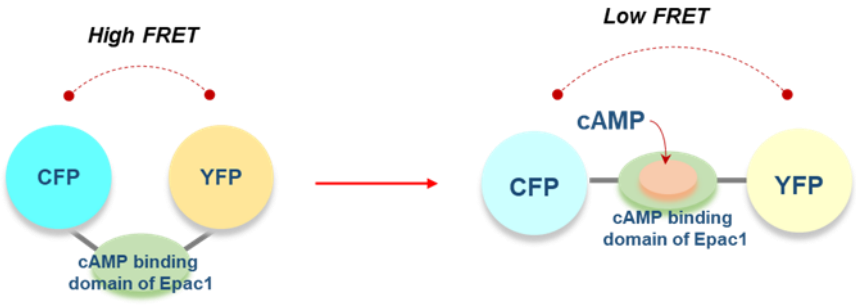

Figure 7.: Working of Epac1-camps FRET sensor. Epac1-camps FRET sensor consists of a single cAMP binding site of Epac1 flanked YFP and CFP. Binding of cAMP to the sensor leads to a conformational change causing a decrease in YFP and an increase in CFP fluorescence leading to FRET signal. This figure was adapted from the study by Borner et al., 2011 [75]. CFP – Cyan fluorescent protein, YFP – Yellow fluorescent protein, FRET- Förster resonance energy transfer, Epac1- Exchange protein directly activated by cAMP 1, cAMP – 3','5- Cyclic adenosine monophosphate.

1.4. Aim of the thesis

All the three subtypes of β-adrenergic receptors (β_1, β_2 and β_3- ARs) are expressed and exhibit functional differences in brown adipocytes. Amongst these, β_1-ARs have been reported to be important in early stages of brown adipocyte differentiation facilitating proliferation. β_3-receptors are the most widely studied receptors in humans, mice and rodents for brown adipose tissue function and activation regulating whole body energy expenditure. However, how these β-ARs and their cAMP signals are compartmentalised due to their regulation by PDEs in adipocytes is still unknown. Apart from β-ARs, G_s-coupled adenosine receptors (A_{2A} and A_{2B}) have also been reported to positively regulate brown adipose tissue activation and function. Therefore, this led to addressing another question of interest, if different G_s-coupled-GPCRs, for example β-ARs and adenosine receptors (A_{2A} and A_{2B}) both of which are involved in regulating brown adipocyte thermogenesis exhibited different or similar pattern of compartmentalisation. Therefore, the main aim of this thesis was:

1. To identify the expression of the negative regulators of cAMP, the PDEs in pre- and mature brown adipocytes.
2. To elucidate the expression of PDEs in different compartments of brown adipocytes.
3. To establish real-time measurements of cAMP in brown adipocytes using FRET in the context of independent β_1, β_2 and β_3-AR stimulation and to elucidate whether PDE2, PDE3 and PDE4 regulate β-ARs compartmentalisation differently in pre- and mature brown adipocytes.
4. Using FRET based biosensor Epac1-camps for real-time cAMP measurement, to identify if stimulation of adenosine receptors A_{2A} and A_{2B} receptors also form similar patterns of compartmentation as β-ARs when inhibited with PDE2, PDE3 and PDE4 in pre- and mature brown adipocytes.

2. Materials and Methods

2.1. Materials

2.1.1. Animals

The following mouse lines were used for this project.

Table 1.: List of mouse lines used.

Mouse line	Genetic background	Source
Epac1-camps	FVB/N	Viacheslav Nikolaev Lab [68]
WT	C57BL/6J	Charles river

2.1.2. Antibodies

2.1.2.1. Primary Antibodies

The following Primary Antibodies were used for Western Blot. Primary antibodies were prepared in their respective dilutions in a solution of TBST containing 5% BSA.

Table 2.: List of primary antibodies used.

Antibody	Source	Dilution	Manufacturer	Article number
Anti Calnexin	Rabbit	1:1000	Sigma	208880
Anti LaminA/C	Rabbit	1:1000	Cell Signaling	20325
Anti PDE2A	Rabbit	1:1000	Abcam	14604
Anti PDE3A	Rabbit	1:1000	Chen Yan Lab	
Anti PDE3B	Rabbit	1:1000	Emilio Hirsch Lab	
Anti PDE4A	Rabbit	1:1000	Abcam	ab14607
Anti PDE4B	Rabbit	1:1000	Abcam	ab170939
Anti PDE4D	Rabbit	1:1000	Abcam	ab171750
Anti Tubulin	Mouse	1:1000 or 1:2000	Dianova	DLN-009993
Anti VDAC	Rabbit	1:1000	Cell Signaling	48665

2.1.2.2. Secondary Antibodies

The following Secondary Antibodies used for Western Blot. Secondary antibodies were prepared in their respective dilutions in a solution of TBST containing 5% BSA.

Table 3.: List of secondary antibodies used.

Antibody	Isotype	Dilution	Manufacturer	Article number
Anti-Rabbit Dylight (H+L) IgG 800	Goat	1:15000	Cell Signalling	5151S
Anti-Mouse Dylight (H+L) IgG 680	Goat	1:15000	Cell Signalling	5470S

2.1.3. Chemicals and Reagents

The following chemicals and reagents were used for this project. All the compounds used for this project were prepared, used and stored according to the manufacturer's instructions.

Table 4.: List of chemicals and reagents used.

Chemical and Reagents	Manufacturer	Article number
β-Mercaptoethanol	Sigma-Aldrich	M6250
(-)-Isoproterenol hydrochloride	Sigma-Aldrich	I6504
2-Propanol	Carl Roth	6752.4
3-isobutyl-1-methylxanthine (IBMX)	Sigma-Aldrich	I5879
3,3',5-Triiodo-L-thyronine (T3)	Sigma-Aldrich	T6397
8-Br-2'O-Me-cAMP-AM	BioLog	B 028
Agarose Standard	Carl Roth	3810.4
Albumin Factor V	Carl Roth	8076.3
Ammoniumperoxydisulphate (APS)	Carl Roth	9592.2
Bay 60-6583	Tocris	4472
Bay 60-7550	Cayman	10011135
Bovine serum albumin (BSA)	Sigma-Aldrich	A7030
Bromophenolblue	Carl Roth	T116.1
Calcium chloride dihydrate	Carl Roth	5239.1
CGP 20712 dihydrochloride	Tocris	1024
CGS 21680 hydrochloride	Tocris	1063
Cilostamide	Cayman	14455
CL-316243	Tocris	1499
Collagenase Type 2	Worthington	LS004177
Complete, EDTA-free Protease Inhibitor Cocktail	Sigma-Aldrich	04693132001
Coomassie brilliant blue G 250	Merck	115444
Dexamethasone	Sigma-Aldrich	D4902

Dimethyl sulfoxide	Carl Roth	A994.2
Disodium ethylenediaminetetraacetate		
D-Mannitol	Sigma-Aldrich	M4125
Dulbecco's Modified Eagle's Medium (DMEM), high glucose, GlutaMAX Supplement	Gibco	61965059
DMEM, high glucose, GlutaMAX Supplement, pyruvate	Gibco	31966021
DMEM, high glucose, HEPES, no phenol red	Gibco	21063029
Ethanol (96%)	Carl Roth	P075.4
Ethanol (99.8%)	Carl Roth	9065.4
Fetal bovine serum	Sigma-Aldrich	F7524
Forskolin	Sigma-Aldrich	F6886
Free glycerol reagent	Sigma-Aldrich	F6428
Glycine	Carl Roth	3908.3
Glycerine	Carl Roth	3783.1
HEPES	Carl Roth	9105.2
Hydrochloric acid 37%	Carl Roth	4625.2
Immersol 518 F/30°C	Carl Zeiss	444970-9000-000
InnuSOLV	Analytik Jena AG	845-SB-2090100
L-(-)-Norepinephrine (+) – bitartrate salt monohydrate	Sigma-Aldrich	A9512
Magnesium chloride hexahydrate	Carl Roth	7791-18-6
Methanol (99.9%)	Carl Roth	4727.1
N,N,N',N'-Tetramethyl ethylenediamine (TEMED)	Sigma- Aldrich	T7024
Nonfat dried milk powder	PanReac AppliChem	A0830, 1000
Oil-Red O	Sigma-Aldrich	09755
Penicillin/Streptomycin	Merck Millipore	A2213
Percoll	Sigma-Aldrich	P1644
Phosphoric acid	Carl Roth	6366.1
Potassium chloride	Carl Roth	6781.1
PageRuler™Prestained Protein Ladder	Thermo Scientific	26616

PageRuler™Prestained Protein Ladder	Thermo Scientific	26619
PageRuler™Prestained Protein Ladder	NEB	P7712S
Rolipram	Tocris	0905
Rotiphorese gel 30 (37.5:1)	Carl Roth	3029.1
Sodium azide	Roth	K305.1
Sodium chloride	Carl Roth	3957.1
Sodium orthovanadate	Sigma-Aldrich	S6508
LightCycler 480 SYBER Green 1 Master Mix	Roche	04887352001
Tris	Carl Roth	AE15.2
Tris HCl	Carl Roth	9090.3
Tryphan blue stain	Gibco	15250-061
Trypsin-EDTA (0.05%), phenol red	Gibco	25300-054
Tween 20	Carl Roth	9127.2
Water	Sigma-Aldrich	W3500

2.1.4. Consumables and Kits

The following Consumables and Kits were used for this project.

Table 5.: List of Consumables and Kits used.

Description	Manufacturer	Article number
6-well plate	Sarstedt	83.3920
12-well plate	Sarstedt	83.3921
24-well plate	Sarstedt	83.3922
96-well plate	Sarstedt	83.3924.005
cAMP ELISA Kit	Enzo	ADI-901-006
Cell counting chamber slide, Countess	Invitrogen	C10283
Cell scraper, 18 cm	BD Falcon	353085
Cryo Pure Tube 1.8 mL		72.379.992
Disposable needle 0.90*70 mm	Braun	4665791
Glass plate, with 1.5 mm spacer	Bio-Rad	1653312
Glass plate, short	Bio-Rad	1653308
ibiTreat, µ-Dish$^{35mm, high}$	Ibidi	81156
Microscope cover glasses, 25 mm	Marienfeld	0110650
Microtube 1.5 mL, safe seal	Sarstedt	72.706.400

Nitrocellulose blotting membrane	GE Healthcare	10600002
ProtoScript II First Strand cDNA Synthesis Kit	NEB	E6560S
Serological pipette, 5 mL	Corning	4487
Serological pipette, 10 mL	Corning	4488
Serological pipette, 25 mL	Corning	4489
Sterile syringe filter w/0.2 µM	VWR	514-0061
Sterile syringe filter w/0.4 µM	VWR	514-0063
Tube, 15 mL, 129*17 mm, PP	Sarstedt	62.554.502
Tube, 50 mL, 114*20 mm, PP	Sarstedt	62.547.502
TC Dish 100*20 mm Standard	Sarstedt	83.3902
TC Dish 150*20mm Standard	Sarstedt	83.3903
Whatman Gel Blot Paper, GB003	GE	10426892

2.1.5. Equipment and Devices

The following Equipment and Devices were used for this project.

Table 6.: List of equipment and devices used.

Description	**Manufacturer**	**Model**
Autoclave	Faust	Varioklav 135 T
Automated cell counter	Invitrogen	Countess
Beam splitter	Photometrics	DualView-∧
Centrifuge	Beckman Coulter	Avanti JXN-26
Centrifuge	Eppendorf	5810
Centrifuge	Eppendorf	5804R
Centrifuge	Sigma	Sigma 8k, 12510-H rotor
CO_2 incubator	Thermofisher Scientific	Hera cell 150i
Electrophoresis cell	BioRad	Mini-PROTEAN Tetra Vertical Electrophoresis cell
Imaging system for western blots	Licor	Odyssey Fc
Inverted microscope	Leica	DMI 4000 B
Laser scanning confocal microscope	Carl Zeiss Microscopy GmbH, Jena, Germany	LSM 700 VRGB (445)
Light source	CoolLED	*pE*-100, 425 nm

PCR System	Applied Biosystems	7900 HT Fast Real Time PCR system
Shaker	Edmund Bühler	TH15K5-15, Control
Spectrophotometer	Thermofisher Scientific	Nanodrop 2000
SW 32 Rotor	Beckman Coulter	Optima L-100 XP ultracentrifuge
SW 55 Ti Rotor	Beckman Coulter	Optima L-100 XP ultracentrifuge
Photometer	Eppendorf	BioPhotometer D30
Plate reader	Perkin Elmer	EnSpire Multimode Plate reader
Potter	Sartorius	S
Thermocycler	Biometra	T-Personal Thermal Cycler
Thermoomixer	Eppendorf	Comfort
Water bath for cell culture	Memmert	WNB22

2.1.6. Primer Sequences

The following Primer Sequences were used for this project. They were ordered from Microsynth AG.

Table 7.: List of Primer sequences used.

Gene name	Species	Primer sequence (5'→ 3')
β_1-AR forward	Murine	CCG TCG TCT CCT TCT ACG TG
β_1-AR reverse	Murine	CTC GCA GCT GTC GAT CTT CT
β_2-AR forward	Murine	AAC GAC AGC GAC TTC TTG CT
β_2-AR reverse	Murine	GCC AGG ACG ATA ACC GAC AT
β_3-AR forward	Murine	ATC ACT CTG TCT CCA GGC TC
β_3-AR reverse	Murine	TGC CTATTG TGA GAG ATG GTC C
A_1 forward	Murine	ATC CTC ACC CAG AGC TCC AT
A_1 reverse	Murine	TGT CTT GTA CCG GGA GAG GGA
A_3 forward	Murine	TCA TGT CCT TGC TGG CCA TT
A_3 reverse	Murine	AGT GGT AAC CGT TCT ATA TCT GAC T
A_{2A} forward	Murine	GCC AGA CAA GAG GCA GGT AT
A_{2A} reverse	Murine	CAG CCG TGT ACC CAC TCA AA
A_{2B} forward	Murine	GCG TCC CGC TCA GGT ATA AA

A_{2B} reverse	Murine	CAATGCCAAAGGCAAGGACC
HPRT forward	Murine	GTC CCA GCG TCG TGA TTA GC
HPRT reverse	Murine	TCA TGA CAT CTC GAG CAA GTC TTT
PDE1A forward	Murine	CAA CAA TGG TTG CCC AGT CG
PDE1A reverse	Murine	CTG TTG AGT CCG TCA GGA GAG
PDE1B forward	Murine	AGT TGC TGA CTC GGC ATA GC
PDE1B reverse	Murine	CCC ATA GCC TGT CTC CAA GG
PDE1C forward	Murine	AAC CCT CGT GGG AAG AAC TC
PDE1C reverse	Murine	TTC CGG TGT TGG AGT GAT CC
PDE2A forward	Murine	CTA GGC GCC GTT ATC GAC AT
PDE2A reverse	Murine	ACA CAC CAG TCT GGA CTC CC
PDE3A forward	Murine	AGT AAC CAT CAA GCG AGG GC
PDE3A reverse	Murine	TGC GAA TAA GGT CTG CCA CA
PDE3B forward	Murine	AAA GCG CAG CCG GTT ACTAT
PDE3B reverse	Murine	CCA CTG CTT CAA GTC CCA GT
PDE10A forward	Murine	CTA TCG GCG GGT TCC TTA CC
PDE10A reverse	Murine	CAG ACA CGC AAT TAG CAG GC
PDE11A forward	Murine	ATT AGC CAC AGA CCT CAC GC
PDE11A reverse	Murine	AAC ACA TCT CGG TGG CTT GT
PDE4A forward	Murine	ACT CAC ACA CCT GTC GGA AA
PDE4A reverse	Murine	TGG GAT CTC CAC TTC GTG CT
PDE4B forward	Murine	TCT CAC GCT TCG GAG TCA AC
PDE4B reverse	Murine	GTG AGT ACC CAG CCA CAT TGA
PDE4C forward	Murine	GCC CAC GTG GTC TTC ACA AT
PDE4C reverse	Murine	CGG ACT GAG CGT CTA GGA GA
PDE4D forward	Murine	GGA GAT TCT CGC GGC CAT TT
PDE4D reverse	Murine	TAG GAC CGA GGA GTC GTT GT
PDE7A forward	Murine	CTC GCA GAG ACG TGG AGC TA
PDE7A reverse	Murine	GTT TCA AAT CCT GCT CGG CTC
PDE7B forward	Murine	CCA TGG GCT CAT CCA CCA TT
PDE7B reverse	Murine	TGG TAT GGG TTG TGA CCG TG
PDE8A forward	Murine	AGT ACG CAG GGT GGA CAA AG
PDE8A reverse	Murine	ATG CCA ACT GGA GCA GTT CA

2.1.7. Software

The following Software and their respective versions were used for this project.

Table 8.: List of Software used.

Software and versions	Manufacturer
Enspire Workstation 4.13.3005.1482	Perkin Elmer
Microsoft Office 360 2016	Microsoft
Prism 6	GraphPad
Image Studio Software 5.2.5	Licor
Micromanager 2.0.0 Beta3 coupled with Image J	National Institutes of Health
SDS 2.4	Applied Biosystems
RQ Manager 1.2.1	Applied Biosystems
Zen 2010	Carl Zeiss

2.2. Methods

2.2.1. Buffers and Solutions

Stated below are general buffers that were prepared for use during experiments. A description of other Buffers and Solutions are stated for the respective method they were used for.

2.2.1.1. Preparation of Phosphate buffered saline (PBS)

The pH was adjusted to 7.4 with 5M NaOH, and autoclaved at 121°C for 20 min. It was stored at RT. From 10X PBS, 1 part of 10X PBS was mixed with 9 parts of distilled water to make 1X PBS.

Table 9.: Preparation of 10X PBS, pH 7.4.

Reagent	Concentration
NaCl	137 mM
KCl	2.7 mM
Na_2HPO_4	8.1 mM
KH_2PO_4	1.5 mM

2.2.1.2. Preparation of Tris buffered saline (TBS)

The pH was adjusted to 7.6 and was autoclaved at 121°C for 20 min. It was stored at RT. From 10X TBS, 1 part of 10X TBS was mixed with 9 parts of distilled water to make 1X TBS.

Table 10.: Preparation of 10X TBS, pH 7.6.

Reagent	Concentration
Tris	198.1 mM
NaCl	1.5 M

2.2.2. Isolation, Culture, Immortalisation, and Cryopreservation of primary BAT-mesenchymal stem cells from new-born mice

This protocol was adapted from the protocol described earlier [31]. Interscapular brown adipose tissue (iBAT) pads were isolated from new-born pups of C57BL/6J (wildtype, WT) or FVB/N (transgenic, TG, containing Epac1-camps-FRET biosensor) background with a tweezer. Two lobes of the iBAT were placed in 1 mL of the Digestion buffer with collagenase-type II (Table 12) and were minced finely. This was then added to a 15 mL tube containing 2 mL of the Digestion buffer with collagenase-type II (Table 12). The contents were shaken very 10 min in a shaker at 120 RPM heated to 37°C (TH15K5-15, Control, Edmund Bühler) for 30 min till the fat pad pieces were no longer seen. The suspension was then filtered through a

100 µM nylon mesh into a fresh 15 mL tube. The suspension was kept on ice for 30 min. The middle layer formed (about 1 mL) was collected, filtered through a 30 µM nylon mesh into a 50 mL tube and centrifuged at 700 g (Centrifuge 5810, Eppendorf) for 10 min. At this stage fat pads from all the pups were combined and resuspended in BAT culture medium (Table 13). For 2 lobes of BAT from each pup, the pellet was resuspended 3 mL of BAT culture medium and seeded on 1 well of a 6 well plate. This was considered as Passage 0 (P0). The plate was incubated overnight in the incubator at 37°C, 5% CO_2 and 95% (conditions: 5% CO_2 and 95% H_2O, Hera cell 150i CO_2 incubator, Thermo Scientific). After overnight incubation, the BAT-Mesenchymal stem cells (MSCs) were immortalised with lentiviral transduction of large T-antigen containing Simian virus 40 (SV40) (200 ng in 800 µL/6well) under phosphoglycerate kinase (PKG) promotor in BAT culture medium. The next day the well was filled up to 3 mL BAT culture medium. 24 h post immortalisation, BAT culture medium was replaced by BA growth medium (BA GM) (Table 14) and the medium was changed every 2 days till the cells reached 90 % confluency. The cells from all the wells of the 6 well plate were washed with PBS (Table 9), trypsinised with 200 µL trypsin for 5 min and pooled together. After pooling, the cells were seeded onto 6 well plates. From one 6 well plate, the cells were split into 2 100*20 mm tissue culture (TC) dishes. The cells were grown up to 90% confluency and from each 100*20 mm TC dish, the cells were frozen in a cryo tube in BA GM containing 10% DMSO for cryopreservation in -150°C. These cells were considered P2, were expanded and used at P4.

2.2.2.1. Preparation of isolation buffer for BAT isolation

Digestion buffer for BAT isolation can be stored at 4°C up to 1 month. The pH was adjusted to 7.4 with 5M NaOH, and the solution was made up to the required volume with MilliQ water and filtered with a 0.2 µM filter mesh.

Table 11.: Preparation of Isolation buffer for BAT isolation.

Reagent	Concentration
NaCl	123 mM
KCl	5 mM
$CaCl_2$	1.3 mM
Glucose	5 mM
HEPES	100 mM

2.2.2.2. Preparation of digestion buffer for BAT isolation

Digestion buffer for BAT isolation with collagenase-type II and fatty acid-free BSA was prepared fresh prior to the isolation and was prewarmed at 37°C in a water bath (Memmert).

Table 12.: Preparation of digestion buffer for BAT isolation.

Reagent	Concentration
Isolation Buffer	(Table 11)
Fatty acid-free BSA	1.5%
Collagenase-Type II	2 mg/mL

2.2.2.3. Preparation of BAT culture medium

BAT culture medium can be stored at 4°C up to 1 month.

Table 13.: Preparation of BAT culture medium.

Reagent	Concentration
DMEM, high glucose, GlutaMax-I without Pyruvate	As required
FBS	10%
Penicillin/Streptomycin	1%
HEPES	10 mM
Insulin	4 nM
T3	4 nM
Sodium ascorbate	25 µg/mL

2.2.2.4. Preparation of brown adipocyte growth medium

The prepared BA GM can be stored at 4°C up to 1 month.

Table 14.: Preparation of brown adipocyte growth medium.

Reagent	Concentration
DMEM, high glucose, GlutaMax-I without Pyruvate	As required
FBS	10 %
Penicillin/Streptomycin	1 %

2.2.3. Routine cell culture of primary brown adipocytes

Cryopreserved cells were thawed in the water bath (Memmert) at 37°C for 2 min. The cells were then mixed in 4 mL BA GM and centrifuged at 1000 RPM (Centrifuge 5810, Eppendorf) for 5 min to wash out DMSO. The cell pellet was resuspended in the required volume of BA GM. BA were differentiated as described previously [88]. One million cells per 6 well plate from P4 were seeded (Day -4) in BA GM (Table 14). The same number of cells per well was maintained depended on the type of plate used. Medium change was performed every 48 h

for 11 days. BA GM was replaced by BA differentiation medium (DM) (Table 15) on Day-2 of differentiation. After Day -1, BA DM was replaced with BA induction medium (IM) (Table 16). BA IM was changed to BA DM after 48 h and 2 more times subsequently. A schematic representation of BA differentiation and medium change is represented below (Figure 8). Depending on the need of the experiments, cells were harvested on Day -2 (pre-BA) and Day 7 (mature BA) of differentiation.

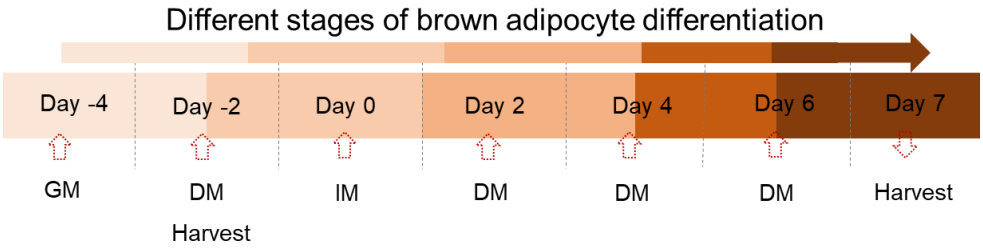

Figure 8.: Representation of the different stages of brown adipocyte differentiation. Representation of the routine cell culture protocol of brown adipocytes. The cells were harvested either on Day-2 or Day 7 of brown adipocyte differentiation depending on the experiment's requirement.

2.2.3.1. Preparation of brown adipocyte differentiation medium

BA DM can be stored in 4°C up to 1 month. Prior to use, BA DM was warmed in a water bath (Memmert) at 37°C for 30 min.

Table 15.: Preparation of brown adipocyte differentiation medium.

Reagent	Concentration
DMEM, high glucose, Glutamax-I Supplement without Pyruvate	As required
FBS	10 %
Penicillin/Streptomycin	1 %
Insulin	20 nM
T3	1 nM

2.2.3.2. Preparation of brown adipocyte induction medium

BA DM was prepared as stated above (Table 15). The reagents used for and BA IM were freshly prepared prior to use. 3-isobutyl-1-methylxanthine (IBMX) was weighed, dissolved in DMSO and was preheated to 97°C for 2 min in a thermomixer (Thermomixer Comfort, Eppendorf).

Table 16.: Preparation of brown adipocyte induction medium.

Reagent	Concentration
BA DM	As required
Dexamethasone	1 µM
IBMX	0.5 mM

2.2.4. Oil Red O Staining of brown adipocytes

Oil Red O (ORO) has been used as a measure for the quantitative analysis of differentiated adipocytes. It makes use of the principle of selectively staining triglycerides and cholesteryl oleates [89].

Differentiated brown adipocytes were first washed once with PBS. The cells were then fixed with 4% PFA for 15 min at RT. The cells were then washed twice with PBS and stained with ORO working solution (Table 18) for 4 h at RT. The cells were then washed thrice with water and the plates were dried overnight.

2.2.4.1. Preparation of Oil Red O Stock solution

The reagents were stirred overnight. The solution was stored at RT.

Table 17.: Preparation of Oil Red O Stock solution.

Reagent	Concentration
Oil red O	5 mg/mL
2-Propanol	As required

2.2.4.2. Preparation of Oil Red O working solution

ORO working solution was prepared 2 h prior to staining. The reagents from the Oil red O stock (Table 17) were mixed and was filtered.

Table 18.: Preparation of Oil Red O working solution.

Reagent	Concentration
Oil red O stock (Table 17)	3 mg/mL
Water	40 %

2.2.5. Isolation of mRNA

Cells were washed with PBS. Cells were lysed in Trizol (InnuSOLV RNA Reagent, Analytik Jena AG) (1 mL/6well). The cells were scraped with a pipette tip and transferred to a 1.5 mL tube. 200 µL of chloroform was added, the contents were mixed well and incubated at RT for

5 min. The contents were centrifuged for 10 min at 13000 RPM (Centrifuge 5415R, Eppendorf) at 4°C. The upper phase (~500 µL) was transferred to a fresh 1.5 mL tube and 500 µL of 99% 2-Propanol was added to this. The contents were mixed well and centrifuged for 10 min at 13000 RPM (Centrifuge 5415R, Eppendorf) at 4°C.The supernatant was removed, and the pellet was washed in 75% ethanol (EtOH) (Table 19), briefly vortexed and was centrifuged for 10 min at 13000 RPM (Centrifuge 5415R, Eppendorf) at 4°C. The final step was repeated 3 times and the pellet was air dried for 15-20 min. The dry pellet was dissolved in 20-30 µL of nuclease-free water and the concentration of mRNA was measured in the spectrophotometer (Nanodrop 2000, Thermofisher Scientific). mRNA prepared was stored in -80°C.

2.2.5.1. Preparation of 75% ethanol

75% EtOH was prepared.

Table 19.: Preparation of 75% ethanol.

Reagent	Concentration
98% EtOH	75%
MilliQ water	Made up to required volume

2.2.6. Synthesis of cDNA

cDNA was synthesised using Protoscript II First strand cDNA synthesis kit (E6560S, NEB) and using the program (Table 21) on a thermal cycler block (T-Personal Thermal Cycler, Biometra) as described by the manufacturer's instructions.

2.2.6.1. cDNA synthesis with Protoscript II First Stand cDNA synthesis Kit

The contents were made up to the following volume as specified. To the prepared cDNA 380 µL of nuclease free water was added to obtain a final dilution of 1:20 for qPCR reaction.

Table 20.: Reagent set-up for cDNA synthesis with Protoscript II First strand cDNA synthesis Kit.

Reagents	Amount (20 µL)
mRNA	1 µg
ProtoSctript II Reaction Mix (2X)	10 µL
ProtoScript ii Enzyme Mix (10X)	2 µL
Random Primer Mix	2 µL
Nuclease free water	6 µL

2.2.6.2. Program set-up for synthesis of cDNA

Table 21.: Program set-up for the synthesis of cDNA.

Temperature	Time
25°C	5 min
42°C	60 min
80°C	5 min

2.2.7. Real-time qPCR

A master mix of primers (1:10 dilution), cDNA (1:20 dilution) and Light Cycler 480 SYBR Green 1 Master Mix (04887352001, Roche Life Sciences) was made. Each sample was loaded in duplicates. RT-qPCR was performed in 7900 HT Fast Real Time PCR system (Applied Biosystems) with software SDS 2.4 at stages (Stage 1 95/10, Stage 2 95/15 and 60/1) repeated 40X). RQ Manager 1.2.1 was used for analysing the RT-PCR respectively.

2.2.8. Isolation and quantification of Protein lysates

200 µL/ 6 well of radio immunoprecipitation assay buffer (RIPA) lysis buffer (Table 22) was added. The cells were isolated using a cell scraper and collected in a 1.5 mL tube. The proteins were centrifuged at 13000 RPM (Centrifuge 5415R, Eppendorf) at 4°C. The supernatant containing the protein was collected. The amount of protein was determined by Bradford assay. The protein concentration was determined using a defined BSA standard curve. A mixture of 2 µl cell or tissue lysate with 98 µl 0.15 M NaCl solution was mixed with 1 ml Coomassie solution (Table 23) and incubated for 2 min. After the incubation time, the absorption was measured at 595 nm in a calorimeter (BioPhotometer D30) by Bradford assay.

2.2.8.1. Preparation of RIPA buffer

RIPA buffer was prepared and stored at 4°C. RIPA-lysis buffer fresh before use.

Table 22.: Preparation of RIPA buffer Stock solution and Lysis buffer.

Reagents	Concentration
NaCl	150 mM
Tris-HCl	50 mM
Nonidet P40	1% (v/v)
Sodium deoxycholate	0.25% (w/v)
SDS	0.1% (w/v)
RIPA- lysis buffer was freshly prepared before use	
Reagents	**Concentration**
RIPA stock	900 µL

Sodium fluoride	10 mM
Sodium orthovandate	1 mM
Complete® EDTA- free	40 L/mL

2.2.8.2. Preparation of Coomassie solution

Coomassie solution was prepared and stored at 4°C.

Table 23.: Preparation of Coomassie solution.

Reagents	Concentration
Coomasie brilliant blue G250	0.01%
EtOH	5%
Phosphoric acid	8.5%
MilliQ Water	Made up to required volume

2.2.8.3. SDS-PAGE electrophoresis and immunodetection of Proteins

Protein lysates were prepared in 5x Laemmli buffer (Table 24) containing 5% β-mercaptoenthanol and made up to the final volume with RIPA buffer (Table 22). They were heated at 97°C (Thermomixer, Eppendorf) for 10 mins.

The protein lysates were subjected to 8%, 10% or 12% (Table 25) SDS-polyacrylamide gel electrophoresis in 1X electrophoresis buffer (Table 26) at 120V for 1:30 h. The proteins were transferred with a protein cassette in the following order – (from cathode – 3 Whatmann filter papers, protein containing gel, nitrocellulose membrane, 3 Whatmann filter papers) and subjected to electrophoresis transfer in 1X transfer buffer (Table 27) at 1000 mA for 1 h. During the transfer, it was ensured that the transfer equipment was maintained on ice. After transfer, the membranes were blocked in blocking buffer (Table 28) for 1 h at room temperature (RT). The membrane was briefly washed in TBS. The membrane blotted with primary antibodies (Section 2.1.2.1) were incubated overnight at 4°C. Post primary antibody incubation, the membranes were washed 3 times for 5 min in TBST. The membranes were incubated with secondary antibodies for 1 h at RT (Section 2.1.2.2). After primary antibody incubation, the membranes were washed 3 times for 5 min in TBST. All the blots were detected on Odyssey Fc (Licor). The density of the protein bands was quantified with Image Studio software (5.2.5, Licor).

2.2.8.4. Preparation of 5X SDS Sample Loading Buffer

5X SDS Sample Loading buffer (Lämilli) was prepared and aliquoted at -20°C.

Table 24.: Preparation of 5X Lamilli buffer,

Reagents	Concentration
Tris (pH 6.8)	250 mM
SDS	10%
Glycine	50%
Bromophenol blue	0.02%
For membrane proteins, to the same composition of 5X Lamilli, urea was added	
Urea	5 M

2.2.8.5. Preparation of Gels for SDS-PAGE Electrophoresis

1.5 M Tris, 1 M Tris and 20 % APS were prepared and stored at 4°C.

Table 25.: Preparation of Resolving and Stacking Gel for SDS-PAGE electrophoresis.

Resolving Gel			
Reagents	**8% (Amount mL)**	**10% (Amount mL)**	**12% (Amount mL)**
Distilled water	4.6	4	3.3
30 % Acrylamide mix	2.7	3.3	4
1.5 M Tris (pH 8.8)	2.5	2.5	2.5
20 % APS	0.05	0.05	0.05
TEMED	0.006	0.004	0.004
Stacking Gel			
Reagents		**Amount (mL)**	
Distilled water		2.1	
30 % Acrylamide mix		0.5	
1 M Tris (pH 6.8)		0.38	
20 % APS		0.015	
TEMED		0.03	

2.2.8.6. Preparation of 10X Electrophoresis buffer

10X Electrophoresis buffer was prepared and stored at RT. It was made to 1X with distilled water.

Table 26.: Preparation of 10X Electrophoresis buffer.

Reagent	Concentration
SDS	1% (w/v)
Tris-base	250 mM
Glycine	1900 mM

2.2.8.7. Preparation of 10X Transfer buffer

10X Transfer buffer was prepared and stored at RT. It was made 1X with distilled water.

Table 27.: Preparation of 10X Transfer buffer.

Reagent	Concentration
Tris-base	250 mM
Glycine	1900 mM

2.2.8.8. Preparation of Blocking buffer

Blocking buffer was prepared fresh before use.

Table 28.: Preparation of Blocking buffer.

Reagent	Concentration
Milk powder	5%
TBS	1X

2.2.9. Lipolysis assay of mature brown adipocytes

Triglycerides are hydrolysed by lipase to glycerol and free fatty acids by which is measured by coupled enzymatic reactions [90]. The free endogenous glycerol is measured by free glycerol reagent. Adenosine-5'-triphosphate (ATP) phosphorylates glycerol to glycerol-1-phoshate (G-1-P) and adenosine-5'-diphosphate (ADP) in the presence of glycerol kinase (GK). This is then oxidised to dihydroxyacetone phosphate (DAP) and hydrogen peroxide (H_2O_2) by glycerol phosphate oxidase (GPO). H_2O_2 couples with 4-aminoantipyrine (4-AAP) and sodium N-ethyl-*N*-(3-sulfopropyl) *m*-anisidine (ESPA) producing quinoeimine dye that has an absorption at 540 nm.

Lipolysis is performed on Day 7 of BA differentiation. The cells were washed 1 time with PBS, followed by 3 washes with Lipolysis medium (Table 29). Lipolysis medium (400 µL/12 well plate, 200 µL/24 well plate) with or without the substances were added and incubated for 2 h at 37°C (Conditions: with 5% CO_2 and 95% H_2O; Hera cell 150i CO_2 incubator, Thermo Scientific). The measurement was performed in duplicates in a 96 well plate. Free glycerol reagent was prewarmed to RT, 60 µL of it was added followed by 40 µL of the lipolysis supernatant of respective treatments. For measurement of standard, 5 µL of Glycerol standard reagent, 95 µL of free glycerol reagent was added and the plate was incubated for 5 min at 37°C (Incubator, Advantage Lab). The 96 well plate was measured in the plate reader (EnSpire Multimode Plate reader, PerkinElmer) at an absorbance of 540 nm, and the increase in absorbance was directly proportional to the amount of free glycerol release in the sample.

The glycerol release was normalised to the protein content of the cells and proteins were isolated as described (Section 2.2.8) and the amount of protein was determined by Bradford assay.

2.2.9.1. Preparation of Lipolysis medium

Lipolysis medium was prepared fresh before the experiment and was prewarmed in the water bath (Memmert) at 37°C.

Table 29.: Preparation of Lipolysis medium.

Reagent	Concentration
DMEM (4.5 g/l D-glucose, -pyruvate, without phenol red)	Made up to required amount
Fatty acid-free BSA	2%

2.2.10. Fractionation of mature brown adipocytes

Fractionation was performed to isolate different sub-cellular fractions of mature brown adipocytes according to a method previously described [91]. The method was optimised and established for mature brown adipocytes isolated from new-born pups of C57BL/6J (WT) strain. Throughout the experiment it was ensured that all the buffers and glassware used were cooled on ice.

2.2.10.1. Cell culture of mature brown adipocytes

To perform fractionation a large amount of differentiated murine brown adipocytes were needed. For this, in 15 150*20 mm TC dishes 9*10^6 cells were seeded respectively, and differentiation of brown adipoytes protocol was performed as described (Section 2.2.3).

2.2.10.2. Homogenisation of mature brown adipocytes

1. The medium was removed, and the cells were first washed with PBS. 4 mL of pre-cooled $1B_{cells}$-1 buffer (Table 31) was added on each plate and the cells were scraped with a cell scraper gently ensuring the final volume of the cells collected was 25 mL.
2. Cells were centrifuged at 600 g for 5 min at 4˚C (Centrifuge 5804R, Eppendorf).
3. The Teflon Potter Elvehjem homogeniser (Sartorius Potter S) and glass vessel (30 mL) were precooled in ice for 1 hour, and the glass chamber was filled with ice and water.
4. Before homogenising, 200 µL of the **Cell homogenate** was saved.
5. The cells in 25 mL of IB_{cells}-1 transferred to the 30 mL glass vessel and were homogenised at 1500 rpm (Sartorius Potter S) by moving the Teflon pestle gently up and down 25 times.

- ✓ It was ensured that the strokes were given gently so that the integrity of the cellular organelles were not damaged and that the cell homogenate did not change colour to black while being homogenised.

6. Cells were centrifuged at 600 g for 5 min at 4˚C (Centrifuge 5804R, Eppendorf). The supernatant was collected in a fresh 50 mL tube and stored on ice.
7. To the homogenised cell lysate, 25 mL of IB_{cells}-1 buffer was added again, and steps 5 and 6. were repeated thrice until a final volume of 100 mL was obtained.
8. The pellet obtained from step 7. constituted the **Nuclei and unbroken cells** was dissolved in 500 µL of IB_{cells}-1 buffer and saved on ice.

2.2.10.3. Isolation of Cytoplasmic, Plasma membrane, Lysosomal and Endoplasmic reticulum fraction

1. 100 mL of supernatant collected in from Section 2.2.10.2 step 7 was centrifuged at 600 g for 5 min at 4˚C twice (Centrifuge 5804R, Eppendorf).
   - ✓ At both the stages of centrifugation, it was ensured that there was no pellet formed. This testifies that there would be no contamination from the nuclei in the steps to follow.
2. The supernatant was centrifuged at 7000 g for 10 min at 4˚C (Sigma 8K Centrifuge, Sigma).
3. The supernatant obtained from step 3 comprised of the cytosol containing lysosomes and microsomes and the pellet contained the mitochondrial fraction.

- **Isolation of Lysosomal and Plasma membrane fraction**

The supernatant obtained in Section 2.2.10.3 step 3 was transferred to a fresh 50 mL tube and sub-fractionation was further carried out by centrifuging at 20,000 g for 30 min at 4˚C (Avanti JXN-26, Beckman Coulter). The pellet was dissolved in 200 µL of IB_{cells}-1 buffer and comprised of the **Lysosomal and Plasma membrane** fractions.

- ✓ **Isolation of Cytoplasmic and Endoplasmic reticulum fraction**

The supernatant was added into polypropylene centrifuge tubes (1 x 3 ½ inches) and further centrifuged for 28500 RPM for 1 hr (SW 32 Rotor, Optima L-100 XP ultracentrifuge, Beckman Coulter). The pellet obtained comprised of **Endoplasmic reticulum (ER)** fraction and was saved by resuspending in 200 µL IB_{cells}-1 buffer. The supernatant comprised the **Cytosolic** fraction.

- ✓ Depending on the need of the experiment, the supernatant obtained from step X. can be stored on ice up to 1.5 h before proceeding.

2.2.10.4. Isolation of crude mitochondria, mitochondrial associated membranes and pure mitochondrial fractions

- ✓ **Isolation of crude mitochondrial fraction**

1. The pellet obtained in Section 2.2.10.3 step 3 comprised of the mitochondrial fraction. It was gently resuspended in 10 mL of ice cold IB_{cells}-2 buffer (Section 2.2.10.5.3). The mitochondrial suspension was centrifuged at 7000 g for 10 min at 4˚C (Sigma 8K centrifuge, Sigma).
    - ✓ Gentle resuspension was done with a 5 mL pipette so as not to damage the integrity of the mitochondria.
2. The supernatant was discarded, the mitochondrial pellet was again resuspended in 10 mL of ice cold IB2 buffer and was resuspended at 10,000 g for 10 min at 4˚C (Sigma 8K centrifuge, Sigma).
3. The supernatant was discarded, and the pellet of crude mitochondria was resuspended 1 mL of cold Mitochondrial resuspension buffer (MRB) (Table 32). About 50 µL of the pellet was stored and this comprised of the **Crude mitochondrial** fraction.
    - ✓ The pellet was resuspended in MRB with a cut tip of a 1 mL pipette to avoid damage to the mitochondrial integrity.
    - ✓ The pellet dissolved in MRB was gently crushed with the Teflon Potter Elvehjem homogeniser with 2 hand strokes.

- ✓ **Isolation of mitochondrial associated membranes and pure mitochondria**

1. 4 mL of Percoll medium (Table 34) was added to the polyallomer centrifuge tubes (1/2 x 2 inches). To this, 500 µL of the crude mitochondrial suspension obtained was added on top of the Percoll medium along the side of the tube. 200 µL of MRB was carefully layered on top of the crude mitochondrial fraction till the tube was full.
2. This fraction was then centrifuged at 28000 RPM for 30 min at 4˚C (SW 55 Ti Rotor, Optima L-100 XP ultracentrifuge, Beckman Coulter). The fraction obtained in this step comprised of the Mitochondrial associated membranes (MAM), as the middle layer and pure mitochondria on the bottom (Figure 9). MAM, comprises of the ER and mitochondria, serves as one of the main source of interorganelle lipid transport, amongst other functions [92,93].

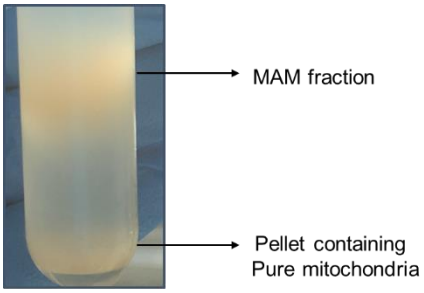

Figure 9.: Fractions of Mitochondrial associated membranes and Pure mitochondria. Representation of MAM and pure mitochondrial fraction obtained after centrifugation.

✓ **Isolation of mitochondrial associated membranes**

1. The middle layer of the MAM obtained from above was gently removed and diluted 10 times with MRB and centrifuged at 6300 g for 10 min at 4˚C (Sigma 8K centrifuge, Sigma).
    - ✓ Gentle resuspension was done with a 5 mL pipette so as not to damage the integrity of the mitochondria.
2. The MAM supernatant was added to polypropylene centrifuge tubes (1 x 3 ½ inches) and the tubes were filled up to the rim with MRB and centrifuged at 28500 RPM for 1 h at 4˚C (SW 32 Rotor, Optima L-100 XP ultracentrifuge, Beckman Coulter).
    - ✓ MAM was resuspended in MRB with a cut tip of a 1 mL pipette to avoid damage to the cellular integrity.
3. The supernatant obtained was discarded and the pellet comprising the **MAM** was dissolved in 200 µL MRB and stored on ice.
    - ✓ MAM was resuspended in MRB with a cut tip of a 1 mL pipette to avoid damage to the cellular integrity.

✓ **Isolation of pure mitochondria**

1. The pure mitochondrial pellet obtained from the MAM fraction was diluted in 10 mL MRB, gently removed and diluted 10 times with MRB and centrifuged at 6300 g for 10 min at 4˚C (Sigma 8K centrifuge, Sigma).
2. The supernatant was discarded, and the pellet was again resuspended in 20 mL MRB and was centrifuged at 6300 g for 10 min at 4˚C. The pellet obtained from this step comprised of the pure mitochondria which was dissolved and stored in 200 µL MRB.
    - ✓ Gentle resuspension was done with a 5 mL pipette so as not to damage the integrity of the mitochondria.
    - ✓ Pure mitochondria was resuspended in MRB with a cut tip of a 1 mL pipette to avoid damaging the mitochondrial integrity.

2.2.10.5. Buffers for Fractionation

All the buffers for the sub-cellular fractionation were prepared from the protocol described by [91]. 1 M Tris-HCL, 0.5 M EGTA, 100 mM EGTA adjusted to pH 7.4 were prepared and stored at RT. For buffers that needed to be cooled, MilliQ water was precooled overnight at 4˚C.

2.2.10.5.1. Preparation of Starting buffer

The pH of the Starting buffer was adjusted to pH 7.4 with KOH or HCl and made up to the required volume with precooled MilliQ water. The buffer was kept on ice throughout the procedure.

Table 30.: Preparation of Starting buffer, pH 7.4.

Reagents	Concentration
Mannitol	225 mM
Sucrose	75 mM
Tris-HCL (1 M, pH 7.4)	30 mM

2.2.10.5.2. Preparation of Isolation buffer for cells -1 (IB_{cells}- 1)

IB_{cells} -1 buffer was made by adding 150 mL starting buffer with the required concentration of EGTA or alternatively prepared as stated below.

Table 31.: Preparation of Isolation buffer for cells -1 (IBcells-1), pH 7.4.

Reagents	Concentration
EGTA (100 mM, pH 7.4)	0.01 mM
Mannitol	225 mM
Sucrose	75 mM
Tris-HCL (1M, pH 7.4)	30 mM

2.2.10.5.3. Preparation of Isolation buffer for cells -2 (IB_{cells}-2)

Isolation buffer for cells -2 (IB_{cells}-2) has the same preparation as that of the starting buffer (Table 31).

2.2.10.5.4. Preparation of Mitochondrial resuspending buffer (MRB)

The pH of the Mitochondrial resuspension buffer (MRB) was adjusted to 7.4 with KOH or HCl and was made up to the required volume with precooled MilliQ water. The buffer was kept on ice throughout the procedure.

Table 32.: Preparation of mitochondrial resuspension buffer, pH 7.4.

Reagents	Concentration
EGTA (100 mM, pH 7.4)	0.5 mM

Mannitol	250 mM
HEPES (0.5 M, pH 7.4)	5 mM

2.2.10.5.5. Preparation of Basal buffer for Percoll medium

The pH of the Basal buffer for Percoll was adjusted to 7.4 with KOH or HCl and was made up to the required volume with precooled MilliQ water. The buffer was kept on ice throughout the procedure.

Table 33.: Preparation of Basal buffer for Percoll medium, pH 7.4.

Reagents	Concentration
EGTA (100 mM, pH 7.4)	1 mM
Mannitol	225 mM
HEPES (0.5 M, pH 7.4)	25 mM

2.2.10.5.6. Preparation of Percoll medium

The mixture of Percoll medium with Basal solution for Percoll medium was prepared fresh before the step of the experiment.

Table 34.: Preparation of Percoll medium.

Reagent	Concentration
Percoll Medium	30 % (vol/vol)
Basal solution for Percoll medium	(Table 33)

2.2.11. Förster Resonance Energy Transfer Imaging with confocal microscopy

For measurement of FRET in preadipocytes, pre-BA were plated on round glass coverslides (Ø 25mm) inserted in a 6 well plate and measurements were performed post seeding on Day-2. A coverslide with adherent and confluent brown adipocytes was mounted onto a self-made microscopy cell chamber. The FRET buffer was added and removed of the chamber with a self-made perfusion system using syringes. Initial proof of principle experiments of BA transfected with Epac1-camps FRET sensor were performed using the Laser scanning confocal microscopy (LSM 700 VRGB (445)) with the settings as mentioned (Table 35).

2.2.11.1. Settings to measure FRET in pre-BA with Laser scanning confocal microscopy

The following settings were used for LSM 700 VGRB to measure FRET in pre-BA.

Table 35.: Settings used for measuring FRET in pre-BAs with Laser scanning confocal microscopy.

Parameters on the LSM 700 VRGB	Settings Used
Objective	Plan-Aprochromat 63x/1.40 Oil DIC M27
Filter	Ch1: SP 5555, Ch2: BP 505-600
Beam splitters	MBS: MBS 445/488/555/639, DBS1: 515 nm
Lasers	445 nm: 2.0 %
Scaling	(X: 0.382 µm, Y: 0.382 µm)
Pinnhole	459 µM
Time per frame	10 s

2.2.11.2. Preparation of FRET buffer

For FRET measurements, FRET buffer was used and was prepared from a protocol described previously [94]. The pH was adjusted to 7.4 with 1M NaOH. The buffer was stored at RT.

Table 36.: Preparation of FRET buffer, pH 7.4.

Reagents	Concentration
$CaCl_2$	1 mM
HEPES	10 mM
KCl	5.4 mM
$MgCl_2.6H_2O$	1 mM
NaCl	144 mM

2.2.12. Förster Resonance Energy Transfer Imaging Set-up

This protocol was adapted as described previously [95]. The principle components of the FRET imaging set-up consisted of: an inverted microscope (Leica DMI 4000 B, Leica), a light source (CoolLED, *pE*-100, 440 nm), a beam-splitter (DualView-ʌ, Photometrics) equipped with ET480/40 excitation, ET535/30 emission filters, dcrx505 dichoric mirror and a T510lpxrxt-UF2 longpass filter (Chroma Technologies) and scientific Complementary metal–oxide–semiconductor camera (sCMOS) (Photometrics Prime sCMOS) connected to a computer via the interface of an Arduino UNO I/O switch board.

Detailed explanation of the FRET equipment set-up is as follows:

1. A single-wavelength light emitting diode (LED) (CoolLED *pE*-100, 440 nm) selectively exciting the donor, enhanced cyan fluorescent protein (CFP) was connected to the epifluorescence illumination port of the microscope.
2. The excitation filter (ET480/40M) for CFP, the dichroic mirror (dcrx505), the longpass filter (T510lpxrxt-UF2) and the emission filter (ET535/30M) was first installed into the

filter cube of the beam splitter (DualView-ʌ). The filter cube was then mounted onto the bracket into the interior of the beam-splitter.

3. Communication between the computer and the light source was established by connecting the Arduino I/O (Arduino Uno) board to the LED by a BNC cable and two single Raspberry Pi wires connected into the pins GND (0) and 8 of the board. The board was then connected to the USB-port of the computer.
4. The beam-splitter was connected to the inverted microscope via the C-mount of the inverted microscope. The sCMOS camera was connected on the output view of the beam-splitter. The alignment was made such that the top of the camera was in parallel to the beam-splitter.

To enable the viewing of the output signal on the computer the following steps were followed:

Micro-Manager version 2.0 Beta was installed. The Arduino board was connected to the USB port of the computer. To program the Ardunio to work with the Micro-Manager, first the Arduino software was installed and the source code supporting Micro-Manager was downloaded and copied into the Arduino sketch window. The hardware was configured as follows: Micro-Manger → Tools → Hardware Configuration Wizard → Camera, Ardunio board with components (Ardunio-Switch, Arduino-Hub and Arduino-Shutter devices) were added. To enable the opening of the shutter, the following options were chosen: Tools → Devise Property Browser. Arduino Switch State →1 and the Auto-shutter state was enabled; File → Save System State was installed. The final FRET set-up is represented below (Figure 10).

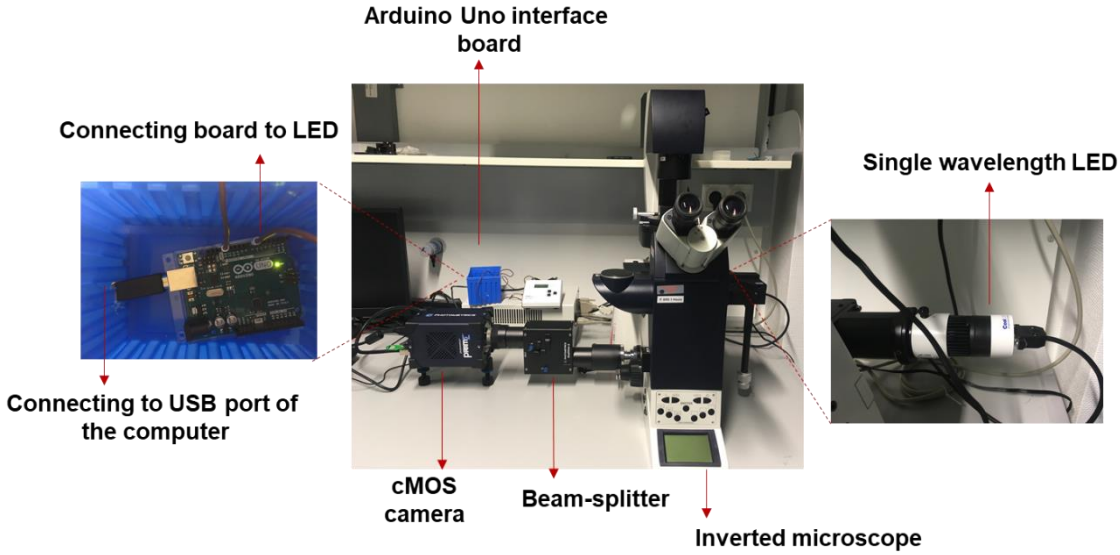

Figure 10.: FRET imaging set-up. The principle components of the FRET imaging set-up consisting of: an inverted microscope (Leica DMI 4000 B, Leica), a single wavelength LED as a light source (CoolLED, *pE*-100, 440 nm), a beam-splitter (DualView-ʌ, Photometrics) and sCMOS camera (Photometrics Prime sCMOS) connected to a computer through a USB port via the interface of an Arduino UNO I/O switch board.

2.2.13. Parameters for FRET measurements in pre- and mature brown adipocytes

MSCs and pre-BA were isolated from new born TG pups ubiquitously expressing Epac1-camps FRET biosensor as described (Section 2.2.2). For the measurement of FRET in pre-BA, BA were plated on round glass coverslides (Ø 25mm) inserted in a 6 well plate and measurements were performed post seeding on Day-2 of differentiation. A coverslide with adherent and confluent BAs was mounted onto a self-made microscopy cell chamber. For measurements in mature BAs (Day 7); MSCs and pre-BA were seeded on single wells of ibidi dishes (ibiTreat, µ-Dish$^{35mm, high}$) and were differentiated (Figure 10). FRET experiments were performed by using the FRET set-up with an oil immersion objective with a 40x magnification.

The settings used for these measurements on Micro-Manager 2.0 Beta software were: Exposure time: 100 ms; LED intensity: 75%, Binning: 1*1, Preset: State 1. Images of the CFP and YFP emission channels were acquired every 10 ms with an exposure time of 100 ms. Prior to starting the experiments, a sharp image of the BA was adjusted with the microscope and a region of interest (ROI) covering both the images together from top to bottom; left and right from the channels was selected.

For FRET measurements in both the stages of differentiation, the medium was removed and washed with FRET buffer prior to the experiment. The pharmacological compounds of interest were diluted in FRET buffer and were made in increasing concentrations considering the number of times the sample was diluted. The concentrations of the compounds used were maintained constant post dilution. 400 µL or 1 mL of the desired compound solution was pipetted gently into the measuring chamber and onto the ibidi slides respectively. It was assured that the FRET ratio reached a stable baseline before adding the compounds.

2.2.14. Correction of spectral bleed through factor for calculation of FRET measurements

Spectral bleed through (SBT) occurs in the region of maximum emission of the acceptor wherein the emission spectrum of the acceptor and donor channel overlap. This causes the fluorescence of the donor to be detected in the channel of the acceptor [96] and therefore, must be corrected by determined by calculating the SBT factor ‘b’. However, while using CFP/YFP as a FRET pair, there is no acceptor SBT making it less prone to artefacts [97].

The value of ‘b’ was determined by transfecting HEK293a cells with a plasmid encoding the donor (CFP) fluorophore. HEK293a cells were seeded onto a round glass coverslide (Ø 25mm) inserted in a 6 well plate.

The intensity of the LED light source was set to 75% and exposure time was set to either 10 ms or 5 ms depending on the brightness of the image. A single frame measurement was

performed for HEK293a cells as mentioned earlier (Section 2.2.12), the image of the YFP and CFP emission channels recorded were split into separate channels. The FRET ratio was calculated for the ROI determined for an individual HEK293a cell transfected with the CFP (donor) plasmid as:

$$\text{FRET ratio} = \frac{Average\ of\ YFP\ intensity}{Average\ of\ CFP\ intensity}$$

Individual YFP and CFP intensities were obtained for every measurement. An average of the individual YFP intensities (containing the spectral bleed through from the CFP channel) was calculated for HEK293a cells. For the current FRET-set up, the value of the spectral bleed through factor 'b' amounted to 0.5.

Therefore, in both the measurements of pre- and mature BA, the spectral bleed through factor 'b' was corrected from the obtained FRET ratios obtained from every frame. The corrected FRET ratio was calculated as follows:

$$\text{FRET ratio corrected} = \frac{YFP}{CFP} - b = \text{FRET ratio} - b$$

2.2.15. Calculation of FRET values to plot for Concentration-response curves

The calculations were performed as follows to obtain the normalised FRET ratios to calculate R_0 and R_{max} to plot Concentration-response curve:

1. Individual YFP and CFP signal intensities was quantified the from MicroManager 2.0 plugin from which the FRET ratio (YFP/CFP) was calculated.
2. From the FRET ratio, the spectral bleedthrough was corrected as mentioned (Section 2.2.14) to obtain corrected FRET ratio (FRET $ratio_{corr}$).
3. Before the addition of any compound the average of FRET $ratio_{corr}$ of 5 frames was calculated and this value obtained was considered as baseline (R_0).
4. All the values of FRET $ratio_{corr}$ were divided by R_0 to obtain the normalized FRET ratio (FRET $ratio_{norm}$).
5. Post the addition of any stimulator of cAMP response (here as e.g. β-AR Agonist (β-AR Ago)), the cAMP response (Figure 11, red arrow) was calculated as average of 5 frames of the normalized FRET $ratio_{norm}$.
6. Cells were stimulated with IBMX (100 µM) + Fsk (10 µM) to achieve a maximal saturation of the Epac1-camps FRET sensor. The average of FRET $ratio_{norm}$ corresponding to 5 frames before the measurement ended was taken. This value corresponded to R_{max} (Figure 11).
7. The value of β-AR Ago response and R_{max} were subtracted from 1, respectively.

8. cAMP produced by β-AR Agonist (β-AR Ago) stimulation was calculated in relation to the maximum FRET response R_{max} by dividing β-AR Ago response/ R_{max} and multiplied by 100 to obtain values in terms of percentage (%) (Figure 11).
9. For the concentration-response curves, for every concentration of compound used, the % change of cAMP FRET response in relation to R_{max} was calculated vs compound concentration.

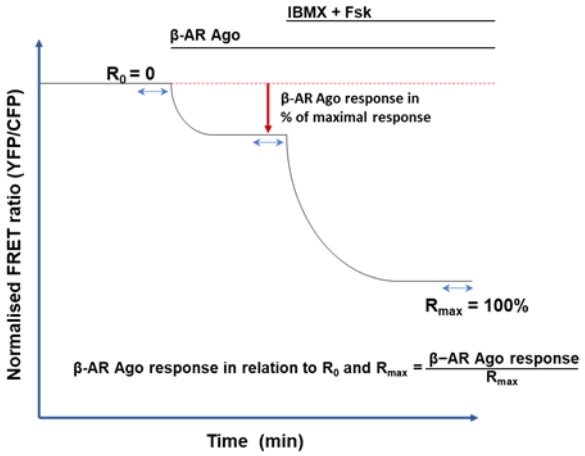

Figure 11.: A schematic plot of normalized FRET ratio vs Time representing the calculation of concentration-response curve in relation to R_0 and R_{max}. Step wise depiction of the calculation of concentration-response curves in relation to R_0 and R_{max} with β-AR Ago responses as a stimulator of cAMP as an example followed by the addition of IBMX and Fsk to attain the maximum stimulation of the cytosolic Epac1-camps FRET sensor.

2.2.16. Calculation for the conversion of the FRET ratio into a bar graph

The quantification of FRET experiments to depict PDE inhibition as percentage in relation to the IBMX response was performed as follows:

1. The normalized FRET ratio (FRET $ratio_{norm}$) was calculated as mentioned earlier (Section 2.2.15).
2. cAMP produced by the addition of an agonist, e.g. β-AR Ago stimulation was calculated when a stable baseline was achieved by taking the average of FRET $ratio_{norm}$ corresponding to 5 frames. This value corresponded to β-AR Ago response (Figure 12). Similarly, after the addition of the PDE inhibitor, the average of FRET $ratio_{norm}$ corresponding to 5 frames was calculated on reaching a stable baseline (Figure 12).
3. To obtain the maximal response of the Epac1-camps FRET sensor, IBMX (100 µM) was added on following the addition of PDE inhibitor (Figure 12). The average of FRET $ratio_{norm}$ corresponding to 5 frames upon reaching stable baseline was calculated. This value corresponded to R_{max}.

4. The value of β-AR Ago response, PDE inhibition and R_{max} were subtracted from 1 respectively.
5. To calculate the change in FRET, corresponding to regulation of PDE inhibition upon respective β-AR initiated cAMP production, the value of PDE inhibition obtained was subtracted from the value of β-AR Ago response and divided by value of R_{max}. This value was subtracted from β-AR Ago response (Figure 12). The fraction was multiplied by 100 to obtain values in terms of percentage (%). These change in FRET values were plotted as bar graphs. A schematic representation of the calculation is shown below.

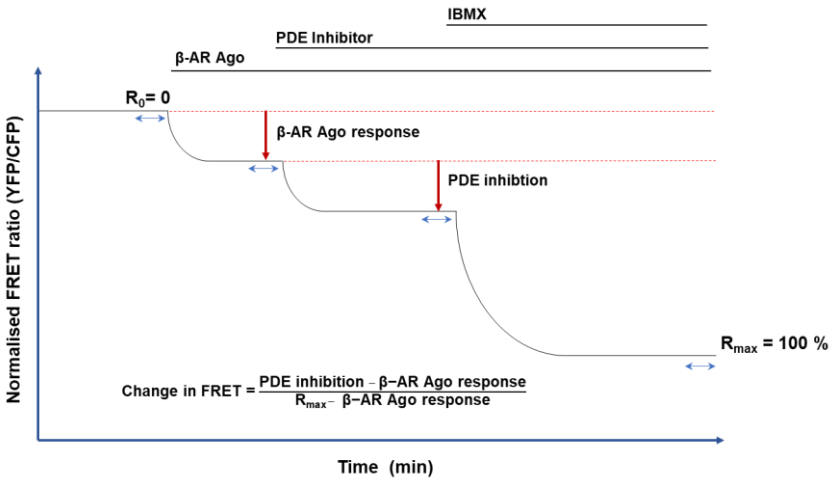

Figure 12.: A schematic plot of normalized FRET ratio vs Time representing how the changes in FRET are converted into bar graphs. Stepwise depiction on how to calculate the % of PDE inhibition during β-AR initiated cAMP production as an example in relation to the maximal PDE inhibition by IBMX using the cytosolic Epac1-camps FRET biosensor.

2.2.17. cAMP ELISA of pre- and mature brown adipocytes

cAMP ELISA was performed in pre- and mature brown adipocytes using Direct cAMP ELISA Kit (Cat.No.ADI-901-006, Enzo) and the manufacturer's instructions were followed. cAMP was measured using a plate reader (EnSpire Multimode Plate reader, PerkinElmer) at an absorbance of 405 nm with Enspire Workstation (software version 4.13.3005.1482). Protein was isolated as described (Section 2.2.8) and the amount of protein was determined by Bradford assay. The cAMP concentration was normalised to the protein content of the cells.

3. Results

3.1. Expression of PDEs in pre- (Day -2) and mature (Day 7) brown adipocytes

To study the regulation of phosphodiesterases (PDEs) on 3', 5'- cyclic adenosine monophosphate (cAMP) compartmentalisation at different stages of brown adipocyte (BA) differentiation *in vitro*, expression profile of cAMP and dual-specific PDEs was analysed in murine pre- (Day -2) and mature (Day 7) BA expressing the transgenic Epac1-camps FRET biosensor by qPCR and immunoblot analysis.

For detecting the mRNA expression of PDEs in BA, primers specific to each PDE and its respective isoforms were designed using Ensembl Genome Browser. The specific designing of primers for each isoform of PDEs was essential due to the occurrence of different alternative transcriptional start sites and alternative splicing of mRNA precursor molecules. This leads to the transcription of multiple mRNA products and subsequent translation into different proteins from these PDE genes [38]. For this project, primers specific to the cAMP specific PDEs and their respective isoforms namely: PDE4 (PDE4A, PDE4B, PDE4C, PDE4D), PDE7 (PDE7A, PDE7B), PDE8 (PDE8A, PDE8B) and the dual-specific PDEs and their respective isoforms namely: PDE2 (PDE2A), PDE3 (PDE3A, PDE3B), PDE10 (PDE10A) and PDE11 (PDE11A) were designed, and the mRNA expression was studied by qPCR analysis. qPCR analysis of the cAMP specific PDEs showed that PDE4A, and PDE4B were downregulated in mature BA, although the downregulation was not significant. PDE4D showed similar patterns of expression in both pre- and mature BA. The mRNA expression of PDE4A, PDE4B and PDE4D were complemented by immunoblots wherein similar expression patterns were observed (Figure 13 A, C, D, E). Upon studying the expression patterns of dual-specific PDEs, PDE3A and PDE3B were expressed in pre-BA, and were upregulated on mRNA and protein level in mature BA. PDE2A was expressed in pre- and mature brown adipocytes both in transcript and protein level respectively (Figure 13 B, F, G, H). Amongst the other cAMP-specific PDEs, the transcript levels of PDE7 and its isoforms (PDE7A and PDE7B) and PDE8 and its isoforms (PDE8A and PDE8B) were detected, while the PDE4 isoform, PDE4C was not expressed in both Day -2 and Day 7 stages of BA differentiation (Figure 13 A). With respect to the other dual-specific PDEs, namely: PDE1A, PDE2A, PDE3A, PDE3B, and PDE10A were expressed, whereas PDE1B and PDE11A were not detectable in pre- and mature BA (Figure 13 B).

After having studied the expression pattern of the aforementioned PDEs on mRNA levels in pre- and mature BA, for this project, the PDEs of interest were cAMP-specific PDE4, and the dual-specific PDEs PDE2 and PDE3 with their respective isoforms. The qPCR analysis for the

expression of these PDEs was complemented by performing immunoblot analysis and band sizes of these PDEs were referred and confirmed from UniProt database.

The expression of the PDEs - PDE4, PDE3 and PDE2 and their isoforms were therefore detected in different adipose tissue depots, namely: interscapular brown adipose tissue (iBAT), inguinal white adipose tissue (iWAT) and gonadal white adipose tissue (gWAT) by immunoblotting. Heart tissue was used as the positive control to compare the band size of the PDEs with the different adipose tissue depots as these PDEs are also known to be highly expressed in the heart [38] (Figure 13 C-H). The expression of PDE4A protein was mainly found in iBAT whereas the protein expression of PDE4B, PDE4D, PDE2A, PDE3A and PDE3B was detected in the iBAT, iWAT and gWAT (Figure 13 F-H). These results have been published by our working group and Figure 13 A-H corresponds to Supplementary 2 A-H in the publication [98].

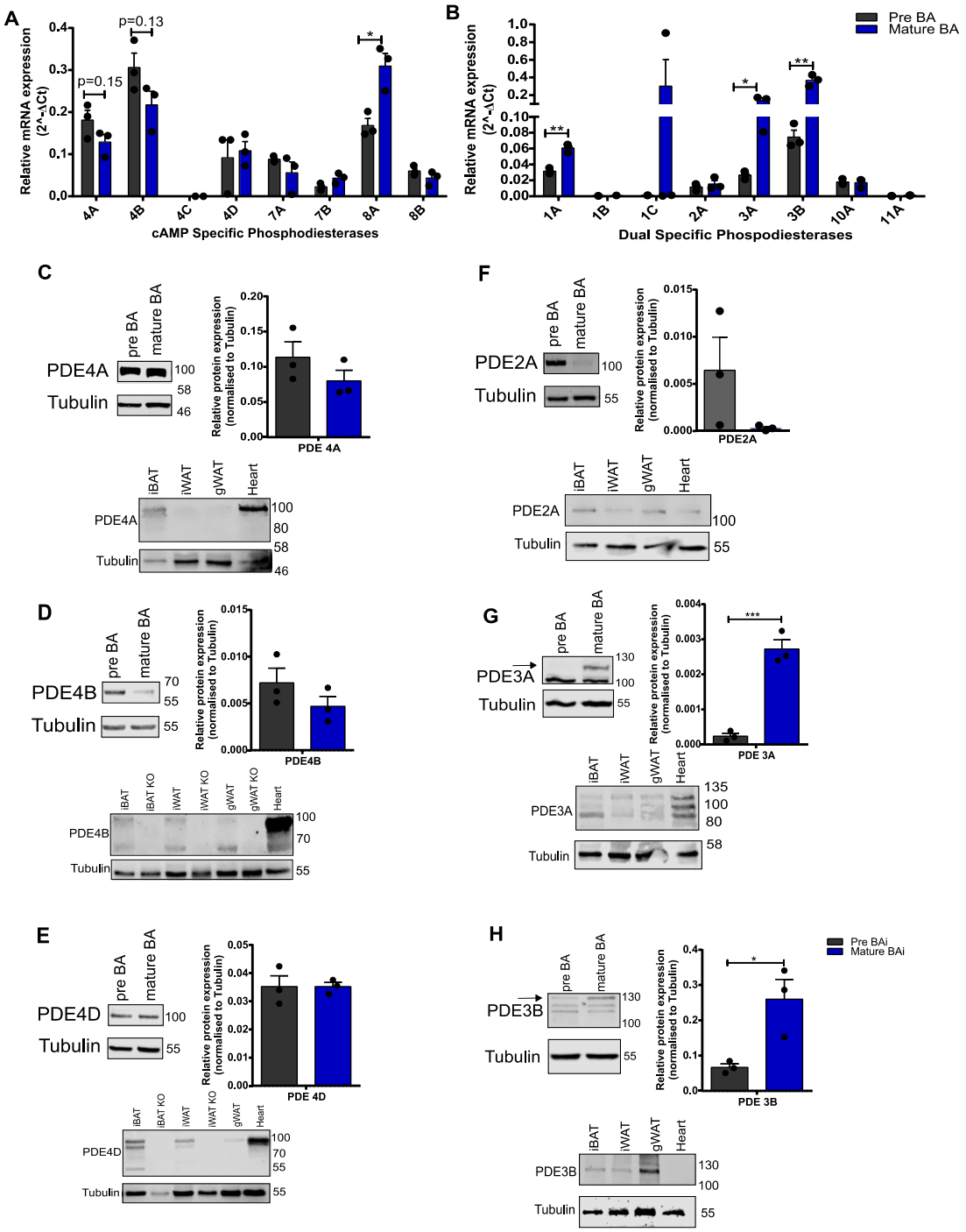

Figure 13.: Expression profile of cAMP and dual-specific phosphodiesterases in murine brown adipocytes by qPCR and immunoblot analysis. The relative mRNA expression of **(A)** cAMP-specific and **(B)** Dual-specific PDEs in murine pre- (Day-2) and mature (Day 7) BA. n=3. Means are represented as ±S.E.M in the bar graphs and are expressed relative to the mRNA of HPRT. Representative immunoblots showing the expression of PDEs **(C)** PDE4A **(D)** PDE4B **(E)** PDE4D **(F)** PDE2A **(G)** PDE3A **(H)** PDE 3B. n=3. The bar graphs represent means as ±S.E.M from protein lysates of pre-, mature BA, iBAT, iWAT, gWAT and heart. 50 µg of protein for pre-and mature BAs, different adipose tissue depots and heart was loaded. Two-tailed unpaired t-test was employed and the significant differences correspond to *-p<0.05, ***- p<0.005. This figure corresponds to Supplementary Figure 2 published by our group in Kannabiran et al., 2020 [98].

3.2. Subcellular fractionation of brown adipocytes

To study PDE-regulated cAMP compartmentalisation in BA, initially a protocol [91] was optimised to study the subcellular localisation pattern of different organelles in BA. Following this, the subcellular localisation pattern of PDEs were studied in different cellular compartments of BA.

3.2.1. Optimisation of a protocol for subcellular fractionation of brown adipocytes

The first step essential for this work was to optimise a protocol described by [91] for the subcellular fractionation of compartments of BA. The pure fractions of endoplasmic reticulum (ER), cytosol, nucleus, crude mitochondria, pure mitochondria and Mitochondrial associated membranes (MAM). They were validated by their selective and organelle specific markers namely: Calnexin, Tubulin, Lamin A/C and Voltage-dependent Anion channel (VDAC) respectively by immunoblot analysis. The important parameters to be considered and optimised were:

- ✓ The number of strokes applied to open the cells and at the same maintaining the integrity of the organelles without damaging them. If the number of strokes exceeded 25 times followed by the procedure described earlier [91], a contamination of cytosol (Tubulin) was found in all the compartments (Figure 14 A).
- ✓ The number of times the cells can be pelleted and subjected to lysis during the homogenisation process to break open the cells. This would enable obtaining pure isolations of cytosol, ER, MAM and pure mitochondria. When the total number of cells were homogenised by 25 strokes in 25 mL IB_{cells}-1 buffer followed by centrifugation, and the same procedure was repeated once again until a working volume of 50 mL was achieved. VDAC was detected in the plasma membrane (PM) fraction and was not detected in the MAM fraction (Figure 14 B). When the procedure was repeated 2 more times by homogenising the pellet, and the last 50 mL volume of supernatant was subjected to the whole procedure of fractionation, VDAC was detected in the pure mitochondrial fraction (Figure 14 C).

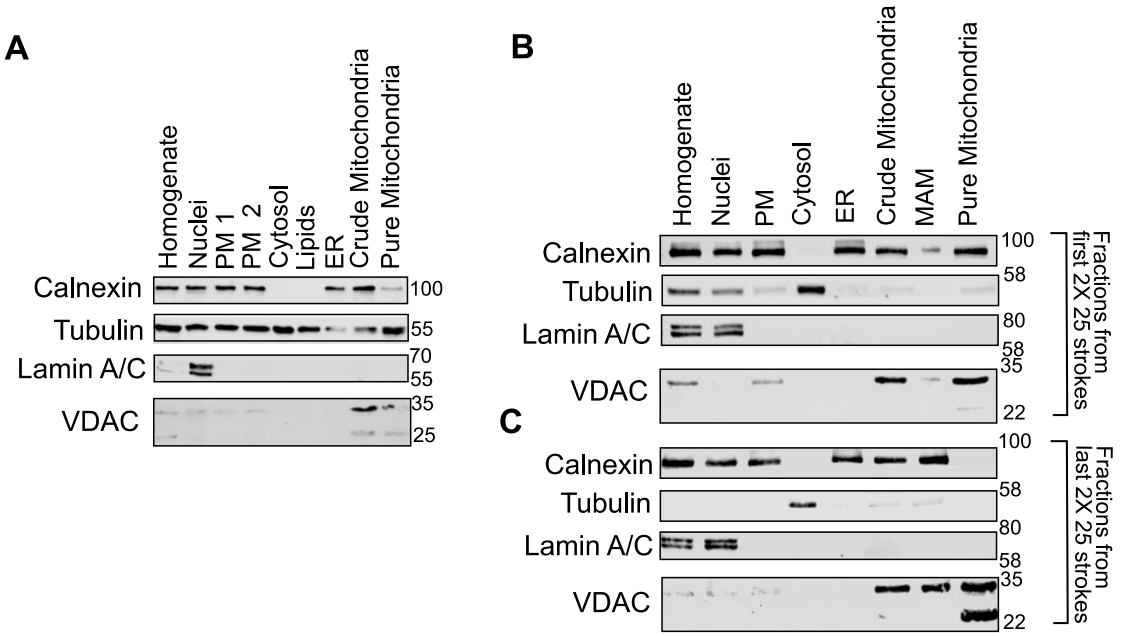

Figure 14.: Optimisation of steps for the subcellular fractionation of mature brown adipocytes. Representative immunoblot of subcellular fractions of mature BA described in Step (1) **(A)** and Step (2) **(B)** first 2 times of 25 strokes with 50 mL working volume of supernatant. **(C)** The same pellet homogenised further 2 times with 25 strokes up to a final volume of 50 mL of supernatant. 8 µg of protein was loaded.

Taking these parameters into account, it was concluded that the cells had to be diluted in 25 mL IB_{cells}-1 buffer for the first time, homogenised with 25 strokes to break open the cells, followed by centrifugation, and the supernatant had to be collected. This step had to be repeated 4 times till the final volume of the supernatant was 100 mL. The final optimised protocol for subcellular fractionation of mature BA is described (Section 2.2.10) and a schematic diagram of the steps followed is illustrated below (Figure 15 A). The immunoblot (Figure 15 B) revealed subcellular fractions obtained from the optimised protocol were pure as validated by the respective organelle specific markers.

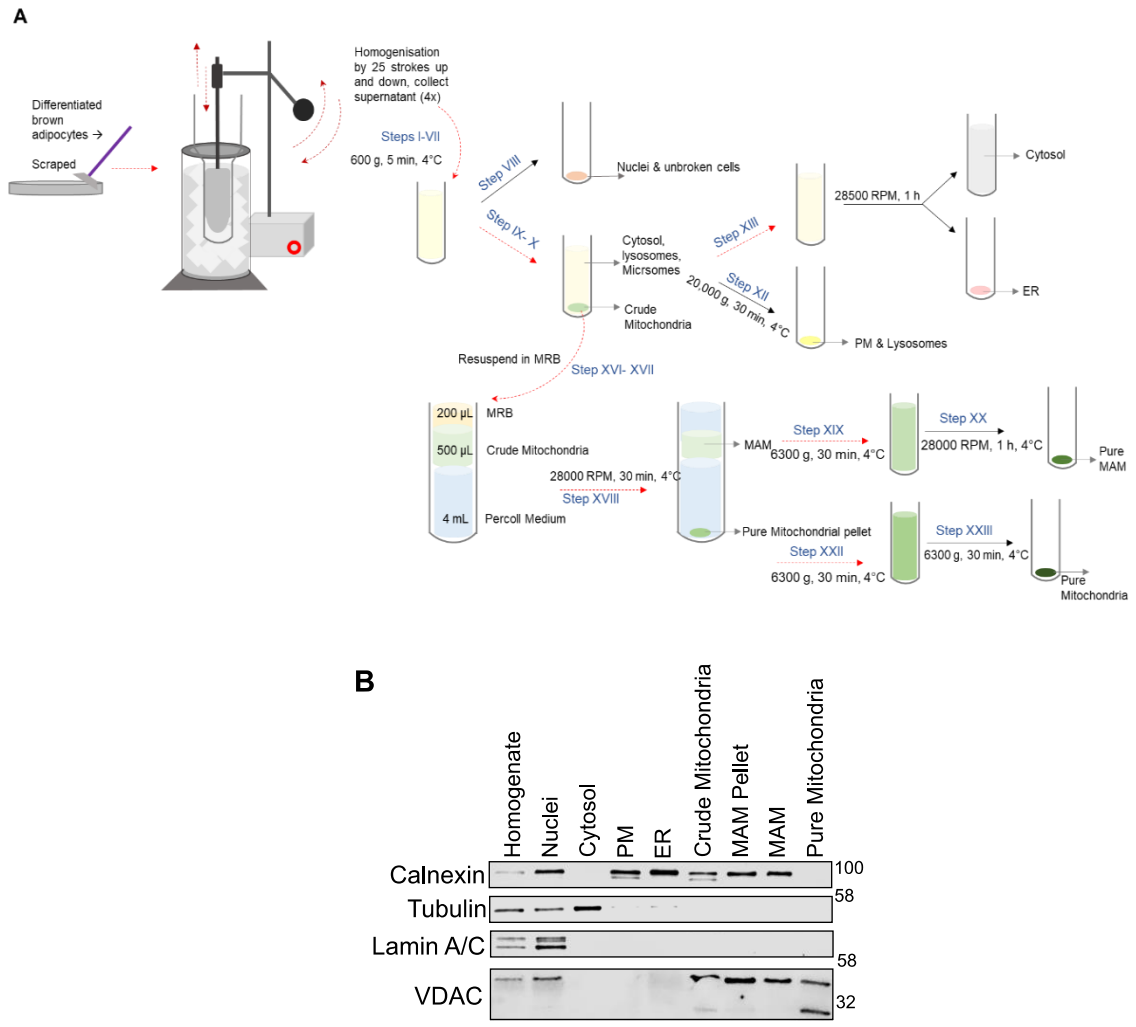

Figure 15.: Optimised steps for the subcellular fractionation of brown adipocytes. (A) Schematic illustration of the optimised protocol for the subcellular fractionation of mature BA adapted from a protocol described earlier by Wieckowski et al., 2009 [78]. **(B)** Representative immunoblot showing the validation of various subcellular compartments. The markers used were: Calnexin for Endoplasmic reticulum ER), Tubulin for Cytosol, Lamin A/C for nucleus, Voltage-dependent anion channel (VDAC) for mitochondria and mitochondrial associated membrane (MAM). 8 µg of protein was loaded.

3.3. Localisation of PDEs in different subcellular compartments of brown adipocytes

PDEs are known for their spatial and temporal attribution due to their various localisation patterns within the cells to control the intracellular concentrations of second messengers cAMP and cGMP causing intercellular compartmentalisation [38]. Therefore, by using the lysates of the different isolated subcellular compartments by fractionation of mature BA as described above, immunoblots were performed with the aim to detect the localisation of the PDEs of interest in different organelles of the BA. Immunoblot analyses of PDE3A, PDE3B, PDE4B, PDE4B, PDE4A (Figure 16 A) and PDE2A (Figure 16 B) revealed their presence

mainly in the cytosolic fraction, indicating their potential functional role majorly in the cytosol. Interestingly, the isoform of PDE3, PDE3A was found to be localised in the ER and the isoform PDE3B was detected in both ER and cytosol (Figure 16 A). This result was an initial indication of different PDE isoforms being expressed or localised in different organelles of BA and that these PDEs could regulate different pools of cAMP indicating differences in cAMP compartmentation. These results have been published. Figure 16 corresponds to Supplementary Figure 3 in the publication [98].

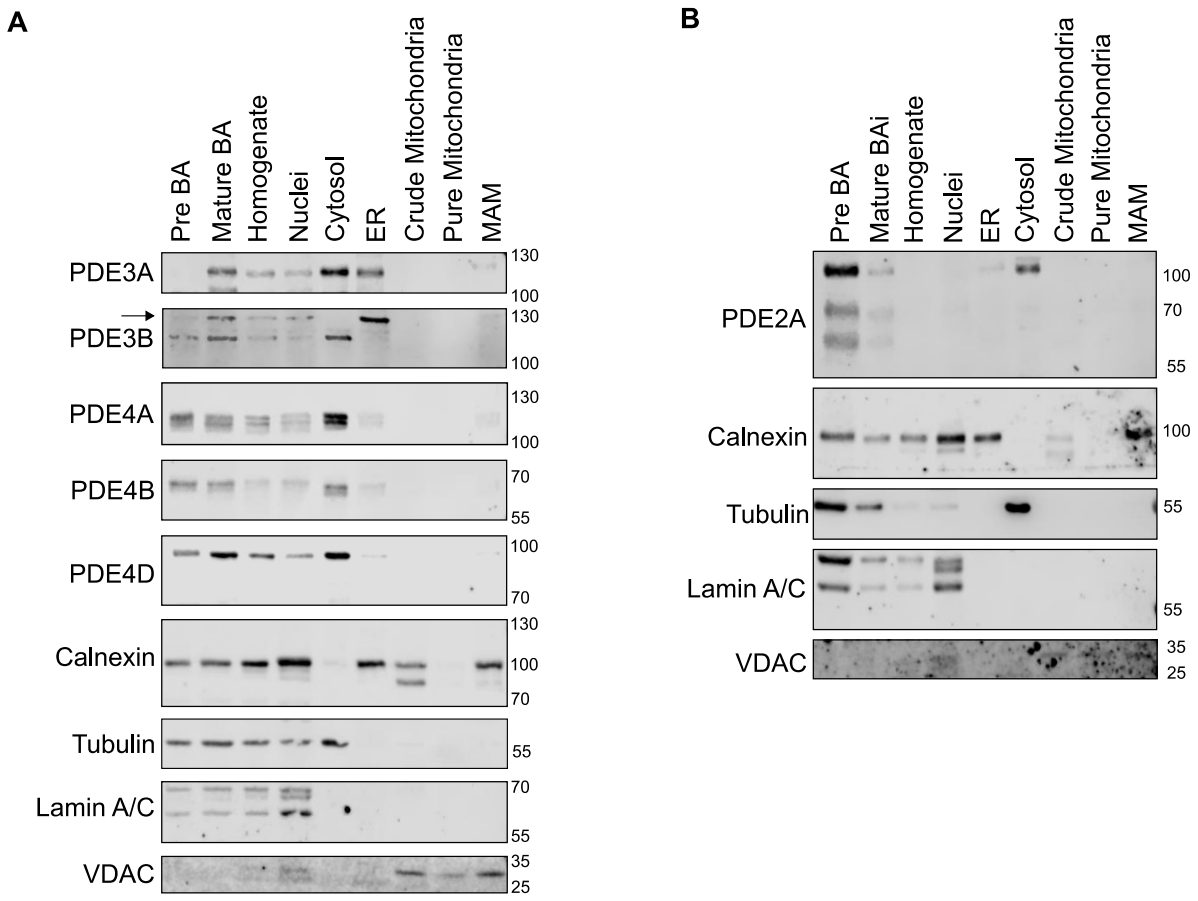

Figure 16.: Protein expression profile of cAMP and dual-specific phosphodiesterases in different subcellular fractions prepared by subcellular fractionation of mature brown adipocytes. Representative Immunoblots showing the expression of PDEs in fractions from lysates obtained from one representative procedure of mature brown adipocyte subcellular fractionation. **(A)** PDE3A, PDE3B, PDE4B, PDE4D and PDE4A **(B)** PDE2A with markers for different cellular fractions namely: calnexin (ER), Tubulin (cytosol), Lamin A/C (Nuclei), VDAC (crude and pure mitochondria, MAM). The immunoblots demonstrate the quality of the fractionation. 8 µg of protein from each subcellular fraction was loaded. Total cell lysates of murine pre- and mature BA are also depicted wherein 18 µg of protein lysate was loaded. This figure corresponds to Supplementary Figure 3 published by our group in Kannabiran et al., 2020 [98].

3.4. Real-time dynamics of cAMP in brown adipocytes measured by FRET

For this study, Förster resonance Energy transfer (FRET) was used as the technique to study the local changes in cAMP in response to any molecule that causes its production or degradation in pre-and mature BA. A cytosolic version (Epac1-camps) of FRET sensor was used as most of the PDEs of interest were found to be localised majorly in the cytosol (Figure 16). Preadipocytes were isolated from iBAT of new-born transgenic (TG) mice that ubiquitously express the cytosolic cAMP sensor, Epac1-camps. The global cytosolic sensor consists of a fusion protein comprised of yellow florescent protein (YFP), followed by the cAMP binding domain of Epac1 and cyan fluorescent protein (CFP) under the control of cytomegalovirus (CMV)/hybrid chicken β-actin (CAG) promoter [68]. A change of intramolecular FRET between CFP and YFP upon binding of cAMP enables the detection and analysis of changes in intracellular cAMP concentrations by the sensor. The first step was to determine the optimal imaging system to be used for measuring FRET in BA.

3.4.1. Measurement of cAMP dynamics in preadipocytes by confocal microscopy

The initial aim was to determine the responsiveness of the isolated and cultured BA expressing Epac1-camp to any stimulator of cAMP production in BA with an optimal imaging system. Experiments were first performed in a confocal microscope (LSM 700) with settings as described (Section 2.2.11.1). Epac1-camps expressing preadipocytes were measured in Day-2 of differentiation. The complete scanned area or the field of view was marked as the region of interest (ROI). HBSS was used as a buffer for these experiments and hence the compounds were dissolved in the same. DMSO was the solvent used for the two stimulators of cAMP production namely: 8-Br-2'-O-Me-cAMP-AM, a cell permeable analogue of cAMP and forskolin (Fsk), an activator of adenylyl cyclases (AC). The compounds were added after the FRET ratio reached a stable baseline (Figure 17). The cells were stimulated with 8-Br-2'-O-Me-cAMP-AM (20 µM) and Fsk (10 µM) showed an immediate change in the FRET ratio indicating the occurrence of FRET due to cAMP production (Figure 17). These experiments confirmed the *bona fide* functioning of the cytosolic Epac1-camps FRET sensor in BA.

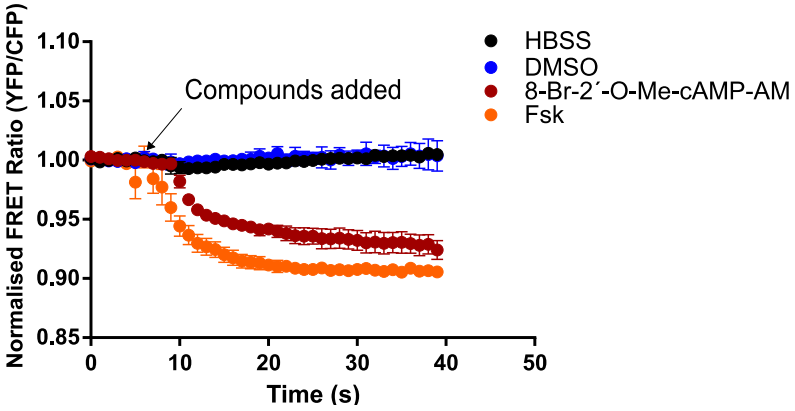

Figure 17.: Real-time cAMP dynamics in pre- and mature murine transgenic brown adipocytes expressing Epac1-camps FRET biosensor measured by laser scanning confocal microscopy. The ratio of YFP/CFP is represented as FRET traces of pre-BA expressing Epac1-camps FRET biosensor stimulated with HBSS, DMSO, 8-Br-2'-O-Me-cAMP-AM (20 µM), Fsk (10 µM) in different experiments respectively. A decrease in ratio of YFP/CFP is representative of an increase of intracellular cAMP levels. n=3-5. All the data are represented as ± S.E.M.

A self-made perfusion system was made in order to facilitate the addition and removal of compounds for enabling measurements in the laser scanning confocal microscope. The sensitivity of the focal planes to movements made measurements difficult when the compounds were added to and removed from the cells. Therefore, the study opted for a more stable self-built and established FRET-set up for FRET measurements.

3.4.2. Measurement of cAMP dynamics in brown adipocytes by a self-built FRET imaging set-up

The self-built FRET imaging system was set up as mentioned (Section 2.2.12) and FRET measurements mentioned from here on performed with the same set-up. The working principle of the FRET set-up is as follows: Epac1-camps expressing BA are excited at 440 nM, which corresponds to the excitation wavelength of the CFP (donor channel) with a light source (CoolLED, pE 100). The light emitted from the sample enters the aperture of the beam splitter (Dual-view Λ, Photometrics) which upon falling on the dichroic mirror splits the image into two. The light of the excited image (CFP, donor channel) is directly reflected by the mirror to the sCMOS sensor as this corresponds to the shorter wavelength (480 nm). The light from the emission filter (YFP, acceptor channel) is first reflected via two mirrors and then the transmitted image (YFP, acceptor channel); corresponding to the longer wavelength (535 nm) is sensed by the sCMOS sensor (Figure 18 A). The image is split into two as an output in the computer, where the left image depicts the output of CFP emission after Epac1-camps expresing BAs were excited at a 440 nM and the right image depicts the output of YFP emission as a result of energy transfer as observed for pre- BAs on Day -2 (Figure 18 B) and lipid-laden mature BA on Day 7 (Figure 18 D) of differentiation respectively. The signal

intensities depicting FRET ratio were calculated by taking the whole area of confluent cells from YFP and CFP channels as the ROI.

A decrease in FRET was observed in response to cAMP production and was confirmed by a change in signal intensities of individual YFP and CFP channels in pre- (Figure 18 C) and mature (Figure 18 E) BA when either of them was subjected to an initial concentration of β-AR receptor agonist Isoproterenol (ISO, 100 nM) followed an unselective global PDE inhibitor 3-isobutyl-1-methylxanthin (IBMX, 100 µM) and Forskolin (Fsk, 10 µM) eliciting a maximal cAMP response. The differences in the intensity of the channels between pre- (Figure 18 C) and mature BA (Figure 18 E) were observed. This was an indication of different fluorescent properties and photobleaching characteristics of the two fluorophores in the Epac1-camps expressing pre-and mature BA. A part of these results has been published and the Figure 18 D-F corresponds to Figure 1 A-D in the publication [98].

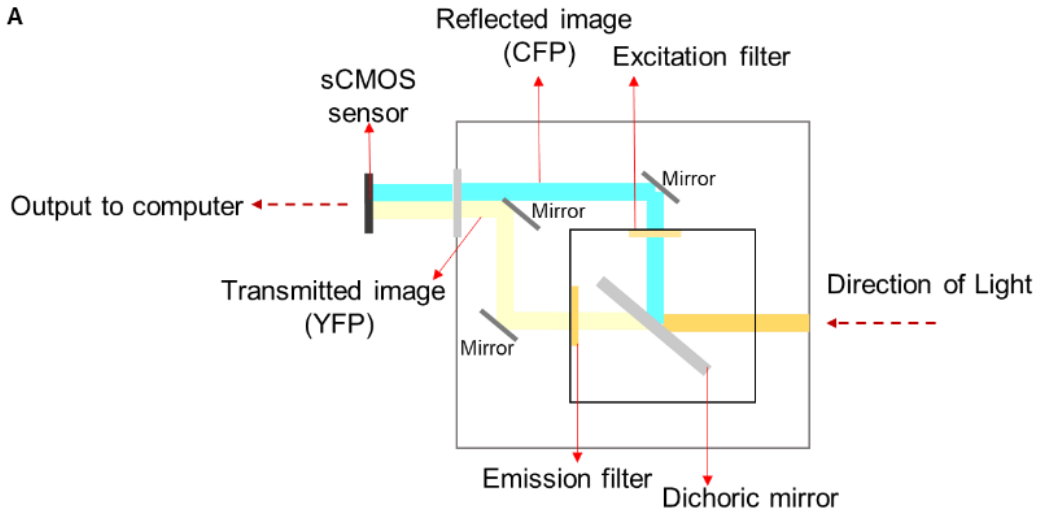

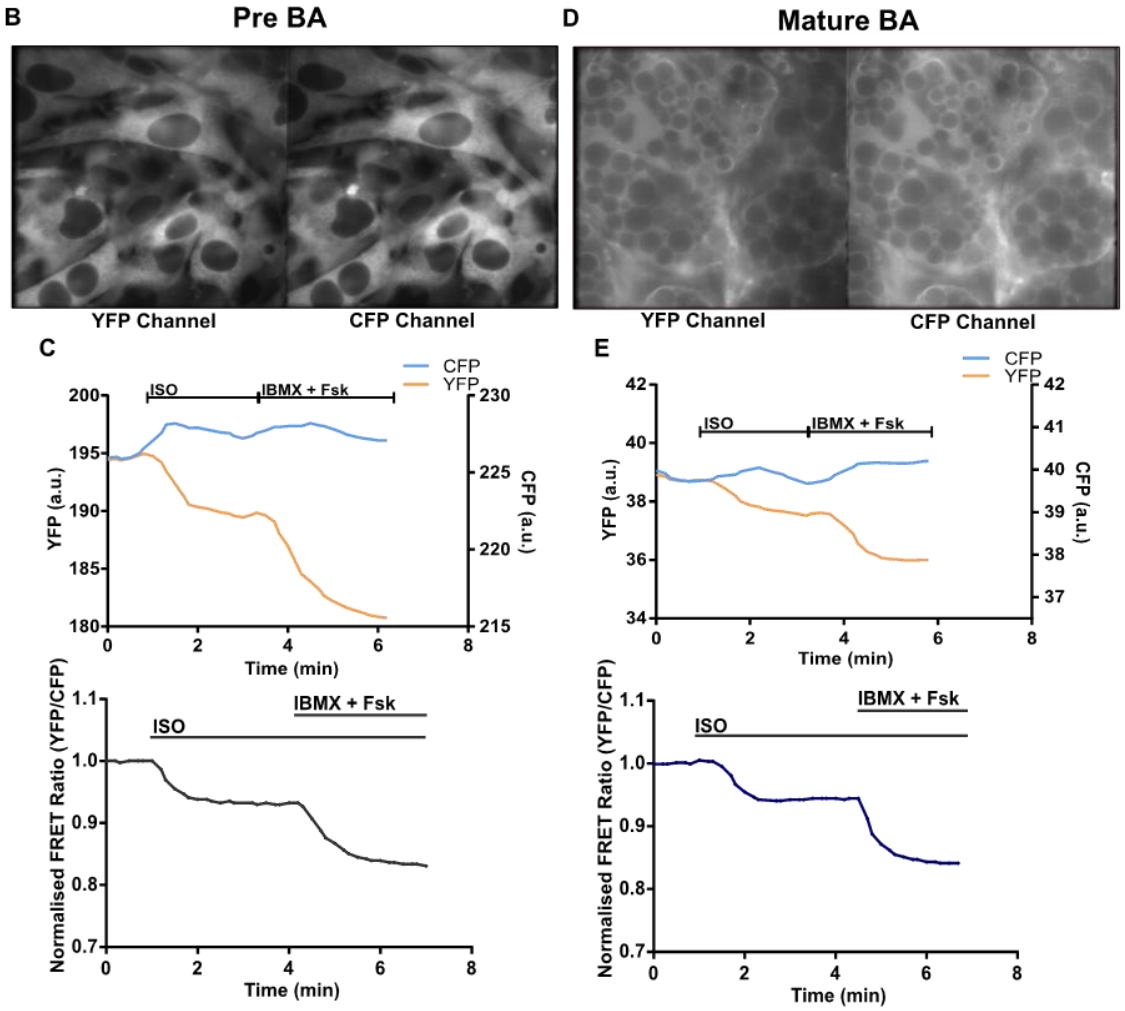

Figure 18.: Real-time cAMP dynamics measured in pre- and mature murine transgenic brown adipocytes expressing Epac1-camps FRET biosensor with a self-built FRET-imaging set-up. (A) Schematic representation of the working principle of the FRET Imaging set-up. Representative images of individual YFP (left) and CFP (right) channels of **(B)** pre-BA and **(D)** mature BA ubiquitously expressing the cytosolic Epac1-camps FRET biosensor. Respective single intensity traces of YFP and CFP in **(C)** pre-BA and **(D)** mature BA followed by their respective YFP/CFP ratio shown as FRET traces. Pre- and mature BA were stimulated by ISO (100 nM) to activate β-AR and then by IBMX + Fsk (100 µM + 10 µM) to obtain maximal FRET response of the FRET biosensor. An increment in the levels of intracellular cAMP is represented as a decrease in YFP/CFP ratio. n=1. The means in the data are represented as ±S.E.M. The figure panel (B-E) corresponds to Figure 1 A-D published by our group in Kannabiran et al., 2020 [98].

3.5. Expression of β-adrenergic receptors in murine brown adipocytes

The first part of this study involved addressing cAMP compartmentation upon the activation of β-AR. To do so, initially the mRNA expression profile of all the β-AR subtypes was confirmed in pre- and mature BA of transgenic Epac1-camps (FVB/N) expressing the cytosolic FRET biosensor. The expression pattern of β-AR receptors from transgenic Epac1-camps FRET biosensor expressing pre- and mature BA was then compared to the mRNA expression of conventionally used pre- and mature BA from C57BL/6J mice. The expression of all the three subtypes of β-ARs, namely: β_1-AR, β_2-AR, β_3-AR was observed in pre- and mature BA of both the strains of mice as expected. The expression of β_3-AR was low in pre-BA. It was strongly upregulated upon differentiation of brown adipocytes to mature BA on Day 7 in both the strains (Figure 19 A-E). It was observed that the expression pattern β-AR between transgenic Epac1-camps cytosolic biosensor expressing and C57BL/6J pre- and mature BA respectively were similar. A part of these results have been published and Figure 19 A-C corresponds to Supplementary Figure 1 A-C in the publication [98].

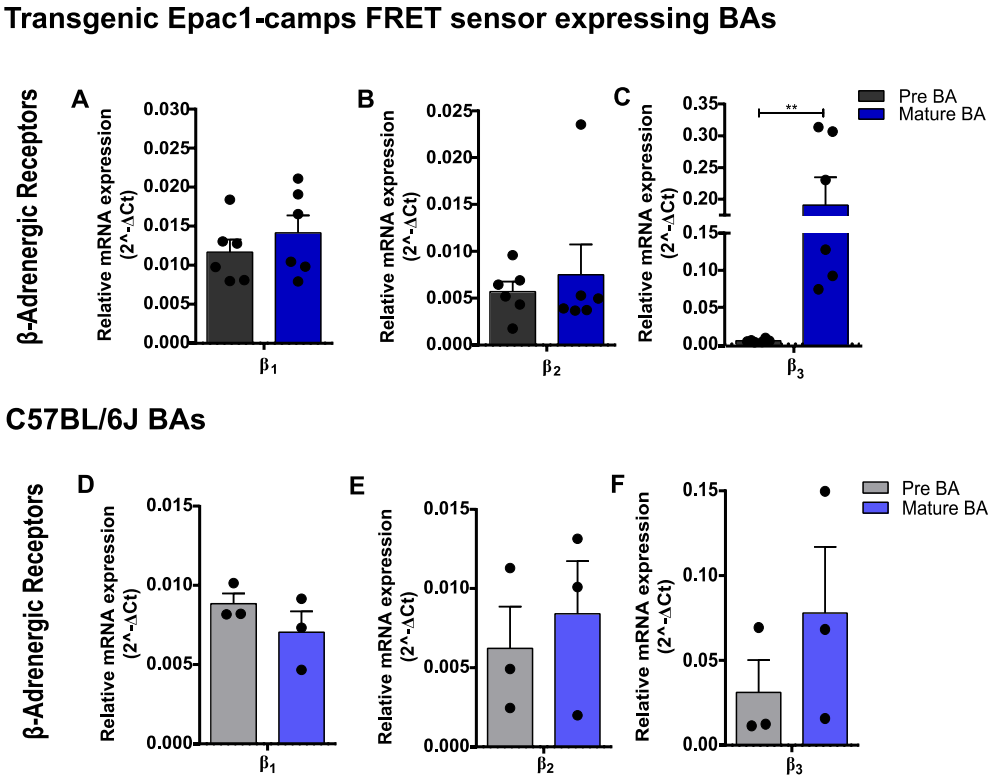

Figure 19.: Expression of β-ARs in murine pre- and mature brown adipocytes. Relative mRNA expression of **(A, D)** β_1, **(B, E)** β_2, **(C, F)** β_3 adrenergic receptors in transgenic Epac1-camps FRET sensor expressing (n=6) and C57BL/6J (n=3) pre- and mature murine BA respectively. The means in the bar graphs are represented as ±S.E.M and are expressed relative to hypoxanthine-guanine phosphoribosyltransferase (HPRT) mRNA. Two-tailed unpaired t-test was employed, and the significant differences correspond to **-p<0.05. The figure (A-C) corresponds to Supplementary Figure 1 (A-C) published by our group in Kannabiran et al., 2020 [98].

3.5.1. Real-time measurements of β-AR induced cAMP in murine brown adipocytes

To study the role of PDEs on β-AR initiated cAMP responses, the next step was to determine the submaximal concentrations of ligands for activating different β-AR subtypes without saturating response of the cytosolic FRET biosensor in pre- and mature brown adipocytes. FRET measurements were performed to activate β-AR using different concentrations of ISO, a synthetic agonist of β-AR; NE, a physiological agonist of β-AR; and CL 316,243 (CL), a selective β_3-AR agonist. The respective different β-AR agonist stimulations were followed by the addition of IBMX (100 µM) and Fsk (10 µM) to attain maximal cAMP response from the FRET biosensor. Concentration response curves were plotted for β-AR induced cAMP responses with the above-mentioned respective agonists (Figure 20 A-C). These responses were deduced with respect to R_0 and R_{max} post addition of the respective compounds (Section 2.2.15). The concentrations of ligands for experiments to be further performed were calculated based on the EC_{50} values obtained from the concentration-response curves (Figure 20 A-C).

The concentrations used to obtain respective β-AR induced cAMP responses by different ligands corresponded to 100 nM for ISO, 100 nM for NE and 50 µM for CL in preadipocytes and 100 nM for ISO, 500 nM for NE and 10 µM for CL in mature adipocytes. These results have been published by our working group and (Figure 20 A-C) corresponds to Figure 1 in the publication [98].

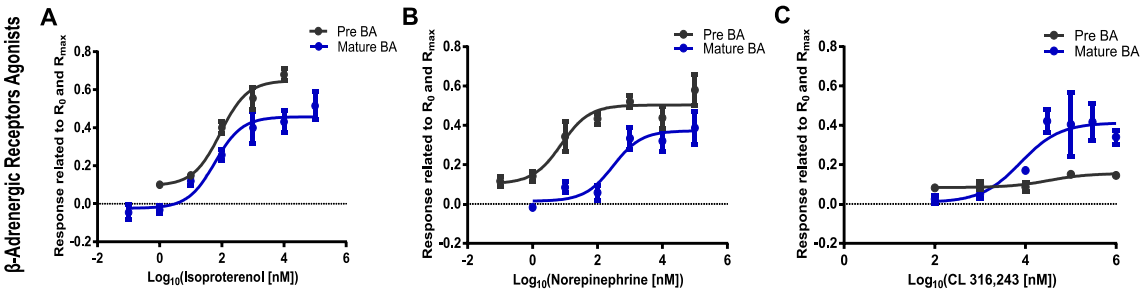

Figure 20.: Concentration-response curves of β-AR induced/cAMP responses in pre- and mature murine brown adipocytes ubiquitously expressing the cytosolic Epac1-camps FRET biosensor. Representation of different magnitudes of cAMP responses by various β-AR ligands as concentration-response curves (A) Isoproterenol (ISO) with EC_{50} values corresponding to 92.8 nM in pre-BA and 60 nM in mature BA (B) Norepinephrine (NE) with EC_{50} values corresponding to 7.7 nM in pre-BA and 353.7 nM in mature BA and (C) CL 316,243 (CL) with EC_{50} values corresponding to 32.8 µM in pre-BA and 7.8 µM in mature BA. FRET responses were calculated by normalizing the values of FRET ratio (R_0) corrected basally. The maximal cAMP FRET responses were generated by addition of IBMX + Fsk to obtain R_{max}. n=3-4. The means in the data are represented as ±S.E.M. This figure corresponds to Figure 1 published by our group in Kannabiran et al., 2020 [98].

3.5.1.1. Validation of the activation of individual β-AR subtypes by their respective agonists by FRET and ELISA

The next step was to perform FRET measurements to specifically activate β_1-AR and β_2-AR respectively. To activate β_1- and β_2-AR individually, the respective β-AR subtype was selectively inhibited. β_1 -AR were selectively activated by blocking β_2-AR by preincubation with the β_2-blocker ICI 118551 (ICI, concentration: 50 nM) followed by addition of the β-AR agonist ISO (100 nM). β_2 -AR were selectively activated by blocking β_1-AR by preincubation with the β_1-AR blocker CGP 20712A (CGP, concentration: 100 nM) followed by addition of the β-AR agonist ISO (100 nM). The synthetic β-AR agonist ISO has been stated to have preferred selectivity and more binding affinity for β_1-AR and β_2-AR in comparison to β_3-AR [99]. Therefore, cAMP responses specific to $\beta_{1/2/3}$-AR subtypes were obtained by selectively activating each receptor accordingly with concentrations of ISO or CL as generated above (Figure 20 A-C) and employing the respective β_1-AR (CGP) and β_2-AR (ICI) blockers as stated above in both pre- and mature BA (Figure 21 A-G). Individual β-AR-induced cAMP responses

were represented as percentage change in FRET derived from FRET traces and was calculated as stated (Section 2.2.16).

It was clear that the change in FRET observed after stimulation with individual β_1- and β_2- ARs elicited a larger response in comparison to the β_3-AR in both pre- and mature adipocytes. Interestingly, a full saturation of the FRET sensor was not observed even though high concentrations of all agonists to selectively activate individual β-AR were used. This was an initial indication suggesting that these cAMP responses elicited by individual β-AR activation could be counterbalanced by the activity of PDEs. Therefore, the next step was to investigate the role of different PDE families in compartmentalising cAMP upon stimulation of β-AR subtypes. These results have been published and Figure 21 A-G corresponds to Supplementary Figure 5 A-G in the publication [98].

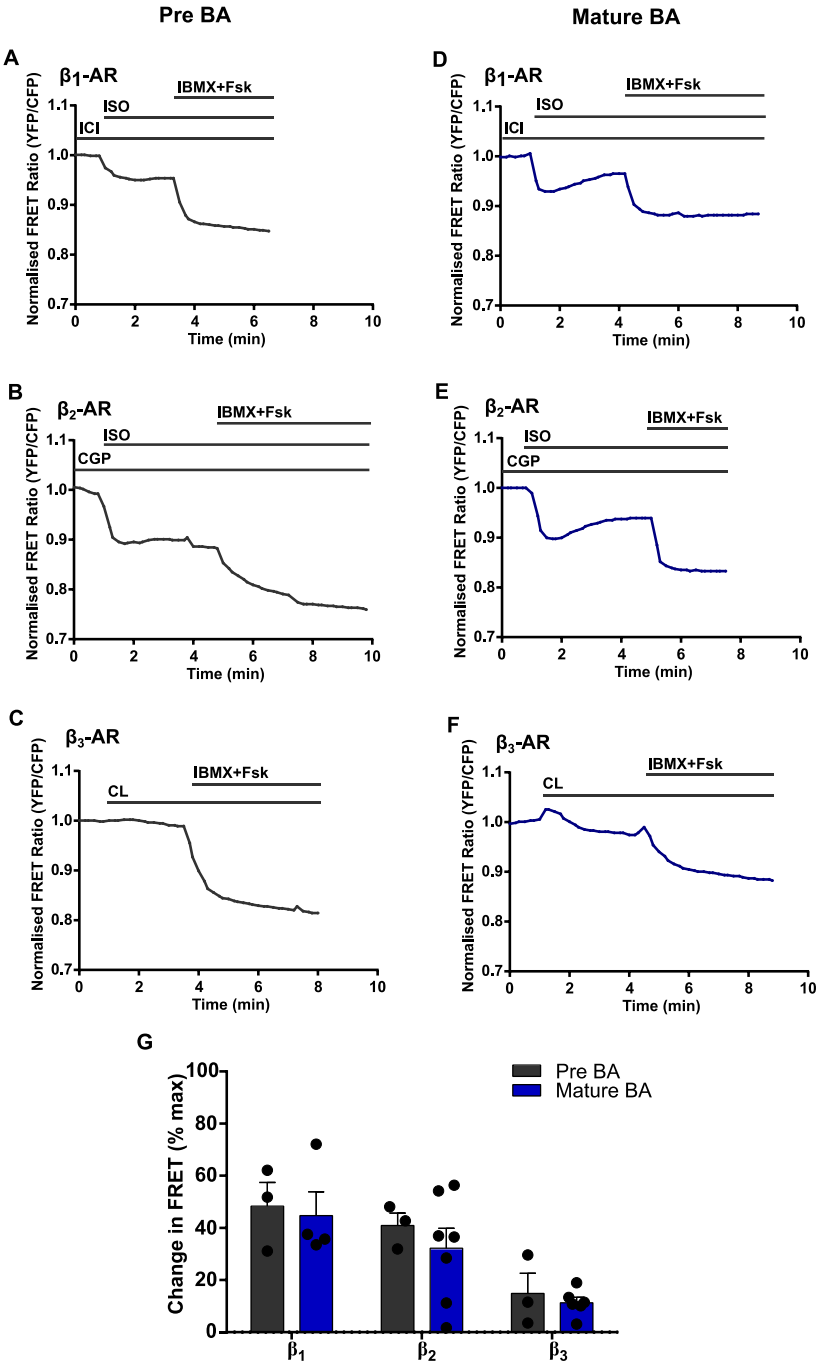

Figure 21.: cAMP responses induced by individual β-AR in murine pre- and mature brown adipocytes measured by FRET. Representation of cAMP responses recorded as FRET traces upon activation of individual β-AR subtype in pre- and mature BA expressing Epac1-camps cytosolic FRET biosensor **(A, D)** Selective activation of β_1-AR by blocking β_2-AR with ICI (50 nM) preincubation followed addition of ISO (100 nM) **(B, E)** Selective activation of β_2-AR by blocking β_1-AR with CGP (100 nM) preincubation followed by addition of ISO (100 nM) **(C, F)** Selective activation of β_3-AR with CL (50 µM used in pre-BA, 10 µM used in mature BA). The maximal cAMP FRET response was achieved by inhibition of all the PDEs with non-specific IBMX (100 µM) and AC activation with Fsk (10 µM). **(G)** FRET responses shown in **(A-F)** were quantified and depicted as the change in FRET by normalizing the values to basal corrected FRET ratio (R_0) and the maximal FRET response obtained by the addition of IBMX + Fsk (R_{max}). n=3-6. The means in the bar graphs are represented as ± S.E.M. This figure corresponds to Supplementary Figure 5 A-G published by our group in Kannabiran et al., 2020 [98].

To further testify the above-mentioned measurements ensuring that addition of ISO along with respective selective β-AR blockers ICI and CGP selectively activated only β_1 and β_2-AR respectively, pre- and mature BA were subjected to application of ICI (50 nM) and CGP (100 nM) together with ISO (100 nM) followed by the maximum saturation of the cAMP response of the FRET biosensor by employing IBMX (100 µM) and Fsk (10 µM). The results revealed that both in pre- and mature BA, ICI and CGP applied together with ISO showed no production of cAMP in comparison to the cAMP production observed upon stimulation with ISO alone (Figure 22 A, B). This confirmed that blocking with either ICI or CGP followed by ISO stimulation led to legitimate β_1/β_2-AR induced cAMP production. These results could also be recapitulated by measuring cAMP production by using another method, namely ELISA. Pre- and mature BA were treated with IBMX (500 µM) to obtain maximal cAMP production as a control, followed by treatment with ISO (100 nM) alone or together with ICI (50 nM), CGP (100 nM) and ISO (100 nM). The cAMP production measured by ELISA also showed that blocking β_1/β_2-ARs completely blunted the ISO stimulated cAMP response (Figure 22 D, E). Furthermore, these results were further complemented by subjecting mature BA with and without pre-treatment with ICI (50 nM) and CGP (100 nM) to block β_1/β_2-AR induced cAMP production followed by stimulation with β_3-AR with CL. Similar levels of cAMP production were observed between β_3-AR stimulated mature BA with or without blocking β_1/β_2-AR (Figure 22 C). Therefore, these data showed that application of ISO was after blocking respective β_1/β_2-AR was selectively activating only β_1- and β_2-AR and had no effect on β_3-AR activation. These results have been published and the Figure 22 A-E corresponds to Supplementary Figure 5 A-G in the publication [98].

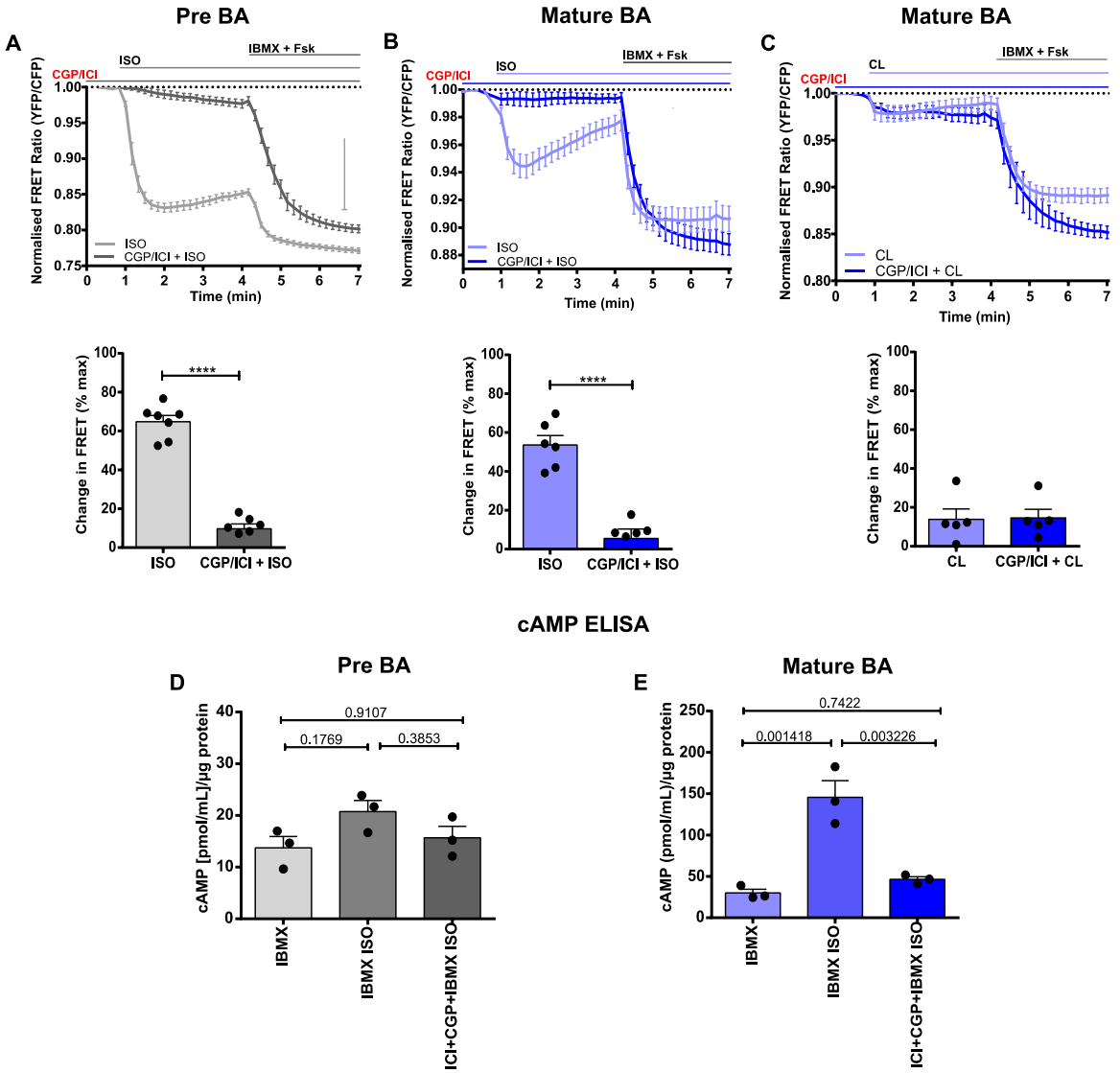

Figure 22.: Assessment of cAMP responses induced by individual β_1/β_2-AR using Epac1-cAMP FRET biosensor and ELISA in murine pre- and mature brown adipocytes. Representation of cAMP responses recorded as FRET traces and their respective quantification in adipocytes expressing Epac1-camps cytosolic FRET biosensor. The FRET measurements were performed by blocking both β_1-AR (CGP, 100 nM) and β_2-AR (ICI, 50 nM) by preincubation in **(A)** pre-BA (n=6) **(B)** mature BA (n=6) followed by stimulation with ISO (100 nM) to activate β-AR and **(C)** mature BA. (n=5) followed by stimulation with CL (10 µM) to activate β_3-AR respectively. The maximal cAMP FRET response was achieved by inhibition of all the PDEs with non-specific IBMX (100 µM) and AC activation with Fsk (10 µM). Bar graphs represent means as ±S.E.M. Two-tailed unpaired t-test was employed, and the significant differences correspond to ****-p<0.0001. Measurement of cAMP accumulation over 15 min by ELISA in **(D)** Pre-BA (n=3) and **(E)** mature BA (n=3) upon stimulation with ISO (10 nM) with or without blocking β_1-AR (CGP, 100 nM) and β_2-AR (ICI, 50 nM) in the presence of IBMX (500 µM). The means in the bar graph are represented as ± S.E.M. 1-way ANOVA followed by Sidak's multiple comparison test was employed. These experiments were performed by Dr. Dominic Gosejacob and Birte Niemann.This figure corresponds to Supplementary Figure 4 published by our group in Kannabiran et al., 2020 [98].

3.5.1.2. Activation of β_1-AR causes PDEs to regulate cAMP responses differently in pre- and mature murine brown adipocytes

The hypothesis that PDE2, PDE3 and PDE4 may differentially control β_1-AR/cAMP dynamics in pre- and mature BA was addressed by performing real-time measurements of cAMP upon selectively stimulating β_1-AR. β_2-AR was selectively inhibited employing the β_2-AR blocker, ICI (50 nM). This was then followed by the addition of β-AR agonist, ISO (100 nM). Post stimulation of β_1-ARs, the contribution of individual PDEs in controlling the β_1-AR-induced cAMP production was studied by adding the respective inhibitors namely: PDE2 with PDE2 inhibitor, BAY 60-7550 (100 nM); PDE3 with PDE3 inhibitor, Cilostamide (10 µM) and PDE4 with PDE4 inhibitor, Rolipram (10 µM). The maximum cAMP response generated by Epac1-camps FRET biosensor was achieved by the addition of IBMX (100 µM), the unselective PDE inhibitor after β_1-AR stimulation followed by inhibition with the individual PDE inhibitors respectively (Figure 23 A-F). In pre-BA, the inhibition of PDE4 contributed to a higher increase in cAMP production which accounted to a value of 1.8-fold ± 0.1 S.E.M (n=6) in comparison to PDE3 inhibition and to a value of 3.5-fold ± 0.6 S.E.M (n=6) in comparison to PDE2 inhibition. The results indicated that upon β_1-AR stimulation, PDE4 is the major PDE family regulating cAMP levels in pre-BA (Figure 23 G). However, in mature BA, upon β_1-AR stimulation, the contribution of PDE2 inhibition to cAMP responses were low while both PDE3 and PDE4 inhibition contributed equally as major regulators of cAMP levels (Figure 23 G). It was interesting to observe that when the responses of β_1-AR initiated cAMP production followed by the addition of different individual PDE inhibitors used were compared between pre- and mature BA, inhibition of PDE3 caused a significant increase in cAMP levels in mature BA in comparison to pre-BA. There were no differences in β_1-AR initiated cAMP responses observed between pre- and mature BA upon PDE2 and PDE4 inhibition (Figure 23 G). This led to a revelation that β_1-AR initiated cAMP responses were controlled differently by different PDEs. In this context, upon β_1-AR activation, PDE3 plays an important role in controlling in mature BA but not in pre-BA. PDE4 is the major PDE that controls β_1-AR initiated cAMP in preadipocytes (Day -2) and differentiated adipocytes (Day 7). The calculations of how the FRET responses are depicted as the percentage of PDE inhibition are stated in Section (2.2.16).

These data have been published by our working group and the Figure 23 A-G corresponds to Figure 2 A-G in the publication [98].

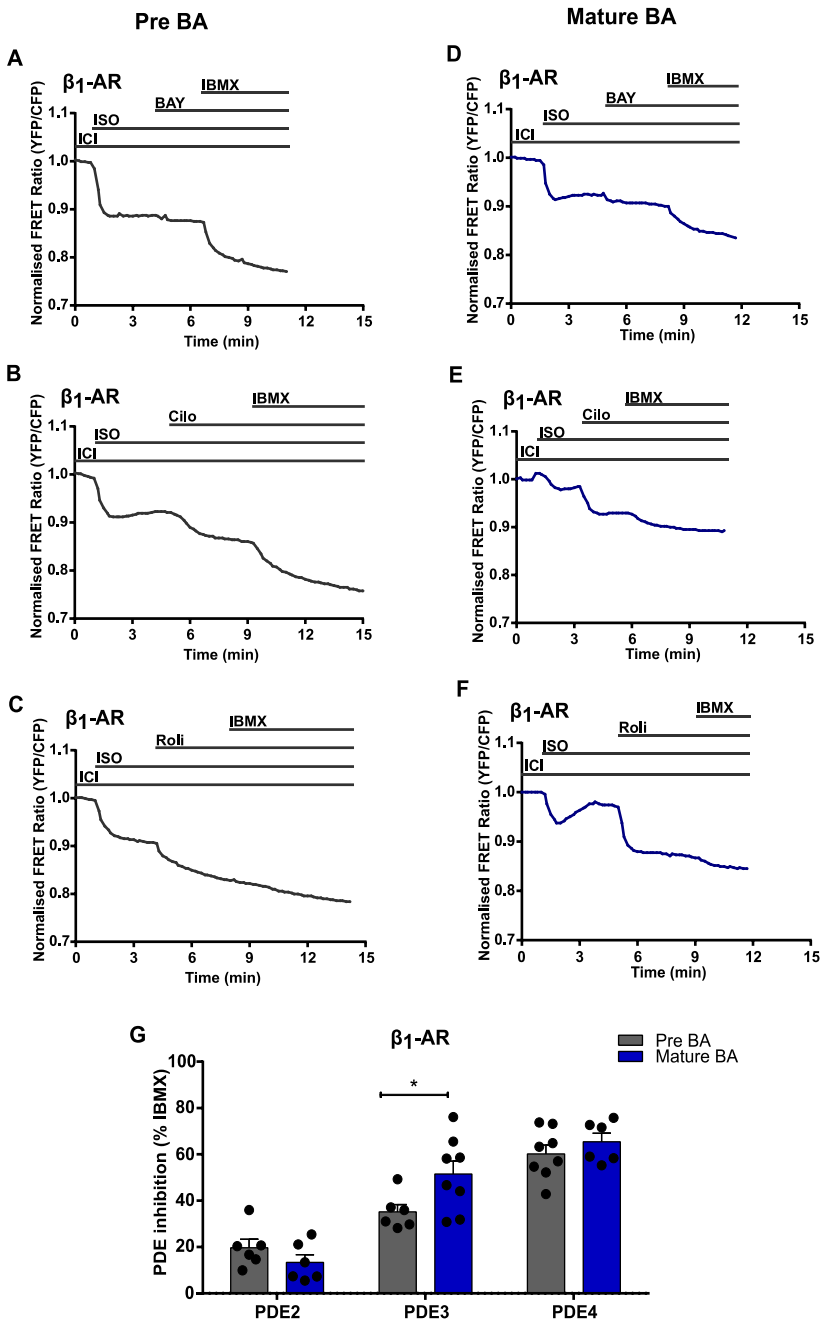

Figure 23.: β1-AR activation exhibits differences in the regulation of real-time dynamics of cAMP by PDEs between pre- and mature murine brown adipocytes. Representation of cAMP responses recorded as FRET traces upon activation of individual β1-AR in pre- and mature BA expressing Epac1-camps cytosolic FRET biosensor. β1-AR were activated by selectively blocking β2-AR (ICI, 50 nM) subsequently stimulated with ISO (100 nM) followed by addition of **(A, D)** PDE2 inhibitor (BAY, 100 nM) **(B, E)** PDE3 inhibitor (Cilo, 10 µM) **(C, F)** PDE4 inhibitor (Roli, 10 µM). The maximal cAMP FRET response was achieved by inhibition of all the PDEs with nonspecific PDE inhibitor, IBMX (100 µM). **(G)** Representation of β1-AR stimulated FRET responses shown in (A-F) quantified and depicted as a percentage of PDE inhibition for each individual family of PDE (PDE2, PDE3 or PDE4) in relation to maximum inhibition of PDEs achieved by using the unselective PDE inhibitor IBMX. n=6-8. Bar graphs represent means as ± S.E.M. 2-way ANOVA followed by Sidak's multiple comparison test was employed, and the significant differences correspond to *- $p<0.05$. This figure corresponds to Figure 3 A-G published by our group in Kannabiran et al., 2020 [98].

3.5.1.3. Activation of β_2-AR causes PDEs to regulate cAMP responses similarly in pre- and mature murine brown adipocytes

The role of PDEs regulating cAMP compartmentation in the context of β_2-AR stimulation was assessed by selectively inhibiting β_1-AR with the β_1-AR blocker CGP (100 nM). This was then followed by the addition of β-AR agonist ISO (100 nM). Post stimulation of β_2-ARs, the contribution of individual PDEs in controlling the β_2-AR-induced cAMP production was studied by adding the respective inhibitors namely: PDE2 with PDE2 inhibitor, BAY 60-7550 (BAY, 100 nM); PDE3 with PDE3 inhibitor, Cilostamide (Cilo, 10 µM) and PDE4 with PDE4 inhibitor, Rolipram (Roli, 10 µM). The maximum cAMP response elicited by Epac1-camps FRET biosensor was achieved by the addition of IBMX (100 µM), after β_2-AR stimulation followed by inhibition with the individual PDE inhibitors respectively (Figure 24 A-F). As observed for β_1-AR induced cAMP responses, in pre-BA, the inhibition of PDE4 showed the maximum increase in β_2-AR initiated cAMP production in comparison to PDE2 and PDE3 inhibition (Figure 24 G). This result suggested that in pre-BA, β_2- AR induced cAMP was controlled majorly by PDE4. Interestingly, in mature BA, β_2- AR activation exhibited similar levels of cAMP post inhibition with PDE2, PDE3 or PDE4 respectively. PDEs were regulated similarly upon. Comparison of how inhibition with individual PDEs behaved on β_2-AR activation between pre- and mature BA revealed that there were no differences observed (Figure 24 G). These results revealed that PDE2, PDE3 and PDE4 inhibition governed β_2-AR induced cAMP in pre- and mature BA in a similar manner.

These data have been published by our working group and the Figure 24 A-G corresponds to Figure 3 A-G in the publication [98].

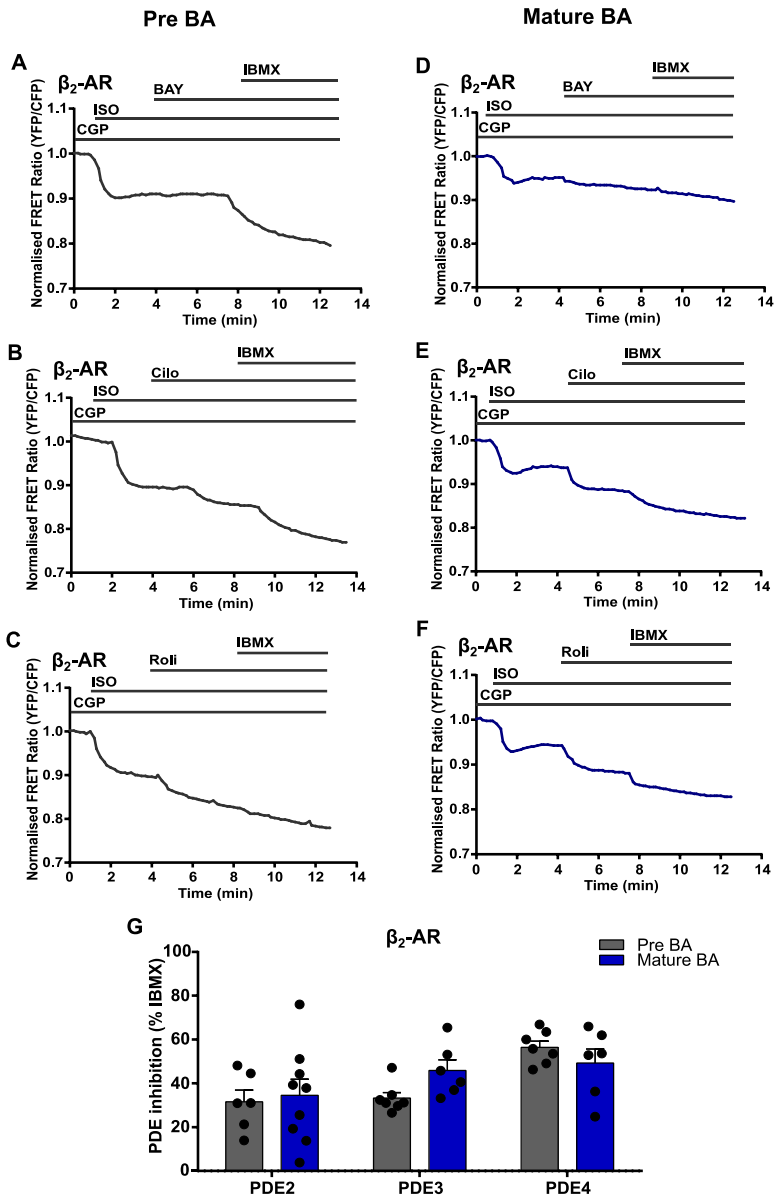

Figure 24.: β_2-AR activation exhibits no differences in the regulation of real-time dynamics of cAMP by PDEs between pre- and mature murine brown adipocytes. Representation of cAMP responses recorded as FRET traces upon activation of β_2-AR subtype in pre- and mature BA expressing Epac1-camps cytosolic FRET biosensor. β_2-AR were activated by selectively blocking β_1-AR (CGP, 100 nM) subsequently stimulated with ISO (100 nM) followed by addition of **(A, D)** PDE2 inhibitor (BAY, 100 nM) **(B, E)** PDE3 inhibitor (Cilo, 10 µM) **(C, F)** PDE4 inhibitor (Roli, 10 µM). The maximal cAMP FRET response was achieved by inhibition of all the PDEs with non-specific PDE inhibitor, IBMX (100 µM). **(G)** Representation of β_2-AR stimulated FRET responses shown in (A-F) quantified and depicted as a percentage of PDE inhibition for each individual family of PDE (PDE2, PDE3 or PDE4) in relation to maximum inhibition of PDEs achieved by using the unselective PDE inhibitor IBMX. n=6-9. The means in the bar graphs are represented as ± S.E.M. 2-way ANOVA followed by Sidak's multiple comparison test was employed. This figure corresponds to Figure 3 A-G published by our group in Kannabiran et al., 2020 [98].

3.5.1.4. Activation of β_3-AR causes PDEs to regulate cAMP responses differently in pre- and mature murine brown adipocytes

β_3-AR was selectively activated using its agonist CL in preadipocytes (50 µM) and mature BA (10 µM). Post stimulation of β_3-AR with CL, the contribution of individual PDEs in controlling the β_3-AR-induced cAMP production was studied by adding the respective inhibitors namely: PDE2 with PDE2 inhibitor, BAY 60-7550 (BAY, 100 nM); PDE3 with PDE3 inhibitor, Cilostamide (Cilo, 10 µM) and PDE4 with PDE4 inhibitor, Rolipram (Roli, 10 µM). The maximum cAMP response elicited by Epac1-camps FRET biosensor was achieved by the addition of IBMX (100 µM), after β_3-AR stimulation followed by inhibition with the individual PDE inhibitors respectively (Figure 25 A-F). In pre- and mature BA, inhibition of PDE2 and PDE3 exhibited no differences in β_3-AR initiated cAMP production (Figure 25 G). Interestingly, β_3-AR stimulation followed by PDE4 inhibition in pre-BA caused a 2.3-fold ± 0.5 S.E.M (n=6) increase in cAMP production to mature BA. This could be reasoned due to the lower expression of β_3-AR in pre-BA and potentially be the reason why PDE4 could have a higher influence in controlling β_3-AR initiated cAMP in pre-BA in comparison to mature BA. Although an increase PDE3 expression was observed in mature BA (Figure 13 G, H) warrants for a more pronounced effect of PDE3- dependent-cAMP degradation upon β_3-AR stimulation in mature BA compared to pre-BA, this effect of was not observed (Figure 25 G). These results were different in comparison to β_1-AR activation wherein the effect of PDE3 inhibition in mature BA was significantly increased in comparison to pre-BA (Day -2). This was therefore a preliminary indication that in mature BA, PDE3 could control different cAMP pools within the cell forming different cAMP sinks and that the existence of these loco-regional cAMP pools generated between β_1-AR and β_3-AR stimulation. In pre-BAs, upon β_3-AR stimulation the regulation of cAMP was strongly controlled by PDE4. Therefore, in pre-BA, PDE4 was the main regulator of cAMP production upon β_1, β_2 or β_3-AR stimulation. These data have been published by our working group and the Figure 25 A-G corresponds to Figure 4 A-G in the publication [98].

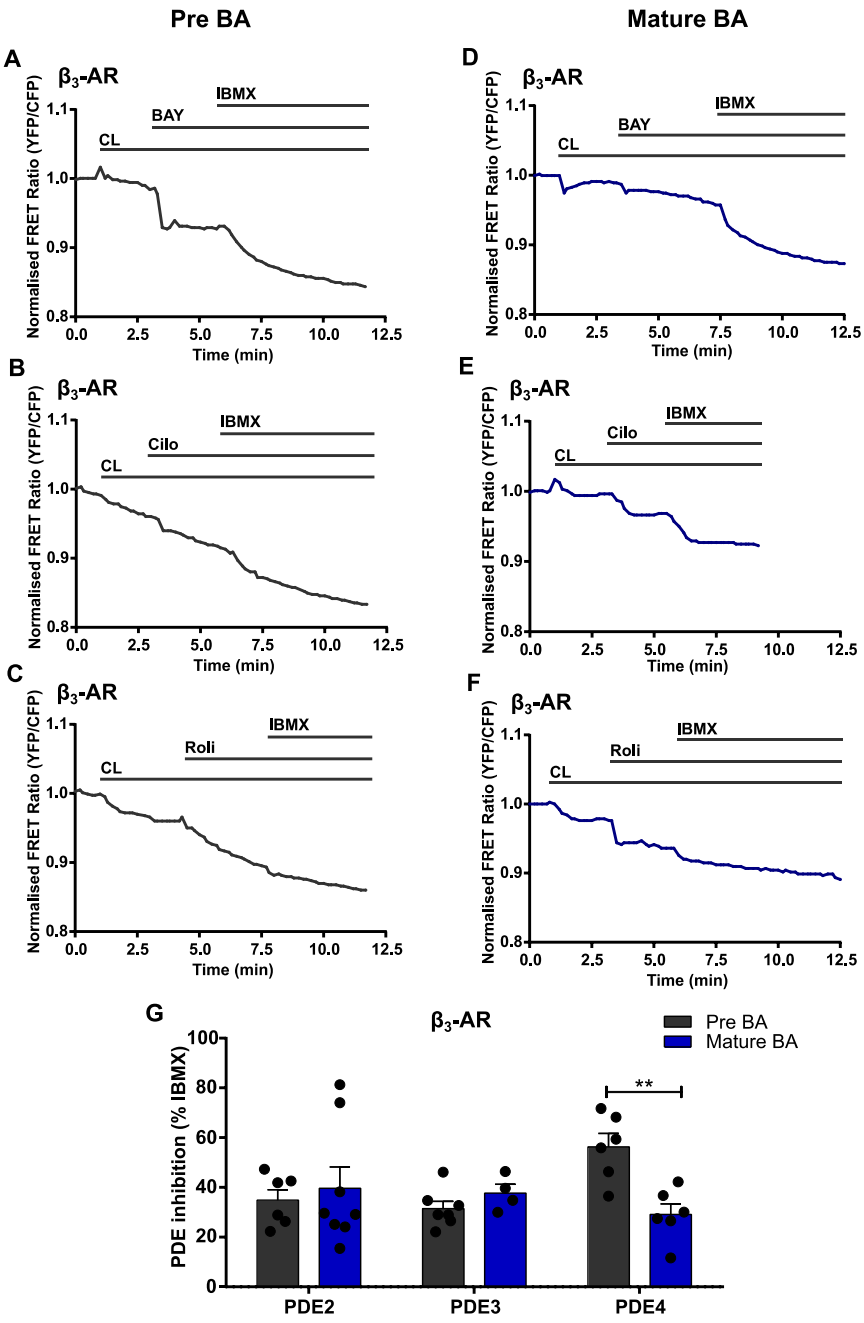

Figure 25.: β_3-AR activation exhibits differences in the regulation of real-time dynamics of cAMP by PDEs between pre- and mature murine brown adipocytes. Representation of cAMP responses recorded as FRET traces upon activation of β_3-AR in pre- and mature BA expressing Epac1-camps cytosolic FRET biosensor. β_3-AR were selectively activated with CL (50 µM was used in pre-BA, 10 µM was used in mature BA) followed by **(A, D)** PDE2 inhibitor (BAY, 100 nM) **(B, E)** PDE3 inhibitor (Cilo, 10 µM) **(C, F)** PDE4 inhibitor (Roli, 10 µM). The maximal cAMP FRET response was achieved by inhibition of all the PDEs with non-specific PDE inhibitor, IBMX (100 µM). **(G)** Representation of β_2-AR stimulated FRET responses shown in (A-F) were quantified and depicted as a percentage of PDE inhibition for each individual family of PDE (PDE2, PDE3 or PDE4) in relation to maximum inhibition of PDEs achieved by using the unselective PDE inhibitor IBMX. n=4-8. The means in the bar graphs are represented as ± S.E.M. 2-way ANOVA followed by Sidak's multiple comparison test was employed and the significant differences correspond to **- p=0.01. This figure corresponds to Figure 5 published by our group in Kannabiran et al., 2020 [98].

3.5.1.5. Validation of cAMP compartmentation imparted by PDEs upon β-AR stimulation by ELISA

The next question to be validated was, if β_3-AR initiated cAMP produced was less restricted by PDEs in comparison to β_1-AR stimulated cAMP in murine mature BA could be reproduced using cAMP ELISA (Figure 26). Therefore, β_1-AR was stimulated by blocking β_2-AR with preincubation of ICI (50 nM) followed by treatment with ISO (10 nM) and β_3-AR was stimulated with CL (10 nM) followed by treatment with PDE inhibitors, PDE3 inhibitor (Cilo, 10 µM) and PDE4 inhibitor (Roli, 10 µM) respectively. DMSO treatment was used as the control. No increase in cAMP levels were detected upon inhibition of PDE3 with Cilostamide regardless of β_1- or β_3-AR stimulation. However, a significant increase in cAMP production was detected upon PDE4 inhibitor Rolipram treatment with β_1-AR activation. Whereas the same increase of cAMP was not observed with β_3-AR activation in mature adipocytes upon PDE4 inhibition. These was coherent with the measurements performed with Epac1-camps expressing BA by FRET indicating differences in PDE4 compartmentation upon β_1-AR/ β_3-AR activation in mature BA. These data have been published and the Figure 26 corresponds to Supplementary Figure 6 in the publication [98].

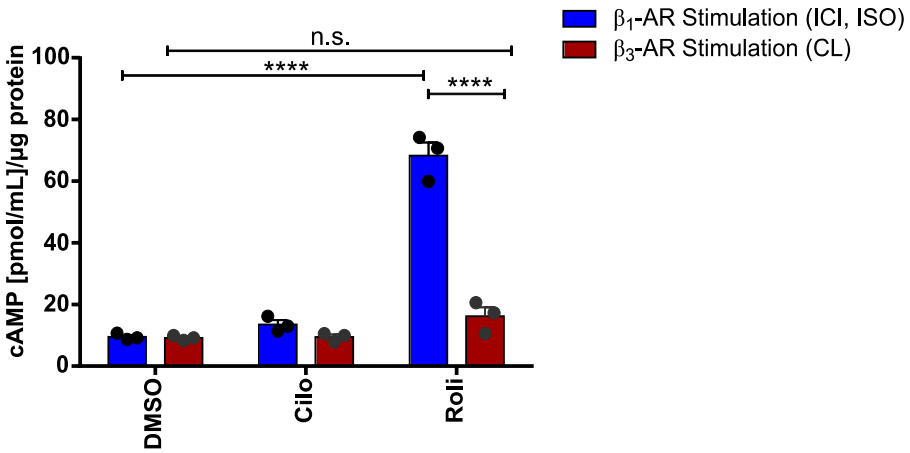

Figure 26.: Measurement of cAMP production upon β_1 or β_3-AR stimulation followed by pre-treatment with PDE inhibitors in murine mature brown adipocytes. Measurement of cAMP (pmol/mL) normalized to the amount of total protein (µg) in murine mature BA by cAMP ELISA. Mature BA were pre-treated with DMSO (Control), PDE3 (Cilostamide 10 µM) and PDE4 (Rolipram 10 µM) inhibitors respectively for 10 min. Prior to the addition of PDE inhibitors, mature BAs were pre-treated with ICI (50 nM) to block β_2-AR and selectively stimulate β_1-AR with ISO (10 nM) and to stimulate β_3-AR, and the cells were treated with 10 nM CL for 15 min. Intracellular cAMP was measured by ELISA (n=3). The means in the bar graphs are represented as ± S.E.M. 2-way ANOVA followed by Holm-Sidak's multiple comparison test was performed and the significant differences correspond to ****- $p<0.0001$. These measurements were performed by Birte Niemann. This figure corresponds to Supplementary Figure 6 published by our group in Kannabiran et al., 2020 [98].

3.5.1.6. Regulation of PDE3/4 function in lipolysis by β-AR in murine brown adipocytes

Lipolysis was used as a read out to assess the functional relevance of regulation of PDE3/4 upon β-AR-induced cAMP compartmentation. $\beta_{1/2}$-AR was stimulated by employing 10 nM ISO and β_3-AR was stimulated by 10 nM CL. The values used to stimulate $\beta_{1/2}$-AR and β_3-AR were chosen close to their EC_{50} ISO (10 nM) [100]. The stimulation was then followed by the inhibition of PDE3 and PDE4 with their respective inhibitors and the activity of lipolysis was quantified. Treatment with β1/2-AR agonist ISO induced lipolysis. This effect of lipolysis was further increased by 2.0-fold ± 0.3 S.E.M (n=6) when ISO was treated together with the combination of Cilostamide (10 μM) and Rolipram (10 μM). The levels of co-treatment with Cilostamide and Rolipram also reached was also comparable to that of effect observed with the unselective PDE inhibitor IBMX (100 μM) as the increase in lipolytic activity with IBMX treatment corresponded to a 2.1-fold ± 0.3 S.E.M (n=6) (Figure 27). However, after selective stimulation of BAs with β_3-AR agonist CL, an increase of 1.5-fold ± 0.2 S.E.M (n=6) in lipolysis was observed in comparison to lipolysis induced after treatment with ISO.

The β_3-AR induced lipolysis by CL response did not increase further with it was co-treated with Cilostamide and Rolipram or IBMX even though the CL concentration employed was close to the EC_{50} [33,34] (Figure 27). This could be due to the fact that the increased amount of β_3-ARs upon brown adipocyte differentiation generate a large amount of cAMP, and that this large amount of cAMP is not counterbalanced by either PDE3/4 or by the global PDE inhibitor, IBMX. Although a tight restriction of β_3-induced cAMP production is observed with upon PDE4 inhibition with the cytosolic Epac1-camps FRET sensor, the same regulation is not observed with lipolysis. This is also a preliminary indication that points out there could be a different cAMP pool governing β_3-AR induced lipolysis in brown adipocytes. These data have been published and Figure 27 corresponds to Supplementary Figure 6 in the publication [98].

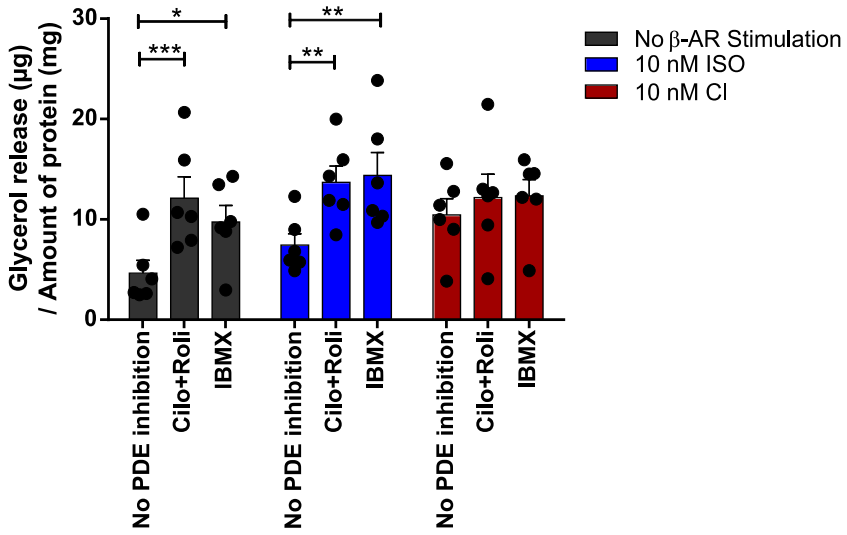

Figure 27.: Regulation of lipolysis upon $\beta_{1/2}$-AR or β_3-AR by PDEs in murine mature brown adipocytes. Measurement of glycerol release (µg) normalised to the amount of total protein (mg) in murine mature BA under conditions of stimulation without and with β-AR stimulation with ISO (10 nM) and CL (10 nM) followed by with or without PDE3 inhibitor Cilostamide (Cilo, 10 µM) + PDE4 inhibitor Rolipram (Roli, 10 µM) and inhibition of all PDEs by IBMX (100 µM) respectively. n=6. Bar graphs represent means as ± S.E.M. 2-way ANOVA followed by Holm-Sidak's multiple comparison test was performed, significant differences correspond to *, **, ***- p<0.05. This figure corresponds to Supplementary Figure 7 published by our group in Kannabiran et al., 2020 [98].

3.5.1.7. Activation of β-ARs collectively reveal similar results as upon selective β_1-AR stimulation

Finally, it was assessed if the regulation of PDEs upon individual β-AR/cAMP production could by reproduced using the physiological and non-selective β-AR agonist NE. All the three β-AR subtypes were non-selectively activated using their physiological activator NE in pre-BA (100 nM) and mature BA (500 nM). This was then followed by treatment with either PDE2 with PDE2 inhibitor, BAY 60-7550 (Bay, 100 nM); PDE3 with PDE3 inhibitor, Cilostamide (Cilo, 10 µM) or PDE4 with PDE4 inhibitor, Rolipram (Roli, 10 µM). The maximum cAMP response elicited by Epac1-camps FRET biosensor was achieved by the addition of IBMX (100 µM) (Figure 28 A-F). Upon stimulation of all three β-AR subtypes, in pre-BA, PDE4 inhibition was indicated to be the main regulator of cAMP production as it caused 1.5-fold ± 0.2 S.E.M (n=4) and 1.6-fold ± S.E.M (n=6) increase in cAMP levels compared to PDE2 and PDE3 inhibition albeit this effect was not significant (Figure 28 G). While in mature BA, PDE3 and PDE4 were observed to the major regulators, and the tight restriction on PDE4 inhibition imparted by selective β_3-AR was lost. As expected, no differences in cAMP increase between pre- and mature BA were observed after inhibition of PDE2, PDE3 and PDE4.

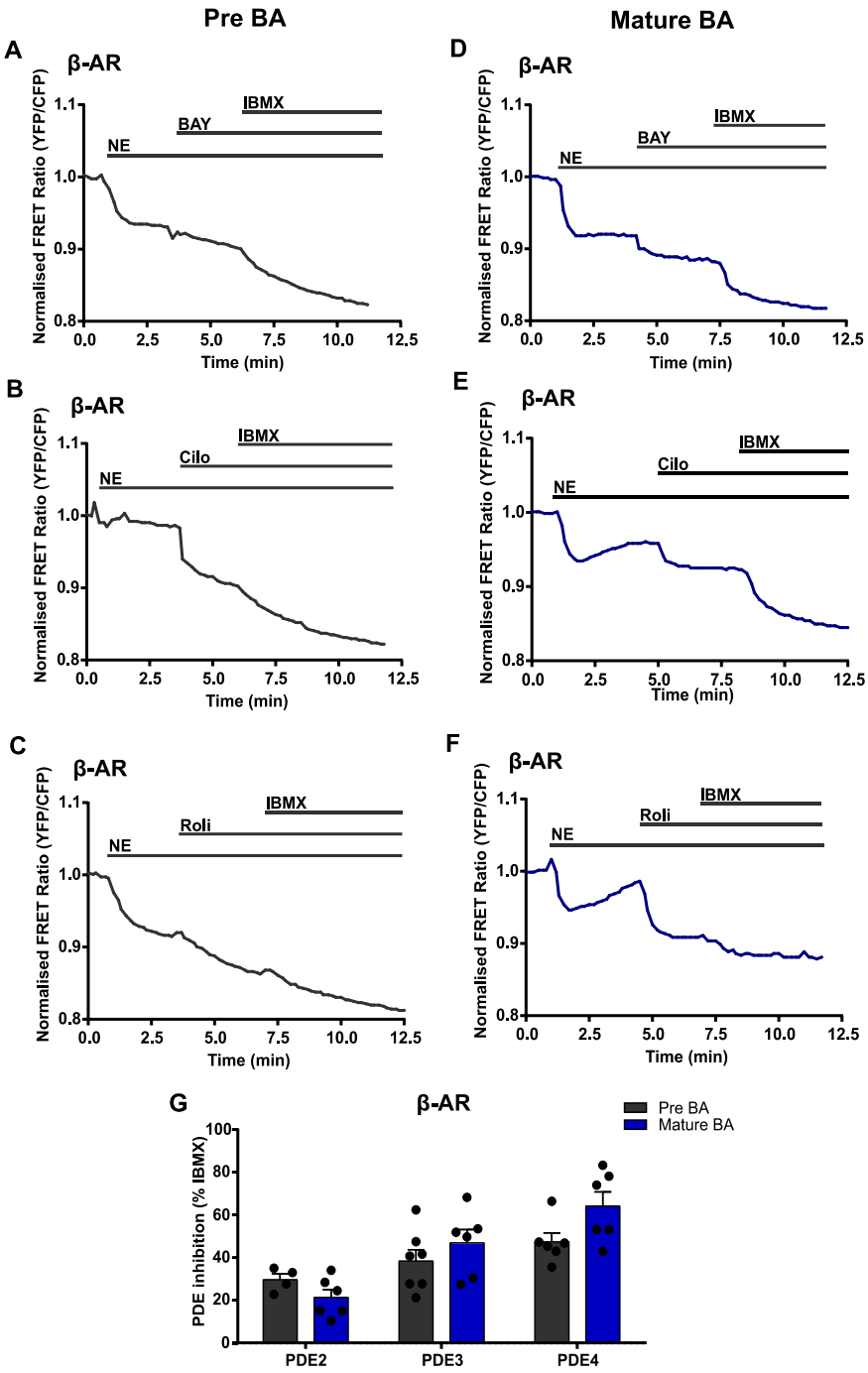

Figure 28.: Regulation of cAMP dynamics by PDEs in pre- and mature murine brown adipocytes upon β-AR activation. Representation of cAMP responses recorded as FRET traces upon activation by non selectively stimulating β-AR with the physiological activator NE (100 nM used in pre-BA and 500 nM used in mature BA) in pre- and mature BA expressing Epac1-camps cytosolic FRET biosensor followed by **(A, D)** PDE2 inhibitor (BAY, 100 nM) **(B, E)** PDE3 inhibitor (Cilo, 10 μM) and **(C, F)** PDE4 inhibitor (Roli, 10 μM). The maximal cAMP FRET response was achieved by inhibition of all the PDEs with non-specific PDE inhibitor, IBMX (100 μM). **(G)** Representation of β-AR stimulated FRET responses shown in (A-F) were quantified and are depicted as a percentage of PDE inhibition for each individual family of PDE (PDE2, PDE3 or PDE4) in relation to maximum inhibition of PDEs achieved by using the unselective PDE inhibitor IBMX. n=6-7. The means in the bar graphs are represented as ± S.E.M. 2-way ANOVA followed by Sidak's multiple comparison test was employed.

3.5.2. Expression of G_s-coupled purinergic receptors in murine brown adipocytes

The second part of this study involved addressing if different G_s-coupled GPCR families showed differences in cAMP compartmentation upon PDE inhibition. Differences in cAMP compartmentation in G_s-coupled purinergic receptors namely A_{2A} and A_{2B} were studied, as the prime importance of purinergic receptors in brown adipocytes was highlighted [32]. Initially mRNA expression of different G_s-coupled adenosine receptors, A_{2A} and A_{2B} was confirmed in transgenic Epac1-camps expressing pre- and mature BA (Figure 29 A). The trend in the mRNA expression pattern of A_{2A} and A_{2B} receptors from transgenic Epac1-camps expressing pre- and mature BA was then compared to the mRNA expression of A_{2A} and A_{2B} receptors from conventionally used pre- and mature BA isolated from mice of C57BL/6J strain. As expected, both the G_s-coupled adenosine receptors – A_{2A} and A_{2B} were expressed in both pre- and mature BA of both the strains (Figure 29 A-D). The expression of A_{2A} was low in pre-BAs and it was strongly upregulated upon BA differentiation to mature BAs in transgenic Epac1-camps BA (Figure 29 A), the same trend was also observed in C57BL/6J mice albeit the effect was not significant (Figure 29 C). The mRNA levels of A_{2B} was high in preadipocytes and decreased strongly upon BA differentiation in both the strains of mice (Figure 29 B-D). While the differences in transcript levels of A_{2B} receptors between pre- and mature BAs was significant in transgenic Epac1-camps expressing mice and not in C57BL/6J strain. It was concluded that the pattern of mRNA expression between both the strains in pre- and mature BA respectively were similar.

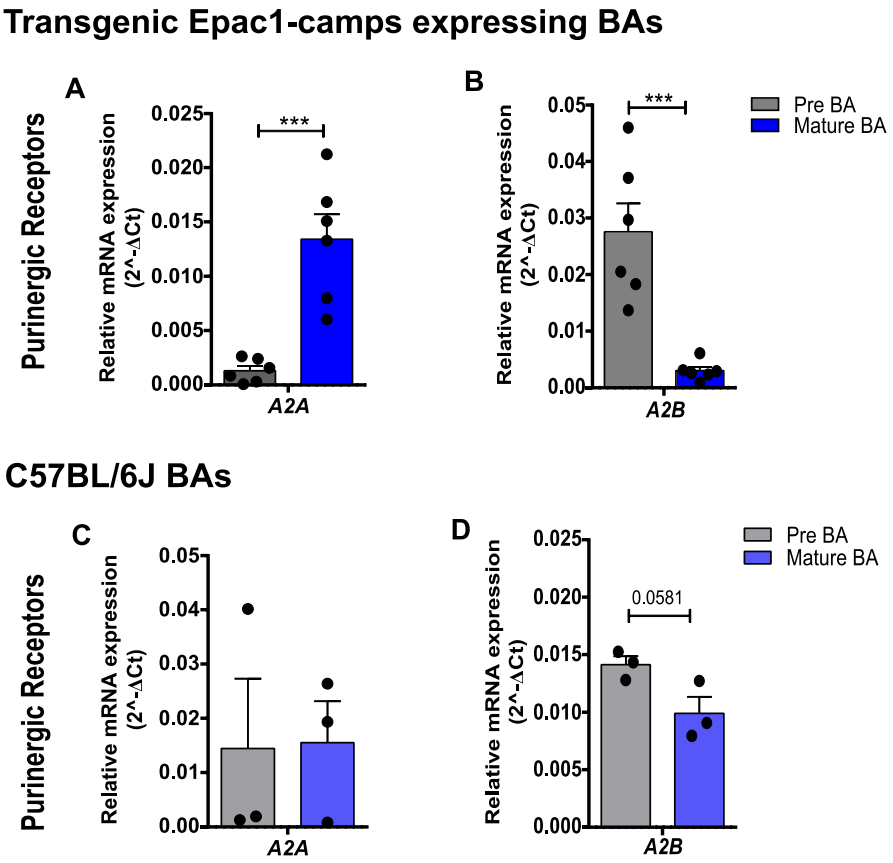

Figure 29.: Expression of adenosine receptors in murine pre- and mature brown adipocytes. Relative mRNA expression of **(A, C)** A_{2A}, **(B, D)** A_{2B} receptors in transgenic Epac1-camps FRET sensor expressing (n=6), and C57BL/6J (n=3) pre- and mature murine BA respectively. The means in the bar graph are represented as ±S.E.M and are expressed relative to hypoxanthine-guanine phosphoribosyltransferase (HPRT) mRNA. Two-tailed unpaired t-test was employed and the significant differences correspond to ***-p<0.05.

3.5.2.1. Real-time measurements adenosine receptor- induced cAMP production in murine brown adipocytes

To study the role of G_s-coupled adenosine receptors-induced cAMP, the submaximal concentrations of ligands for activating different G_s-coupled adenosine receptors without saturating the cytosolic FRET biosensor response in pre- and mature BA was established. FRET measurements were performed to activate G_s-coupled adenosine receptors, A_{2A} and A_{2B} using a physiological agonist of adenosine receptors, Adenosine (ADO) and using synthetic agonist of A_{2A} receptors, CGS21680 (CGS); a synthetic agonist of A_{2B} receptors, Bay 60-6583 (Bay).

Initially a concentration-response curve was established to activate these receptors with various concentrations of the physiological agonist, ADO followed by the addition of IBMX (100 µM) and Fsk (10 µM) to attain maximal cAMP response by the FRET sensor. The respective purinergic receptor-induced cAMP responses were calculated in relation to R_0 and

R_{max} (Section 2.2.15) and were plotted as a concentration response curve (Figure 30). Values of EC_{50} concentration of ADO corresponded to 2.3 µM in preadipocytes and 7.7 nM in mature adipocytes. When FRET measurements were further performed in mature BA with 10 nM concentration of ADO, a weak or almost no cAMP response was observed. This could perhaps be due to the activation of the G_i-coupled GPCR A_1 or a high counteractivity of PDEs upon adenosine receptor activation. Therefore, the concentrations of ADO used in further experiments to obtain respective adenosine receptors/cAMP responses corresponded to 2.3 µM ADO in pre- BA and 10 µM in mature BA respectively.

When the same procedure to obtain concentration-response curved was followed to stimulate A_{2A} and A_{2B} receptors individually and the EC_{50} values obtained from the concentration-response curves could not be used for further experiments (data not shown). This was because the concentration of the ligands calculated with selective stimulation of A_{2A} and A_{2B} receptors were not accurate and were not deducible when applied separately. This can be reasoned due to an on-going hypothesis in the working group and was not confirmed during the scope of this project. It was recently confirmed that in skeletal muscle and brown adipocytes, the G_s-coupled A_{2A} and A_{2B} receptors form heterodimers and therefore, the expression of A_{2B} is necessary for A_{2A} signalling [101]. Therefore, to stimulate A_{2A} and A_{2B} receptors, their synthetic agonists were applied together from a study previously published [32] in both pre- and mature BA-150 nM CGS, 300 nM Bay.

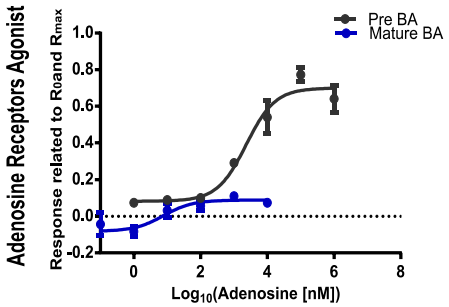

Figure 30.: Concentration-response curves of adenosine receptors induced cAMP responses in pre- and mature murine brown adipocytes expressing Epac1-camps FRET biosensor. Concentration-response curves representing differences in the magnitude of cAMP FRET responses induced by Adenosine (EC_{50} values corresponding to 2.3 µM in pre-BA and 7.7 nM in mature BA). FRET responses were normalized to basal corrected FRET ratio (R_0) and the maximal response obtained by application of IBMX + Fsk (R_{max}). n=3-6. The data represent means as ±S.E.M.

3.5.2.2. Activation of A_{2A} and A_{2B} receptors by Adenosine causes PDEs to differently regulate cAMP responses in pre- and mature murine brown adipocytes

To ensure that A_{2A} and A_{2B} receptors were fully activated, their non-selective physiological agonist, ADO in pre- (2.5 µM) and mature (10 µM) BA was used. This was then followed by treatment with either PDE2 with PDE2 inhibitor, BAY 60-7550 (Bay, 100 nM); PDE3 with PDE3 inhibitor, Cilostamide (Cilo, 10 µM) or PDE4 with PDE4 inhibitor, Rolipram (Roli, 10 µM). The maximum cAMP response elicited by Epac1-camps FRET biosensor was achieved by the addition of IBMX (100 µM) (Figure 31 A-F). In pre-BA, the regulation of cAMP by PDEs PDE4 was the major regulator of cAMP production even upon adenosine-receptors (A_{2A} and A_{2B}) stimulation. No differences in A_{2A} and A_{2B} receptor- initiated cAMP increase was observed upon PDE2 and PDE3 inhibition in pre-BA, while in mature BA, A_{2A} and A_{2B} receptor stimulation had the least restriction on cAMP production upon PDE2 inhibition in comparison to PDE3 and PDE4 inhibition (Figure 31 G).

As observed with β_3-AR initiated cAMP (Section 3.5.1.4), PDE4 inhibition led to a stronger increase (1.8-fold ± 0.3 S.E.M, n=6) of A_{2A} and A_{2B} initiated cAMP with ADO in pre-BA when compared to mature BA. Interestingly, this stronger increase was also observed with PDE2 inhibition (1.3-fold ± 3.5 S.E.M, n=7) in pre-BA (Figure 31 G). Like the β_3-AR, the low expression of A_{2A} receptors in pre-BA might the reason why PDE4 and PDE2 could have a stronger impact in restricting A_{2A} and A_{2B} receptors-initiated cAMP in pre-BA in comparison to mature BA. The Cilostamide-induced effect after A_{2A} and A_{2B} receptors-initiated cAMP (Figure 31 G) in mature adipocytes was similar to the effect observed with β_3-ARs activation (Figure 31 G). Thus, this indicated that PDE2, PDE3 and PDE4 could belong to different loco-regional cAMP pools upon stimulation with A_{2A} and A_{2B} receptors and upon β_3-AR activation in mature BA respectively.

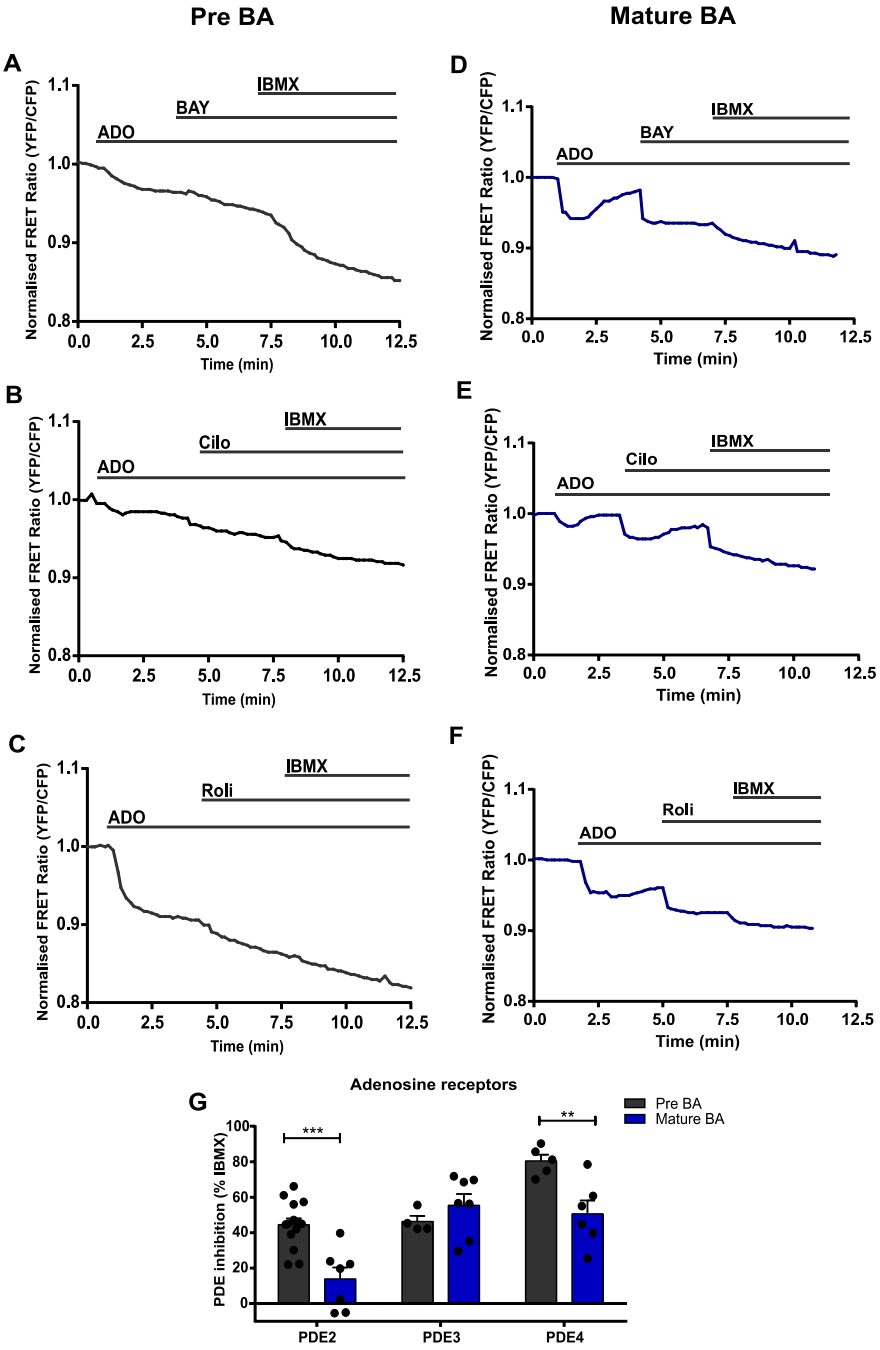

Figure 31.: Differences in regulation of cAMP dynamics by PDEs between pre- and mature murine brown adipocytes upon the activation of Gs-coupled adenosine receptors with Adenosine. Representation of cAMP responses recorded as FRET traces upon activation by selectively stimulating A_{2A} and A_{2B} receptors with the physiological activator Adenosine (ADO, 2.5 µM used in pre-BA and 10 µM used in mature BA) in pre- and mature BA expressing Epac1-camps cytosolic FRET biosensor followed by **(A, D)** PDE2 inhibitor (BAY, 100 nM) **(B, E)** PDE3 inhibitor (Cilo, 10 µM) and **(C, F)** PDE4 inhibitor (Roli, 10 µM). The maximal cAMP FRET response was achieved by inhibition of all the PDEs with non-specific PDE inhibitor, IBMX (100 µM). **(G)** Representation of Adenosine (A_{2A} and A_{2B}) receptors stimulated by FRET responses shown in (A-F) quantified and depicted as a percentage of PDE inhibition for each individual family of PDE (PDE2, PDE3 or PDE4) in relation to maximum inhibition of PDEs achieved by using the unselective PDE inhibitor IBMX. n=4-14. The means in the bar graphs are represented as ± S.E.M. 2-way ANOVA followed by Sidak's multiple comparison test was employed and the significant differences corresponded to **- p=0.01.

3.5.2.3. Selective activation of A_{2A} and A_{2B} receptors together causes PDEs to differently regulate cAMP responses in pre- and mature murine brown adipocytes

G_s-coupled adenosine receptors were selectively activated using A_{2A} receptor agonist CGS (150 nM) and A_{2B} receptor agonist Bay (300 nM) in pre- and mature BA. This was then followed by treatment with either PDE2 with PDE2 inhibitor, BAY 60-7550 (Bay, 100 nM); PDE3 with PDE3 inhibitor, Cilostamide (Cilo, 10 µM) or PDE4 with PDE4 inhibitor, Rolipram (Roli, 10 µM). The maximum cAMP response elicited by Epac1-camps FRET biosensor was achieved by the addition of IBMX (100 µM) (Figure 32 A-F). In preadipocytes, upon stimulation of A_{2A} and A_{2B} receptors, PDE4 was revealed to be the major PDE family regulating cAMP production as its inhibition contributed to a 2.4-fold ± 0.3 S.E.M (n=4) and 2.0-fold ± 0.4 S.E.M (n=5) increase in cAMP in comparison to PDE3 and PDE2 inhibition respectively. While in the mature BAs, both PDE4 contributed as the major regulator cAMP production when compared to PDE3 and PDE2. Interestingly, the regulation of PDE2 on cAMP production was completely lost in comparison to PDE3 and PDE4 in mature BA. The comparison of A_{2A} and A_{2B} receptors induced cAMP production followed by PDE inhibition revealed stimulation an overall lesser control of all the major PDE families studied on cAMP production in mature BA comparison to pre-BA. The effect of cAMP restriction upon PDE2 inhibition was significantly reduced in mature BA (1-fold ± 1.2 S.E.M, (n=5)) when compared to pre-BA (Figure 32 G), an interesting observation adenosine receptors activation in contrast to β-AR stimulation. One might expect the regulation of PDEs upon activation of adenosine receptors in pre- and mature BA to behave similar to the activation of β_3-ARs. The abundant expression of A_{2A} in murine mature BA has been reported [32]. As observed for the β_3-ARs, the low expression of A_{2A} receptors in the pre-BA, might be the reason for the PDEs to have a stronger impact in controlling adenosine receptors-initiated cAMP in preadipcoytes compared to mature BA. Surprisingly, there was also a 2.0-fold ± 0.4 S.E.M (n=5) decrease in Cilostamide-induced effect after adenosine receptors in the pre- BA compared to mature BA, which is in contrast to what was observed after β_3-AR stimulation (Figure 32 G). This might be due to the low expression of A_{2B} receptors or that the concentration of Bay was not sufficient to fully activate A_{2B} receptors in mature BA.

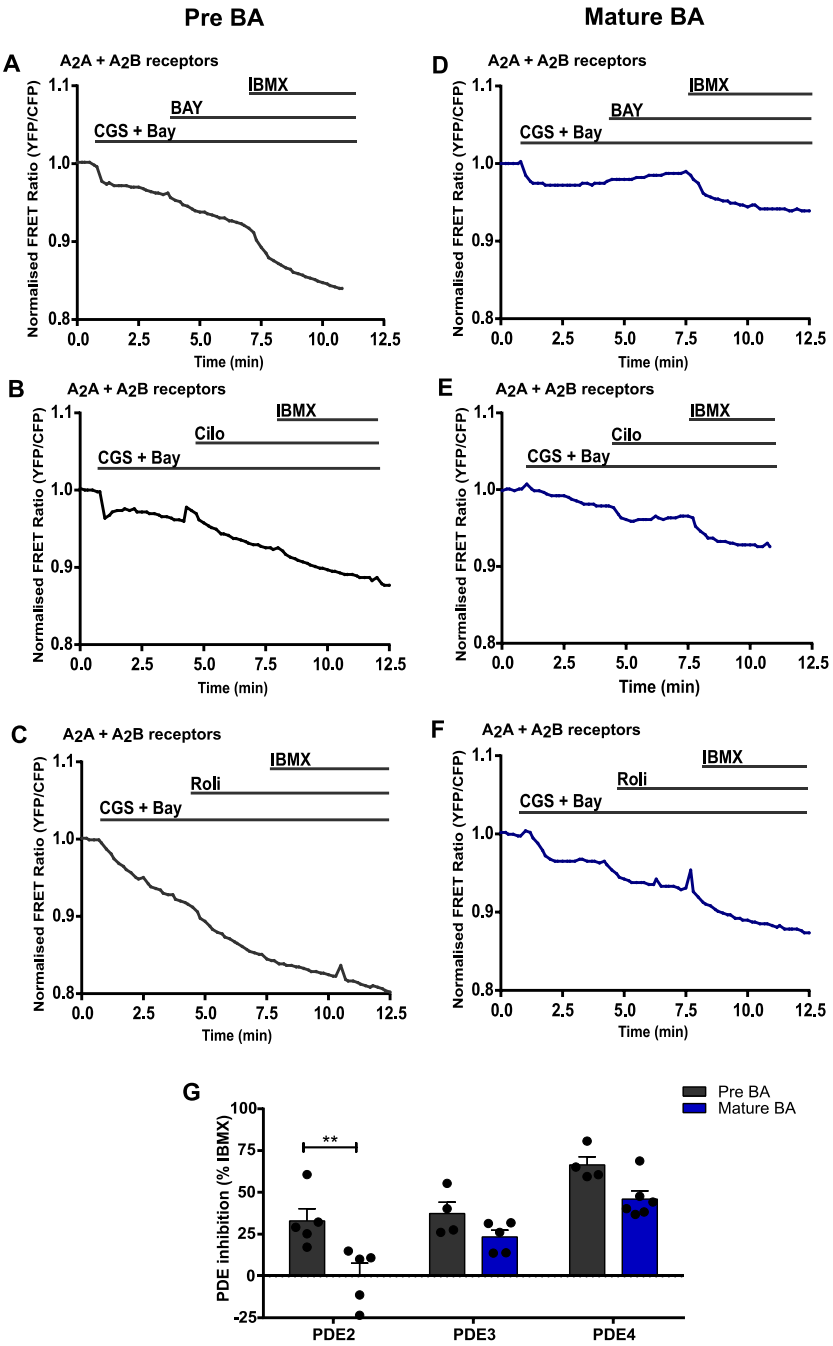

Figure 32.: Differences in regulation of cAMP dynamics by PDEs between pre- and mature murine brown adipocytes upon the activation of Gs-coupled adenosine receptors. Representation of cAMP responses recorded as FRET traces upon activation by selectively stimulating A_{2A} and A_{2B} receptors with ligands CGS21680 (CGS, 150 nM) and Bay 60-6583 (Bay, 300 nM) respectively in pre- and mature BA expressing Epac1-camps cytosolic FRET biosensor followed by **(A, D)** PDE2 inhibitor (BAY, 100 nM) **(B, E)** PDE3 inhibitor (Cilo, 10 µM) and **(C, F)** PDE4 inhibitor (Roli, 10 µM). The maximal cAMP FRET response was achieved by inhibition of all the PDEs with non-specific PDE inhibitor, IBMX (100 µM). **(G)** Representation of A_{2A} and A_{2B} receptors stimulated by FRET responses shown in (A-F) quantified and depicted as a percentage of PDE inhibition for each individual family of PDE (PDE2, PDE3 or PDE4) in relation to maximum inhibition of PDEs achieved by using the unselective PDE inhibitor IBMX. n=4-6. The means in the bar graph are represented as ± S.E.M. 2-way ANOVA followed by Sidak's multiple comparison test was employed**,** and the significant differences corresponded to **- p=0.01.

4. Discussion

4.1. cAMP and dual-specific PDEs are expressed in brown adipocytes

The brown adipose tissue (BAT) has been known to be a thermogenic organ whose main function is to oxidise lipids and convert glucose to heat [8]. Upon β-adrenergic receptor (AR) stimulation, cAMP, an important second messenger regulates important functions of BAT activation, namely, increasing lipolysis, uncoupling protein 1 (UCP1) expression, and glucose uptake [14,25–29]. Major signalling events of cyclic nucleotides are controlled by phosphodiesterases (PDEs). They play an important role in shaping intracellular pools of cyclic nucleotides and are the only route for cyclic nucleotide degradation [35,36].

Therefore, this study aimed at studying the compartmentalisation of cAMP in brown adipocytes regulated by PDEs upon stimulation of G_s-coupled GPCRs studied widely in the field of BAT activation and function, namely the β-ARs (β_1, β_2 and β_3-ARs) [6–13,15] and another set of G_s-coupled GPCRs are the adenosine receptors (A_{2A} and A_{2B}), which have been implicated in positively activating brown adipocyte thermogenesis [32,33].

The presence of cAMP and dual-specific PDEs were confirmed in brown adipocytes (BA). A study reported that the inhibition of PDE3 and PDE4 together upregulated the expression of UCP1 mRNA and led to the induction of lipolysis in brown adipocytes in the absence of adrenergic stimulation [102]. Another study reported the upregulation of PDE2 mRNA in the BAT of Zucker obese rats, though the functional significance of PDE2 still remained an open question [103]. Given the indications of PDE2, PDE3, PDE4 to be involved in the regulation of the BAT, these PDE families were the chosen candidates to study how they regulate cAMP compartmentation upon β-AR or adenosine receptor stimulation in brown adipocytes.

The expression of PDE2, PDE3, PDE4 and their respective isoforms was initially confirmed on mRNA levels in pre- and mature BAs. Interestingly, amongst the different adipose tissue depots studied here (iBAT, iWAT and gWAT), these PDEs and their isoforms were highly expressed in the BAT on protein levels. Furthermore, the expression levels of these isoforms in pre-and mature BAs were complemented on protein levels by immunoblot analysis which revealed similar results to that observed on transcript levels.

Both on mRNA and protein levels, though not significant, the expression of PDE4A, PDE4B decreased in mature BAs in comparison to pre-BA and PDE4D showed similar expression patterns both in pre- and mature BA. Interestingly, a significant upregulation of both PDE3 isoforms, PDE3A and PDE3B were observed in mature BAs on mRNA and protein levels. This observation is in line with the previously described studies that mention the functional importance of PDE3B in regulating lipid accumulation inhibiting lipolysis in mature adipocytes

[55,104–106]. PDE2A was lowly expressed on transcript and protein levels both in pre- and mature BA.

4.2. PDE2, PDE3 and PDE4 isoforms are mainly localised in the cytosol

To separate different cellular compartments in mature BA a protocol was optimised. The key steps in the process to be optimised were the number of strokes used to open the cells without damaging the integrity of the cells and the number of times the cells had to be homogenised to obtain a pure yield of cytosol, endoplasmic reticulum (ER), mitochondrial associated membrane (MAM) and pure mitochondria. Immunoblot analysis of different fractions of mature brown adipocytes revealed the confinement of PDE4A, PDE4B, PDE4D, PDE3A and PDE2A to be confined to the cytosol and PDE3B was the only isoform studied that was localised to ER, as also described for other cell types [38]. However, it should also be noted that in this project, the localisation of PDEs of interest and their isoforms were not checked in cellular fractions of plasma membrane, golgi bodies, lipid droplets or the lysosomes as these fractions were not separated. Steps to isolate the mentioned organelles from the brown adipocytes would require optimisation and further studies in the future.

Since majority of the PDE isoforms for this study were localised in the cytoplasm, a cytosolic FRET sensor (Epac1-camps) was used to study the real-time dynamics of cAMP. The project was carried out with a working hypothesis of the existence of one or more loco-regional cAMP pools in brown adipocytes regulated differently by various PDEs upon G_s-coupled GPCR stimulation.

4.3. cAMP dynamics real-time in brown adipocytes by FRET

Enzyme linked immunoassays have been successfully used to measure intracellular cAMP. However, they do not enable the analysis of spatio-temporal dynamics of cAMP microdomains in real-time. While FRET-based biosensors enable such measurements and have been described for other cell types, they have yet not been performed in primary brown adipocytes [75,95]. This study is the first of its kind describing the use of a FRET biosensor as a tool to study the real-time dynamics of cAMP in BA. Initially the proof-of-principle and the functioning of Epac1-camps FRET biosensor was studied with compounds eliciting a cAMP response using laser scanning confocal microscope. Assembling a self-made perfusion system to enable addition and removal of compounds made image acquisition in the laser scanning confocal microscope difficult as the addition of compounds caused disturbances during imaging due to the sensitivity of the focal planes.

Therefore, this study opted for a more stably established FRET-set-up with FRET imaging system consisting of a light source, an inverted microscope, beam splitter equipped with a

dichroic mirror, a longpass filter and excitation plus emission filters, a sCMOS camera connected to a computer (Section 2.2.11.1) as described for performing FRET measurements of intracellular cAMP concentrations in intact from a protocol described by Börner et al., 2009 [107]. The important parameters for the imaging system namely: exposure time and intensity of light source to excite the CFP donor and to avoid photobleaching occurring due to covalent modification of fluorophores [75,108] was optimised. An exposure time of 100 ms and 75% light intensity gave a good signal-to-noise ratio and hence were used as settings for both pre- and mature BA.

Pre-BA grow in a dense monolayer to differentiate efficiently to mature BA [88]. Therefore, for brown adipocytes, single cell measurements were not possible in both stages of differentiation. Differentiation of BA also gives rise to a layer of mature cells with dense multilocular lipid droplets. The scanned area or the field of view of cells was chosen as a region of interest (ROI) for both pre- and mature brown adipocytes to enable ratiometric analysis of YFP/CFP intensities. Therefore, live cell imaging of cAMP was established in BA to understand its compartmentation regulated by PDEs upon G_s-coupled GPCR receptor stimulation in different stages of BA differentiation.

4.4. Measurement of real-time cAMP revealed different patterns of compartmentation upon β_1 and β_3-AR stimulation in brown adipocytes

The idea of compartmentalised cAMP [8,21,109] has been a question raised due to the co-existence of three different β-ARs, β_1, β_2 and β_3-ARs in brown adipocytes exhibiting different functions [8]. For example, upon treatment of NE, proliferating adipocytes at earlier stages of differentiation in culture showed an increase in the β_1-AR induced cAMP. This was an initial study that showed proliferation of adipocytes was completely controlled by the activation of classical β_1-ARs [20]. While during the process of adipocyte differentiation, treatment with NE leads to activation of β_3-ARs wherein they couple to adenylyl cyclases (AC), triggering classical cAMP/protein kinase A/CREB phosphorylation pathway. This then activates the cellular components of thermogenic state, including an increased amount of mitochondria endowed with oxidative capacity for catabolism of fatty acids. This leads to the increase in the activity of UCP1, thereby causing thermogenesis [8,20,21].

Therefore, the first part of this study sought out to identify differences between the regulation of PDEs - PDE2, PDE3 and PDE4 upon individual β-AR induced cAMP pools in two different stages (pre- and mature BA) of BA differentiation using adipocytes isolated from TG mice expressing the cytosolic Epac1-camps FRET biosensor. The expression of β-ARs in the TG mice with FVB/N background were compared with the mice with C57BL/6J background to address the question of differences in the β-AR expression between different mouse lines. As

expected, all the three β-AR subtypes were expressed in both the adipocytes of the mice backgrounds and the expression of β_3-ARs increased on Day 7 of BA differentiation. This was in-line with the study published that mice with FVB/N and C57BL/6J background respectively showed similar patterns of β-AR expression [110].

The importance of PDE3 and PDE4 in regulating total cAMP levels in mature BA has already been demonstrated [102]. The selective stimulation of the individual β-ARs revealed followed by PDE inhibition revealed that in preadipocytes PDE3 and PDE4 inhibition are involved in the firm regulation of β_1-AR induced cAMP signalling in pre-BA. While all the three PDEs studied, are equally controlled β_3-AR initiated cAMP at low levels in mature brown adipocytes. Interestingly it was also observed that β_2-AR induced cAMP signalling showed no differences upon PDE2/3/4 regulation between pre- and mature murine BA. An upregulation of PDE3 isoforms, PDE3A and PDE3B was observed in mature BA in both mRNA and protein levels. The increased regulation of PDE3 on β_1-AR initiated cAMP in mature BA in comparison to pre-BA can be explained by the significant increase in the expression of both PDE3 isoforms upon BA maturation on both mRNA and protein levels. However, this increase in the control β_3-AR initiated cAMP by PDE3 inhibition due to the high of in expression of PDE3 isoforms in transcript and protein levels is not observed in mature BA. This could be due to the occurrence of different cAMP pools that are controlled differently due to the varied patterns of localisation of PDE3 isoforms [38]. It could also be hypothesised that this spatial separation of cAMP could be due to the establishment of different cAMP signalosomes namely: one with high cAMP concentrations associating β_1-AR and PDE3A/B, while another with β_3-ARs, wherein β_3-ARs could be part of another signalosome or a microdomain that contains low concentrations of PDE3A/B in mature BA. PDE3B in this study and other studies was localised in a different membrane compartment, namely, the ER [38,55]. This could be due to another potential explanation explaining how β_1- and β_3-ARs can be spatially separated on subcellular membrane levels.

In the heart, PDE3 isoforms were reported to be present in different membrane compartments. For example in cardiac myocytes, PDE3A isoforms were present in the sarcoplasmic reticulum (SR) [48] and caveolin-rich membrane microdomains [49] and in microsomal fractions [50]. PDE3B was found to be localised in particulate fractions [51]. It would also be interesting to hypothesise that PDE3 and its isoforms could be localised in other cellular organelles like the golgi bodies, PM or the lysosomes in brown adipocytes. These patterns of localisation would be needed to be tested and the procedure of sub-cellular fractionation for efficient separation of these organelles would have to be optimised in pre- and mature BA.

Although upon β_3-initiated cAMP production, PDE4 showed a high degree of regulation in pre-BA, this regulation was significantly increased upon brown adipocyte differentiation. Interestingly, unlike PDE3, this regulation by PDE4 could be explained at protein levels, as the expression of PDE4 isoforms was not significantly increased upon brown adipocyte maturation. Therefore, a functional redistribution of PDE4 isoforms between β_1-AR and β_3-AR-associated membrane microdomains could be postulated. Such a mechanism was observed in cardiac myocytes wherein PDE2/3 are redistributed functionally between β_1-AR and β_2-AR–associated membrane microdomains during early cardiac hypertrophy [49]. Another possibility could also be the existence of other membrane-associated cAMP pool, localised either for example in the ER, a perilipin/lipid-droplet, PM or golgi bodies that could be distinct from the cAMP pool associated with cytosolic cAMP governed by PDE4 and its isoforms. Such a system has been reported in the heart, where β-AR-cAMP signalling to microdomain-specific second messenger dynamics in the vicinity of the sarcoplasmic/endoplasmic reticulum calcium ATPase (SERCA) due to the privileged receptor–microdomain communication as a PDE3/4-dependent mechanism of cAMP compartmentation [87].

Activation of pan β-ARs with NE and studying the regulation of PDE2, PDE3, PDE4 on cAMP compartmentation revealed results similar to that of β_1-AR activation. This could be due to the higher affinity of NE to β_1-ARs, in the order of β_1-AR > β_3-AR > β_2-AR [99].

The functional aspect of $\beta_{1/2}$- and β_3-AR producing cAMP was investigated by studying lipolysis in mature brown adipocytes. It was observed that $\beta_{1/2}$ -AR induced lipolysis was controlled more by PDE3/4 in comparison to β_3-AR induced lipolysis, indicative of the existence of distinct cAMP pools occurring due to spatial separation. Furthermore, these data could also be recapitulated by ELISA as well as FRET measurements and lipolysis measured with pan β-AR regulation with NE. These results are also in concurrence with the importance of β_1-AR function in pre-BA and the gradual shift to the important role of β_3-AR upon BA maturation [8,20] and also is indicative of the fact that cAMP production and degradation is altered by PDEs thereby allowing cAMP signalling to accustom itself to meet the needs of adipocyte function at specific stages.

4.5. Measurement of real-time cAMP revealed similar behaviour in compartmentation with PDE4 and a difference in PDE2 compartmentation between adenosine receptors- A_{2A} + A_{2B} and β_3-AR signalling in brown adipocytes

The importance of adenosine in activating BAT, the abundant expression of A_{2A} receptors in murine BAT and its ability to increase energy expenditure upon activation has been shown previously [32]. The expression of A_{2A} receptors was also shown to increase oxidative

metabolism in human BAT [33]. These initial implications make the understanding the functionality of A_{2A} and A_{2B} receptors an interesting target to enhance BAT metabolism.

Given the importance of the role of adenosine receptors in BAT activation, it was hypothesised that the activation of different G_s-coupled GPCR families in brown adipocytes could show differences in cAMP compartmentation upon PDE inhibition. The differences between the regulation of PDEs (PDE2, PDE3 and PDE4) upon specific G_s-coupled adenosine receptor induced cAMP pools was studied in two different stages (pre- and mature BA) of BA differentiation using the cytosolic Epac1-camps FRET biosensor. As expected, both A_{2A} and A_{2B} receptor subtypes were expressed in murine brown adipocytes. The stimulation of adenosine receptors with their physiological activator adenosine (ADO) and the selective stimulation of both A_{2A} and A_{2B} receptors with their specific agonists CGS and Bay respectively followed by PDE inhibition by PDE2 and PDE4 respectively, showed that these two PDEs tightly control cAMP production in murine brown preadipocytes. As shown for the β_3-ARs, the low expression of A_{2A} receptors in pre-BA might the reason why PDE4 and PDE2 could have a stronger impact in restricting A_{2A} and A_{2B} receptor-initiated cAMP in pre-BA in comparison to differentiated BA on Day 7.

The PDE3/4 regulation on A_{2A} and A_{2B} receptor-initiated cAMP production was similar to the pattern observed for β_3-initiated cAMP production. This could also indicate that PDE3 and PDE4 could belong to similar loco-regional pools governing cAMP production pertaining to the activation of all G_s-coupled GPCRs receptors in general.

The restriction of PDE2 inhibition in mature BA upon A_{2A} and A_{2B} receptor-initiated cAMP production cannot be explained on the expression of protein levels as for PDE4. The differences between the high restriction of cAMP production on PDE2 inhibition between G_s-coupled adenosine receptors and β-ARs could indicate formation of different loco-regio cAMP pools. This could perhaps occur due to a receptor-associated membrane microdomain switch of PDE2 isoforms that could be more dominant and pronounced in hydrolysing cAMP in upon adenosine receptor activation in comparison to β-ARs in the cytosol [49,87]. Therefore, these data a preliminary indication that PDEs could form different spatial and temporal cAMP-hydrolysing sinks and vary their restriction upon activation of different G_s-coupled GPCRs.

4.6. Limitations and scope of perspectives for the future

In this study, it is noteworthy to acknowledge that brown adipocytes isolated from mice expressing the cytosolic Epac1-camps used for FRET experiments in this study belong to FVB/N background. The expression of β-ARs as validated in this study and in literature confirms similar expression patterns of all the three β-AR subtypes in the brown adipcoytes with FVB/N and C57BL/6J background respectively [110]. Similar patterns of mRNA

expression were also observed for adenosine receptors, A_{2A} and A_{2B} between both the strains of mice. It would be important to also prove that the expression of PDEs on mRNA and protein levels from brown adipocytes of the transgenic cytosolic Epac1-camps mice with FVB/N background and brown adipocytes from mice with C57BL/6J as used in this study are comparable. The same would also hold true for performing fractionation with pre-and mature brown adipocytes from cytosolic Epac1-camps mice. This would help in addressing discrepancies occurring in results due to differences in the background strains of the mice used in the study.

For the stimulation of individual β-ARs used in this study, concentration-response curves were established with various concentrations of their respective physiological agonist to determine the E_{50} value of the compound to be used to achieve a sub-optimal level of receptor activation without saturating the cytosolic FRET sensor. When the same procedure was used to obtain a concentration response with the physiological activator of adenosine receptors, ADO, the values of EC_{50} concentration of adenosine (ADO) corresponded to 2.3 µM in preadipocytes and 10 nM in mature adipocytes. Although 10 nM was the calculated EC_{50} for ADO in mature adipocytes, a weak or almost no cAMP response was observed when the experiments were repeated. This could perhaps be due to the activation of the G_i-coupled adenosine receptor A_1 or a high counteractivity of PDEs upon adenosine receptor activation.

Also, the concentration response curves using the synthetic agonist of A_{2A} receptors, CGS21680 (CGS); and A_{2B} receptors, Bay 60-6583 (Bay) could not be established when applied the compounds were applied individually. This can be reasoned due to an on-going hypothesis in the working group during the scope of this project. It was recently reported that in skeletal muscle and brown adipocytes, the G_s-coupled A_{2A} and A_{2B} receptors form heterodimers and therefore, the expression of A_{2B} is necessary for A_{2A} signalling [101]. As confirmed by mRNA expression levels, A_{2A} receptors are lowly expressed in preadipocytes and their expression in significantly increased upon differentiation. Therefore, to stimulate A_{2A} and A_{2B} receptors to achieve complete activation both the receptors, their agonists were applied together from a study previously published [32].

Considering the study of compartmentation of G_s-coupled adenosine receptors by the method of FRET to be preliminary and the first of its kind in this study, concentration-response curves for ADO and with the synthetic agonists Bay and CGS applied together have to be repeated and re-established in pre- and mature adipocytes with studies in the future.

Another limitation of this study was that the functional aspect of A_{2A} and A_{2B} receptor producing cAMP was not investigated. It would be interesting to observe if A_{2A} and A_{2B} receptor induced lipolysis would also not be controlled by PDE3/4 as observed for β_3-AR induced. Should the

inhibition of PDE3/4 regulate lipolysis differently in the case of A_{2A} and A_{2B} receptor induced lipolysis, it would be an indication of the occurrence of different pools of cAMP due to spatial separation controlling lipolysis that would be mediated by adenosine receptors in comparison to adrenergic receptors.

In conclusion, this study established a real-time live cell imaging approach to analyse brown adipocyte cAMP compartmentation in real-time using a cAMP biosensor. The key findings of this study showed that upon differentiation from pre- to mature murine brown adipocytes a change in PDE-dependent compartmentation of β_1- and β_3-AR-initiated cAMP responses by PDE3 and PDE4 both functionally and via FRET. Adenosine receptor stimulation (A_{2A} and A_{2B}) showed a similar behaviour as observed for β_3-AR compartmentation and PDE2 was regulated differently amongst these two classes of GPCRs.

These patterns of compartmentation have opened up avenues to study cAMP dynamics real-time regulated by with the help of other membrane-targeted FRET biosensors, for example generating FRET sensors specific to the ER, PM, nucleus and lipid droplets. This would require optimisation of stably expressing these targeted sensors via adenovirus transduction in brown adipocytes. It would also be interesting to optimise brown adipocyte fractionation to efficiently isolate the PM, nucleus, lysosomes and the lipids to confirm localisation of PDEs in these organelles.

This study focussed on studying PDEs regulating cAMP sinks with a cAMP specific cytosolic FRET sensor upon activation of different β-AR activation in murine adipocytes. Given the importance of cGMP in positively regulating BAT thermogenesis [31], it would be intriguing to study how PDEs regulate cGMP compartmentation in brown adipocytes isolated from mice expressing a cGMP-specific FRET sensor [111] . It would also be interesting to understand how PDEs regulate cAMP/cGMP crosstalk in brown adipocytes as described in the cardiomyocytes [49,111] in models of mice expressing cAMP and cGMP FRET sensors respectively. Another interesting perspective would also be to study cAMP compartmentation regulated by PDEs in primary white adipocytes. These questions would then be resourceful to interpret how the regulation of PDEs could change between health and disease models of obesity and diabetes.

5. References

[1] WHO, 2018. Fact Sheet - Obesity and Overweight.

[2] Spiegelman B.M., Flier J.S., 2001. Obesity and the regulation of energy balance. Cell 104(4):531–43. https://doi.org/10.1016/s0092-8674(01)00240-9.

[3] World Health Organization, 2009. Global health risks mortality and burden of disease attributable to selected major risks: World Health Organization.

[4] Malik V.S., Willett W.C., Hu F.B., 2013. Global obesity: trends, risk factors and policy implications. Nat Rev Endocrinol 9(1):13–27. https://doi.org/10.1038/nrendo.2012.199.

[5] Bartelt A., Heeren J., 2014. Adipose tissue browning and metabolic health. Nat Rev Endocrinol 10(1):24–36. https://doi.org/10.1038/nrendo.2013.204.

[6] Cypess A.M., Weiner L.S., Roberts-Toler C., Franquet Elia E., Kessler S.H., Kahn P.A. et al., 2015. Activation of human brown adipose tissue by a beta3-adrenergic receptor agonist. Cell Metab 21(1):33–8. https://doi.org/10.1016/j.cmet.2014.12.009.

[7] Cypess A.M., Lehman S., Williams G., Tal I., Rodman D., Goldfine A.B. et al., 2009. Identification and importance of brown adipose tissue in adult humans. N Engl J Med 360(15):1509–17. https://doi.org/10.1056/NEJMoa0810780.

[8] Cannon B., Nedergaard J., 2004. Brown adipose tissue: function and physiological significance. Physiol Rev 84(1):277–359. https://doi.org/10.1152/physrev.00015.2003.

[9] Saito M., Okamatsu-Ogura Y., Matsushita M., Watanabe K., Yoneshiro T., Nio-Kobayashi J. et al., 2009. High incidence of metabolically active brown adipose tissue in healthy adult humans: effects of cold exposure and adiposity. Diabetes 58(7):1526–31. https://doi.org/10.2337/db09-0530.

[10] van Marken Lichtenbelt, Wouter D, Vanhommerig J.W., Smulders N.M., Drossaerts, Jamie M A F L, Kemerink G.J., Bouvy N.D. et al., 2009. Cold-activated brown adipose tissue in healthy men. N Engl J Med 360(15):1500–8. https://doi.org/10.1056/NEJMoa0808718.

[11] Virtanen K.A., Lidell M.E., Orava J., Heglind M., Westergren R., Niemi T. et al., 2009. Functional brown adipose tissue in healthy adults. N Engl J Med 360(15):1518–25. https://doi.org/10.1056/NEJMoa0808949.

[12] Cinti S., 2005. The adipose organ. Prostaglandins Leukot Essent Fatty Acids 73(1):9–15. https://doi.org/10.1016/j.plefa.2005.04.010.

[13] Cinti S., 2009. Reversible physiological transdifferentiation in the adipose organ. Proc Nutr Soc 68(4):340–9. https://doi.org/10.1017/S0029665109990140.

[14] Nicholls D.G., Locke R.M., 1984. Thermogenic mechanisms in brown fat. Physiol Rev 64(1):1–64. https://doi.org/10.1152/physrev.1984.64.1.1.

[15] Frontini A., Cinti S., 2010. Distribution and development of brown adipocytes in the murine and human adipose organ. Cell Metab 11(4):253–6. https://doi.org/10.1016/j.cmet.2010.03.004.

[16] Lo K.A., Sun L., 2013. Turning WAT into BAT: a review on regulators controlling the browning of white adipocytes. Biosci Rep 33(5). https://doi.org/10.1042/BSR20130046.

[17] Pfeifer A., Hoffmann L.S., 2015. Brown, beige, and white: the new color code of fat and its pharmacological implications. Annu Rev Pharmacol Toxicol 55:207–27. https://doi.org/10.1146/annurev-pharmtox-010814-124346.

[18] Prusiner S.B., Cannon B., Lindberg O., 1968. Oxidative metabolism in cells isolated from brown adipose tissue. 1. Catecholamine and fatty acid stimulation of respiration. Eur J Biochem 6(1):15–22. https://doi.org/10.1111/j.1432-1033.1968.tb00413.x.

[19] Mohell N., Nedergaard J., Cannon B., 1983. Quantitative differentiation of alpha- and beta-adrenergic respiratory responses in isolated hamster brown fat cells: evidence for the presence of an alpha 1-adrenergic component. Eur J Pharmacol 93(3-4):183–93. https://doi.org/10.1016/0014-2999(83)90136-x.

[20] Bronnikov G., Houstek J., Nedergaard J., 1992. Beta-adrenergic, cAMP-mediated stimulation of proliferation of brown fat cells in primary culture. Mediation via beta 1 but not via beta 3 adrenoceptors. J Biol Chem 267(3):2006–13.

[21] Collins S., Daniel K.W., Rohlfs E.M., Ramkumar V., Taylor I.L., Gettys T.W., 1994. Impaired expression and functional activity of the beta 3- and beta 1-adrenergic receptors in adipose tissue of congenitally obese (C57BL/6J ob/ob) mice. Mol Endocrinol 8(4):518–27. https://doi.org/10.1210/mend.8.4.7914350.

[22] Hibi M., Oishi S., Matsushita M., Yoneshiro T., Yamaguchi T., Usui C. et al., 2016. Brown adipose tissue is involved in diet-induced thermogenesis and whole-body fat utilization in healthy humans. Int J Obes (Lond) 40(11):1655–61. https://doi.org/10.1038/ijo.2016.124.

[23] Tavernier G., Barbe P., Galitzky J., Berlan M., Caput D., Lafontan M. et al., 1996. Expression of beta3-adrenoceptors with low lipolytic action in human subcutaneous white adipocytes. J Lipid Res 37(1):87–97.

[24] Blondin D.P., Nielsen S., Kuipers E.N., Severinsen M.C., Jensen V.H., Miard S. et al., 2020. Human Brown Adipocyte Thermogenesis Is Driven by β2-AR Stimulation. Cell Metab 32(2):287-300.e7. https://doi.org/10.1016/j.cmet.2020.07.005.

[25] Reed N., Fain J.N., 1968. Stimulation of respiration in brown fat cells by epinephrine, dibutyryl-3',5'-adenosine monophosphate, and m-chloro(carbonyl cyanide)phenylhydrazone. J Biol Chem 243(11):2843–8.

[26] MacDonald J.A., Storey K.B., 1998. cAMP-dependent protein kinase from brown adipose tissue: temperature effects on kinetic properties and enzyme role in hibernating ground squirrels. J Comp Physiol B 168(7):513–25. https://doi.org/10.1007/s003600050172.

[27] Fredriksson J.M., Thonberg H., Ohlson K.B., Ohba K., Cannon B., Nedergaard J., 2001. Analysis of inhibition by H89 of UCP1 gene expression and thermogenesis indicates protein kinase A mediation of beta(3)-adrenergic signalling rather than beta(3)-adrenoceptor antagonism by H89. Biochim Biophys Acta 1538(2-3):206–17. https://doi.org/10.1016/s0167-4889(01)00070-2.

[28] Schreiber R., Diwoky C., Schoiswohl G., Feiler U., Wongsiriroj N., Abdellatif M. et al., 2017. Cold-Induced Thermogenesis Depends on ATGL-Mediated Lipolysis in Cardiac Muscle, but Not Brown Adipose Tissue. Cell Metab 26(5):753-763.e7. https://doi.org/10.1016/j.cmet.2017.09.004.

[29] Holm C., Fredrikson G., Cannon B., Belfrage P., 1987. Hormone-sensitive lipase in brown adipose tissue: identification and effect of cold exposure. Biosci Rep 7(11):897–904. https://doi.org/10.1007/bf01119481.

[30] Chrisman T.D., Garbers D.L., Parks M.A., Hardman J.G., 1975. Characterization of particulate and soluble guanylate cyclases from rat lung. J Biol Chem 250(2):374–81.

[31] Haas B., Mayer P., Jennissen K., Scholz D., Berriel Diaz M., Bloch W. et al., 2009. Protein kinase G controls brown fat cell differentiation and mitochondrial biogenesis. Sci Signal 2(99):ra78. https://doi.org/10.1126/scisignal.2000511.

[32] Gnad T., Scheibler S., Kugelgen I. von, Scheele C., Kilic A., Glode A. et al., 2014. Adenosine activates brown adipose tissue and recruits beige adipocytes via A2A receptors. Nature 516(7531):395–9. https://doi.org/10.1038/nature13816.

[33] Lahesmaa M., Oikonen V., Helin S., Luoto P., U Din M., Pfeifer A. et al., 2019. Regulation of human brown adipose tissue by adenosine and A(2A) receptors - studies with (15)OH(2)O and (11)CTMSX PET/CT. Eur J Nucl Med Mol Imaging 46(3):743–50. https://doi.org/10.1007/s00259-018-4120-2.

[34] Abi-Gerges A., Richter W., Lefebvre F., Mateo P., Varin A., Heymes C. et al., 2009. Decreased expression and activity of cAMP phosphodiesterases in cardiac hypertrophy and its impact on beta-adrenergic cAMP signals. Circ Res 105(8):784–92. https://doi.org/10.1161/CIRCRESAHA.109.197947.

[35] BUTCHER R.W., SUTHERLAND E.W., 1962. Adenosine 3',5'-phosphate in biological materials. I. Purification and properties of cyclic 3',5'-nucleotide phosphodiesterase and use of this enzyme to characterize adenosine 3',5'-phosphate in human urine. J Biol Chem 237:1244–50.

[36] Mongillo M., McSorley T., Evellin S., Sood A., Lissandron V., Terrin A. et al., 2004. Fluorescence resonance energy transfer-based analysis of cAMP dynamics in live neonatal rat cardiac myocytes reveals distinct functions of compartmentalized phosphodiesterases. Circ Res 95(1):67–75. https://doi.org/10.1161/01.RES.0000134629.84732.11.

[37] Pavlaki N., Nikolaev V.O., 2018. Imaging of PDE2- and PDE3-Mediated cGMP-to-cAMP Cross-Talk in Cardiomyocytes. J Cardiovasc Dev Dis 5(1). https://doi.org/10.3390/jcdd5010004.

[38] Bender A.T., Beavo J.A., 2006. Cyclic nucleotide phosphodiesterases: molecular regulation to clinical use. Pharmacol Rev 58(3):488–520. https://doi.org/10.1124/pr.58.3.5.

[39] Conti M., Beavo J., 2007. Biochemistry and physiology of cyclic nucleotide phosphodiesterases: essential components in cyclic nucleotide signaling. Annu Rev Biochem 76:481–511. https://doi.org/10.1146/annurev.biochem.76.060305.150444.

[40] Martinez S.E., Bruder S., Schultz A., Zheng N., Schultz J.E., Beavo J.A. et al., 2005. Crystal structure of the tandem GAF domains from a cyanobacterial adenylyl cyclase: Modes of ligand binding and dimerization. Proc Natl Acad Sci U S A 102(8):3082–7. https://doi.org/10.1073/pnas.0409913102.

[41] Martinez S.E., Wu A.Y., Glavas N.A., Tang X.-B., Turley S., Hol W.G.J. et al., 2002. The two GAF domains in phosphodiesterase 2A have distinct roles in dimerization and in cGMP binding. Proceedings of the National Academy of Sciences 99(20):13260. https://doi.org/10.1073/pnas.192374899.

[42] Weber S., Zeller M., Guan K., Wunder F., Wagner M., El-Armouche A., 2017. PDE2 at the crossway between cAMP and cGMP signalling in the heart. Cell Signal 38:76–84. https://doi.org/10.1016/j.cellsig.2017.06.020.

[43] Russwurm C., Zoidl G., Koesling D., Russwurm M., 2009. Dual acylation of PDE2A splice variant 3: targeting to synaptic membranes. J Biol Chem 284(38):25782–90. https://doi.org/10.1074/jbc.M109.017194.

[44] Acin-Perez R., Russwurm M., Günnewig K., Gertz M., Zoidl G., Ramos L. et al., 2011. A phosphodiesterase 2A isoform localized to mitochondria regulates respiration. J Biol Chem 286(35):30423–32. https://doi.org/10.1074/jbc.M111.266379.

[45] Monterisi S., Lobo M.J., Livie C., Castle J.C., Weinberger M., Baillie G. et al., 2017. PDE2A2 regulates mitochondria morphology and apoptotic cell death via local modulation of cAMP/PKA signalling. Elife 6. https://doi.org/10.7554/eLife.21374.

[46] Lobo M.J., Reverte-Salisa L., Chao Y.-C., Koschinski A., Gesellchen F., Subramaniam G. et al., 2020. Phosphodiesterase 2A2 regulates mitochondria clearance through Parkin-dependent mitophagy. Commun Biol 3(1):596. https://doi.org/10.1038/s42003-020-01311-7.

[47] Vettel C., Lindner M., Dewenter M., Lorenz K., Schanbacher C., Riedel M. et al., 2017. Phosphodiesterase 2 Protects Against Catecholamine-Induced Arrhythmia and Preserves Contractile Function After Myocardial Infarction. Circ Res 120(1):120–32. https://doi.org/10.1161/CIRCRESAHA.116.310069.

[48] Ahmad F., Shen W., Vandeput F., Szabo-Fresnais N., Krall J., Degerman E. et al., 2015. Regulation of sarcoplasmic reticulum Ca2+ ATPase 2 (SERCA2) activity by phosphodiesterase 3A (PDE3A) in human myocardium: phosphorylation-dependent interaction of PDE3A1 with SERCA2. J Biol Chem 290(11):6763–76. https://doi.org/10.1074/jbc.M115.638585.

[49] Perera R.K., Sprenger J.U., Steinbrecher J.H., Hubscher D., Lehnart S.E., Abesser M. et al., 2015. Microdomain switch of cGMP-regulated phosphodiesterases leads to ANP-induced augmentation of beta-adrenoceptor-stimulated contractility in early cardiac hypertrophy. Circ Res 116(8):1304–11. https://doi.org/10.1161/CIRCRESAHA.116.306082.

[50] Zaccolo M., Movsesian M.A., 2007. cAMP and cGMP signaling cross-talk: role of phosphodiesterases and implications for cardiac pathophysiology. Circ Res 100(11):1569–78. https://doi.org/10.1161/CIRCRESAHA.106.144501.

[51] Shakur Y., Holst L.S., Landstrom T.R., Movsesian M., Degerman E., Manganiello V., 2001. Regulation and function of the cyclic nucleotide phosphodiesterase (PDE3) gene

family. Prog Nucleic Acid Res Mol Biol 66:241–77. https://doi.org/10.1016/s0079-6603(00)66031-2.

[52] Movsesian M., Ahmad F., Hirsch E., 2018. Functions of PDE3 Isoforms in Cardiac Muscle.

[53] Movsesian M.A., 1999. Beta-adrenergic receptor agonists and cyclic nucleotide phosphodiesterase inhibitors: shifting the focus from inotropy to cyclic adenosine monophosphate. J Am Coll Cardiol 34(2):318–24. https://doi.org/10.1016/s0735-1097(99)00220-x.

[54] Wechsler J., Choi Y.-H., Krall J., Ahmad F., Manganiello V.C., Movsesian M.A., 2002. Isoforms of cyclic nucleotide phosphodiesterase PDE3A in cardiac myocytes. J Biol Chem 277(41):38072–8. https://doi.org/10.1074/jbc.M203647200.

[55] DiPilato L.M., Ahmad F., Harms M., Seale P., Manganiello V., Birnbaum M.J., 2015. The Role of PDE3B Phosphorylation in the Inhibition of Lipolysis by Insulin. Mol Cell Biol 35(16):2752–60. https://doi.org/10.1128/MCB.00422-15.

[56] Netherton S.J., Jimmo S.L., Palmer D., Tilley D.G., Dunkerley H.A., Raymond D.R. et al., 2002. Altered phosphodiesterase 3-mediated cAMP hydrolysis contributes to a hypermotile phenotype in obese JCR:LA-cp rat aortic vascular smooth muscle cells: implications for diabetes-associated cardiovascular disease. Diabetes 51(4):1194–200. https://doi.org/10.2337/diabetes.51.4.1194.

[57] Beierwaltes W.H., 2006. cGMP stimulates renin secretion in vivo by inhibiting phosphodiesterase-3. Am J Physiol Renal Physiol 290(6):F1376-81. https://doi.org/10.1152/ajprenal.00209.2005.

[58] Chung Y.W., Ahmad F., Tang Y., Hockman S.C., Kee H.J., Berger K. et al., 2017. White to beige conversion in PDE3B KO adipose tissue through activation of AMPK signaling and mitochondrial function. Sci Rep 7:40445. https://doi.org/10.1038/srep40445.

[59] Bolger G.B., 1994. Molecular biology of the cyclic AMP-specific cyclic nucleotide phosphodiesterases: a diverse family of regulatory enzymes. Cell Signal 6(8):851–9. https://doi.org/10.1016/0898-6568(94)90018-3.

[60] Houslay M.D., Adams D.R., 2003. PDE4 cAMP phosphodiesterases: modular enzymes that orchestrate signalling cross-talk, desensitization and compartmentalization. Biochem J 370(Pt 1):1–18. https://doi.org/10.1042/BJ20021698.

[61] Houslay M.D., Schafer P., Zhang K.Y.J., 2005. Keynote review: phosphodiesterase-4 as a therapeutic target. Drug Discov Today 10(22):1503–19. https://doi.org/10.1016/S1359-6446(05)03622-6.

[62] Baillie G.S., Sood A., McPhee I., Gall I., Perry S.J., Lefkowitz R.J. et al., 2003. beta-Arrestin-mediated PDE4 cAMP phosphodiesterase recruitment regulates beta-adrenoceptor switching from Gs to Gi. Proc Natl Acad Sci U S A 100(3):940–5. https://doi.org/10.1073/pnas.262787199.

[63] Grønning L.M., Baillie G.S., Cederberg A., Lynch M.J., Houslay M.D., Enerbäck S. et al., 2006. Reduced PDE4 expression and activity contributes to enhanced catecholamine-induced cAMP accumulation in adipocytes from FOXC2 transgenic mice. FEBS Lett 580(17):4126–30. https://doi.org/10.1016/j.febslet.2006.06.058.

[64] Zhang R., Maratos-Flier E., Flier J.S., 2009. Reduced adiposity and high-fat diet-induced adipose inflammation in mice deficient for phosphodiesterase 4B. Endocrinology 150(7):3076–82. https://doi.org/10.1210/en.2009-0108.

[65] Vagena E., Ryu J.K., Baeza-Raja B., Walsh N.M., Syme C., Day J.P. et al., 2019. A high-fat diet promotes depression-like behavior in mice by suppressing hypothalamic PKA signaling. Transl Psychiatry 9(1):141. https://doi.org/10.1038/s41398-019-0470-1.

[66] Miaczynska M., Pelkmans L., Zerial M., 2004. Not just a sink: endosomes in control of signal transduction. Curr Opin Cell Biol 16(4):400–6. https://doi.org/10.1016/j.ceb.2004.06.005.

[67] Arora K., Sinha C., Zhang W., Ren A., Moon C.S., Yarlagadda S. et al., 2013. Compartmentalization of cyclic nucleotide signaling: a question of when, where, and why? Pflugers Arch 465(10):1397–407. https://doi.org/10.1007/s00424-013-1280-6.

[68] Calebiro D., Nikolaev V.O., Gagliani M.C., Filippis T. de, Dees C., Tacchetti C. et al., 2009. Persistent cAMP-signals triggered by internalized G-protein-coupled receptors. PLoS Biol 7(8):e1000172. https://doi.org/10.1371/journal.pbio.1000172.

[69] Buxton I.L., Brunton L.L., 1983. Compartments of cyclic AMP and protein kinase in mammalian cardiomyocytes. J Biol Chem 258(17):10233–9.

[70] Schwartz J.H., 2001. The many dimensions of cAMP signaling. Proceedings of the National Academy of Sciences 98(24):13482. https://doi.org/10.1073/pnas.251533998.

[71] Sprenger J.U., Nikolaev V.O., 2013. Biophysical techniques for detection of cAMP and cGMP in living cells. Int J Mol Sci 14(4):8025–46. https://doi.org/10.3390/ijms14048025.

[72] Craven K.B., Zagotta W.N., 2006. CNG and HCN channels: two peas, one pod. Annu Rev Physiol 68:375–401. https://doi.org/10.1146/annurev.physiol.68.040104.134728.

[73] Frings S., Seifert R., Godde M., Kaupp U.B., 1995. Profoundly different calcium permeation and blockage determine the specific function of distinct cyclic nucleotide-gated channels. Neuron 15(1):169–79. https://doi.org/10.1016/0896-6273(95)90074-8.

[74] Rochais F., Vandecasteele G., Lefebvre F., Lugnier C., Lum H., Mazet J.-L. et al., 2004. Negative feedback exerted by cAMP-dependent protein kinase and cAMP phosphodiesterase on subsarcolemmal cAMP signals in intact cardiac myocytes: an in vivo study using adenovirus-mediated expression of CNG channels. J Biol Chem 279(50):52095–105. https://doi.org/10.1074/jbc.M405697200.

[75] Borner S., Schwede F., Schlipp A., Berisha F., Calebiro D., Lohse M.J. et al., 2011. FRET measurements of intracellular cAMP concentrations and cAMP analog permeability in intact cells. Nat Protoc 6(4):427–38. https://doi.org/10.1038/nprot.2010.198.

[76] Förster T., 1948. Zwischenmolekulare Energiewanderung und Fluoreszenz. Annalen der Physik 437(1):55–75. https://doi.org/10.1002/andp.19484370105.

[77] Hochreiter B., Garcia A.P., Schmid J.A., 2015. Fluorescent proteins as genetically encoded FRET biosensors in life sciences. Sensors (Basel) 15(10):26281–314. https://doi.org/10.3390/s151026281.

[78] Frackowiak D., 1988. The Jablonski diagram. Journal of Photochemistry and Photobiology B: Biology 2(3):399. https://doi.org/10.1016/1011-1344(88)85060-7.

[79] Nikolaev V.O., Bünemann M., Hein L., Hannawacker A., Lohse M.J., 2004. Novel single chain cAMP sensors for receptor-induced signal propagation. J Biol Chem 279(36):37215–8. https://doi.org/10.1074/jbc.C400302200.

[80] Nikolaev V.O., Lohse M.J., 2006. Monitoring of cAMP synthesis and degradation in living cells. Physiology (Bethesda) 21:86–92. https://doi.org/10.1152/physiol.00057.2005.

[81] Willoughby D., Cooper D.M.F., 2008. Live-cell imaging of cAMP dynamics. Nat Methods 5(1):29–36. https://doi.org/10.1038/nmeth1135.

[82] Zaccolo M., Pozzan T., 2002. Discrete microdomains with high concentration of cAMP in stimulated rat neonatal cardiac myocytes. Science 295(5560):1711–5. https://doi.org/10.1126/science.1069982.

[83] DiPilato L.M., Cheng X., Zhang J., 2004. Fluorescent indicators of cAMP and Epac activation reveal differential dynamics of cAMP signaling within discrete subcellular

compartments. Proc Natl Acad Sci U S A 101(47):16513–8. https://doi.org/10.1073/pnas.0405973101.

[84] Adams S.R., Harootunian A.T., Buechler Y.J., Taylor S.S., Tsien R.Y., 1991. Fluorescence ratio imaging of cyclic AMP in single cells. Nature 349(6311):694–7. https://doi.org/10.1038/349694a0.

[85] Zaccolo M., Giorgi F. de, Cho C.Y., Feng L., Knapp T., Negulescu P.A. et al., 2000. A genetically encoded, fluorescent indicator for cyclic AMP in living cells. Nat Cell Biol 2(1):25–9. https://doi.org/10.1038/71345.

[86] Bos J.L., 2003. Epac: a new cAMP target and new avenues in cAMP research. Nat Rev Mol Cell Biol 4(9):733–8. https://doi.org/10.1038/nrm1197.

[87] Sprenger J.U., Perera R.K., Steinbrecher J.H., Lehnart S.E., Maier L.S., Hasenfuss G. et al., 2015. In vivo model with targeted cAMP biosensor reveals changes in receptor-microdomain communication in cardiac disease. Nat Commun 6:6965. https://doi.org/10.1038/ncomms7965.

[88] Jennissen K., Haas B., Mitschke M.M., Siegel F., Pfeifer A., 2013. Analysis of cGMP signaling in adipocytes. Methods Mol Biol 1020:175–92. https://doi.org/10.1007/978-1-62703-459-3_11.

[89] Ramirez-Zacarias J.L., Castro-Munozledo F., Kuri-Harcuch W., 1992. Quantitation of adipose conversion and triglycerides by staining intracytoplasmic lipids with Oil red O. Histochemistry 97(6):493–7.

[90] McGowan M.W., Artiss J.D., Strandbergh D.R., Zak B., 1983. A peroxidase-coupled method for the colorimetric determination of serum triglycerides. Clin Chem 29(3):538–42.

[91] Wieckowski M.R., Giorgi C., Lebiedzinska M., Duszynski J., Pinton P., 2009. Isolation of mitochondria-associated membranes and mitochondria from animal tissues and cells. Nat Protoc 4(11):1582–90. https://doi.org/10.1038/nprot.2009.151.

[92] Vance J.E., 1990. Phospholipid synthesis in a membrane fraction associated with mitochondria. J Biol Chem 265(13):7248–56.

[93] Vance J.E., Stone S.J., Faust J.R., 1997. Abnormalities in mitochondria-associated membranes and phospholipid biosynthetic enzymes in the mnd/mnd mouse model of neuronal ceroid lipofuscinosis. Biochim Biophys Acta 1344(3):286–99. https://doi.org/10.1016/s0005-2760(96)00153-1.

[94] Kraft A.E., Nikolaev V.O., 2017. FRET Microscopy for Real-Time Visualization of Second Messengers in Living Cells. Methods Mol Biol 1563:85–90. https://doi.org/10.1007/978-1-4939-6810-7_6.

[95] Herget S., Lohse M.J., Nikolaev V.O., 2008. Real-time monitoring of phosphodiesterase inhibition in intact cells. Cell Signal 20(8):1423–31. https://doi.org/10.1016/j.cellsig.2008.03.011.

[96] Chen Y., Mauldin J.P., Day R.N., Periasamy A., 2007. Characterization of spectral FRET imaging microscopy for monitoring nuclear protein interactions. J Microsc 228(Pt 2):139–52. https://doi.org/10.1111/j.1365-2818.2007.01838.x.

[97] Kim J., Li X., Kang M.-S., Im K.-B., Genovesio A., Grailhe R., 2012. Quantification of protein interaction in living cells by two-photon spectral imaging with fluorescent protein fluorescence resonance energy transfer pair devoid of acceptor bleed-through. Cytometry A 81(2):112–9. https://doi.org/10.1002/cyto.a.21150.

[98] Kannabiran S.A., Gosejacob D., Niemann B., Nikolaev V.O., Pfeifer A., 2020. Real-time monitoring of cAMP in brown adipocytes reveals differential compartmentation of beta1 and beta3-adrenoceptor signalling. Mol Metab:100986. https://doi.org/10.1016/j.molmet.2020.100986.

[99] Hoffmann C., Leitz M.R., Oberdorf-Maass S., Lohse M.J., Klotz K.-N., 2004. Comparative pharmacology of human beta-adrenergic receptor subtypes--characterization of stably transfected receptors in CHO cells. Naunyn Schmiedebergs Arch Pharmacol 369(2):151–9. https://doi.org/10.1007/s00210-003-0860-y.

[100] Atgie C., D'Allaire F., Bukowiecki L.J., 1997. Role of beta1- and beta3-adrenoceptors in the regulation of lipolysis and thermogenesis in rat brown adipocytes. Am J Physiol 273(4):C1136-42. https://doi.org/10.1152/ajpcell.1997.273.4.C1136.

[101] Gnad T., Navarro G., Lahesmaa M., Reverte-Salisa L., Copperi F., Cordomi A. et al., 2020. Adenosine/A2B Receptor Signaling Ameliorates the Effects of Aging and Counteracts Obesity. Cell Metab 32(1):56-70.e7. https://doi.org/10.1016/j.cmet.2020.06.006.

[102] Kraynik S.M., Miyaoka R.S., Beavo J.A., 2013. PDE3 and PDE4 isozyme-selective inhibitors are both required for synergistic activation of brown adipose tissue. Mol Pharmacol 83(6):1155–65. https://doi.org/10.1124/mol.112.084145.

[103] Coudray C., Charon C., Komas N., Mory G., Diot-Dupuy F., Manganiello V. et al., 1999. Evidence for the presence of several phosphodiesterase isoforms in brown adipose

tissue of Zucker rats: modulation of PDE2 by the fa gene expression. FEBS Lett 456(1):207–10. https://doi.org/10.1016/s0014-5793(99)00934-5.

[104] Czech M.P., Tencerova M., Pedersen D.J., Aouadi M., 2013. Insulin signalling mechanisms for triacylglycerol storage. Diabetologia 56(5):949–64. https://doi.org/10.1007/s00125-013-2869-1.

[105] Fruhbeck G., Mendez-Gimenez L., Fernandez-Formoso J.-A., Fernandez S., Rodriguez A., 2014. Regulation of adipocyte lipolysis. Nutr Res Rev 27(1):63–93. https://doi.org/10.1017/S095442241400002X.

[106] Arner P., Langin D., 2014. Lipolysis in lipid turnover, cancer cachexia, and obesity-induced insulin resistance. Trends Endocrinol Metab 25(5):255–62. https://doi.org/10.1016/j.tem.2014.03.002.

[107] Sprenger J.U., Perera R.K., Gotz K.R., Nikolaev V.O., 2012. FRET microscopy for real-time monitoring of signaling events in live cells using unimolecular biosensors. J Vis Exp(66):e4081. https://doi.org/10.3791/4081.

[108] Zal T., Gascoigne N.R.J., 2004. Photobleaching-corrected FRET efficiency imaging of live cells. Biophys J 86(6):3923–39. https://doi.org/10.1529/biophysj.103.022087.

[109] Zhao J., Cannon B., Nedergaard J., 1997. alpha1-Adrenergic stimulation potentiates the thermogenic action of beta3-adrenoreceptor-generated cAMP in brown fat cells. J Biol Chem 272(52):32847–56. https://doi.org/10.1074/jbc.272.52.32847.

[110] de Jong, Jasper M A, Wouters R.T.F., Boulet N., Cannon B., Nedergaard J., Petrovic N., 2017. The beta3-adrenergic receptor is dispensable for browning of adipose tissues. Am J Physiol Endocrinol Metab 312(6):E508-E518. https://doi.org/10.1152/ajpendo.00437.2016.

[111] Götz K.R., Sprenger J.U., Perera R.K., Steinbrecher J.H., Lehnart S.E., Kuhn M. et al., 2014. Transgenic mice for real-time visualization of cGMP in intact adult cardiomyocytes. Circ Res 114(8):1235–45. https://doi.org/10.1161/CIRCRESAHA.114.302437.

6. Summary

Compartmentalisation of cAMP in brown adipocytes

3',5'-cyclic adenosine monophosphate (cAMP) is a central second messenger which governs brown adipocyte differentiation and function. Upon β-adrenergic receptors (β-ARs) or G_s-coupled G protein-coupled receptor (GPCR) stimulation in brown adipocyctes, adenylate cyclases are activated which produce cAMP. The levels of cyclic nucleotides are tightly regulated by phosphodiesterases (PDEs) which can generate subcellular microdomains of cAMP. Since the spatio-temporal organization of the cAMP signalling pathway in adipocytes is still unknown, this study aimed at monitoring the real-time cAMP dynamics by live cell imaging in pre- and mature brown adipocytes from transgenic mice expressing Epac1-camps FRET biosensor.

Real-time measurements of cAMP responses were established. The first part of the study focussed on studying the compartmentation of cAMP that occurred between the different β-AR subtypes. Upon individual β-AR activation, PDE4 was the major PDE regulating cytosolic cAMP in brown preadipocytes. Upon brown adipocyte maturation, the upregulation of PDE3 along with PDE4 contributes to control β_1-AR induced cAMP. Unexpectedly, even though the protein levels of PDE3 increased upon maturation, it was resistant to the β_3-AR initiated cAMP and the control of this microdomain by PDE4 was reduced as well.

Therefore, this led to the postulation that distinct cAMP pools could exist in brown adipocytes. One cAMP pool is formed by β_1-AR associated with PDE3 and PDE4, while another pool is centred around β_3-AR and is much less controlled by these PDEs. Functionally, lower control of β_3-AR initiated cAMP by PDE3 and PDE4 facilitates brown adipocyte lipolysis, while lipolysis activated by β_1-AR is under tight control of PDE3 and PDE4.

Another question that was addressed was, if the stimulation of different G_s-coupled GPCRs in brown adipocytes showed similar compartmentation of cAMP. To test this, G_s-coupled adenosine receptors, A_{2A} and A_{2B} receptors were studied. PDE inhibition by PDE2 and PDE4 tightly control cAMP production in murine brown preadipocytes. As shown for the β_3-ARs, the low expression of A_{2A} receptors in preadipocytes might be the reason why PDE4 and PDE2 could have a stronger impact in restricting A_{2A} and A_{2B} receptor-initiated cAMP. The PDE3/4 regulation on A_{2A} and A_{2B} receptor-initiated cAMP production was similar to the pattern observed for β_3-initiated cAMP production indicating that PDE3 and PDE4 could belong to similar loco-regio pools governing cAMP production when G_s-coupled GPCRs receptors associated with BAT thermogenesis are activated. Functional studies addressing the

regulation of PDEs upon G_s-coupled adenosine receptor warrants future studies and confirmation.

In essence and conclusion, a real-time live cell imaging approach to analyse brown adipocyte cAMP dynamics in real-time using a cAMP biosensor was established. This study showed that during differentiation from pre- to mature murine brown adipocytes, there was a change in PDE-dependent compartmentation of β_1- and β_3-AR-initiated cAMP responses by PDE3 and PDE4 inhibition regulating lipolysis. The same effect of PDE3 and PDE4 was seen upon G_s-coupled adenosine receptor stimulation, however, the functional studies need repetition and confirmation. There was a novel effect of an additional difference in the tight regulation of PDE2 in mature brown adipocytes upon G_s-coupled adenosine receptor stimulation, indicating differences in compartmentation of different G_s-coupled GPCRs.

This study has potentially opened up a scope to study cAMP compartmentation mediated by PDEs with different organelle-specific sensors in brown and as well other types of adipocytes in light to G_s-coupled GPCR activation.

II. Publications, Posters and Talks

Published article:

Kannabiran S.A., Gosejacob D., Niemann B., Nikolaev V.O., Pfeifer A., 2020. Real-time monitoring of cAMP in brown adipocytes reveals differential compartmentation of beta1 and beta3-adrenoceptor signalling. Mol Metab:100986.

https://doi.org/10.1016/j.molmet.2020.100986.

Mol Metab. 2020 Jul;37:100986. doi: 10.1016/j.molmet.2020.100986. Epub 2020 Apr1.

Posters and Talks:

10/19 **Talk: Sukanya Arcot Kannabiran**, Dominic Gosejacob, Viacheslav Nikolaev, and Alexander Pfeifer – *Compartmenatlisation of cAMP in brown adipocytes.* – Adenine Nucleotides in Immunity and Inflammation, SFB 1328, Science Afternoon, Hamburg, Germany.

08/19 **Poster: Sukanya Arcot Kannabiran**, Dominic Gosejacob, Viacheslav Nikolaev, Christa Müller and Alexander Pfeifer – *Compartmenatlisation of cAMP and the role of orphan receptor GPR18 in brown adipocytes* – Pharmacology of 7TM-receptors and downstream signalling pathways, RTG1873, Annual Retreat, Bonn, Germany.

03/19 **Poster: Sukanya Arcot Kannabiran**, Dominic Gosejacob, Viacheslav Nikolaev, and Alexander Pfeifer – *Compartmenatlisation of cAMP and in brown adipocytes* – Adenine Nucleotides in Immunity and Inflammation, SFB 1328, Annual Retreat, Hamburg, Germany.

10/18 **Talk: Sukanya Arcot Kannabiran**, Dominic Gosejacob, Viacheslav Nikolaev, Christa Müller and Alexander Pfeifer – *Compartmenatlisation of cAMP and the role of orphan receptor GPR18 in brown adipocytes* – Pharmacology of 7TM-receptors and downstream signalling pathways, RTG1873, Annual Retreat, Bonn, Germany.

01/18 **Poster: Sukanya Arcot Kannabiran**, Dominic Gosejacob, Viacheslav Nikolaev, Alexander Pfeifer – *Compartmenatlisation of cAMP in brown adipocytes* – FFfF

Adenine Nucleotides in Immunity and Inflammation, SFB 1328, Funding Review, Hamburg, Germany.

01/18 **Poster: Sukanya Arcot Kannabiran**, Dominic Gosejacob, Viacheslav Nikolaev, Alexander Pfeifer – *Compartmenatlisation of cAMP in brown adipocytes* – Adenine Nucleotides in Immunity and Inflammation, SFB 1328, Funding Review, Hamburg, Germany.

09/17 **Talk: Sukanya Arcot Kannabiran**, Dominic Gosejacob, Viacheslav Nikolaev, Christa Müller and Alexander Pfeifer – *Compartmenatlisation of cAMP and the role of orphan receptor GPR18 in brown adipocytes* – Pharmacology of 7TM-receptors and downstream signalling pathways, RTG1873, Annual Retreat, Bonn, Germany.

05/17 **Poster: Sukanya Arcot Kannabiran**, Christa Müller and Alexander Pfeifer - *The role of orphan receptor GPR18 in brown adipocytes* – Pharmacology of 7TM-receptors and downstream signalling pathways, RTG1873, Funding Review, Bonn, Germany.